Durham E-Theses

Optical and transport properties of polyaniline films

Tzamalis, Georgios

How to cite:

Tzamalis, Georgios (2002) *Optical and transport properties of polyaniline films*, Durham theses, Durham University. Available at Durham E-Theses Online: http://etheses.dur.ac.uk/4148/

Use policy

Optical and Transport Properties of Polyaniline Films

Georgios Tzamalis

Department of Physics

University of Durham

A thesis submitted to the Faculty of Science at the University of Durham
for the degree of Doctor of Philosophy.

September 2002

Abstract

This thesis presents the results of a comprehensive study on the transport and optical properties of polyaniline (PANI) films. The films are derived by protonation (doping) of the emeraldine base form of polyaniline, as synthesized in Durham, with either 2-acrylamido-2-methyl-1-propanesulfonic acid (AMPSA) or 10-camphorsulfonic acid. Thus, two distinct PANI systems are obtained: PANI-CSA and PANI-AMPSA. The variation of the doping level can affect the metallic properties of the final system, so that samples close to the boundary as well as samples at either side of a disorder induced metal-insulator can be obtained. The relation between the doping level and the degree of disorder, along with the existence of an inherently metallic behaviour in PANI, are investigated through a series of experiments.

Temperature dependent dc conductivity measurements ranging from 10-295 K are performed using a closed loop helium cryostat under dynamic vacuum ($\sim 10^{-5}$ mbar). From the conductivity data curves, typical fingerprints of the metallic behaviour are detected for certain samples and an initial estimate of the degree of disorder is implicitly attained. More specific information regarding the microscopic contributions to the transport mechanisms is obtained via low temperature (down to 1.5 K) magnetoconductance measurements on selected samples. The magnetic field dependence of conductivity for fields up to 14 T is measured and the suitability of the localization-interaction model for the understanding of the transport mechanism in PANI is examined.

Infrared reflectivity (20-9000 cm^{-1}) measurements on samples of both PANI systems are performed. The experimental configuration permits the determination of the sample's absolute reflectivity. The optical constants are deduced from Kramers-Kronig analysis of the reflectivity data. Typical features of metallic behaviour are examined and analysed in the context of the localization modified Drude model. The results are shown to be consistent with the transport measurements, indicating that PANI is a disordered metal close to the boundary of a disorder induced metal-insulator transition.

Declaration

All material contained in this thesis is original and is the result of my own work except where explicit reference is made to the work of others.

This thesis has not been submitted in whole or in part for the award of a degree at this or any other university.

The copyright of the thesis rests with the author. No quotation from it should be published without their prior written consent and information derived from it should be acknowledged.

Acknowledgements

TABLE OF CONTENTS

1 Introduction to Conducting Polymers

Before the discovery of metallic poly(sulfur nitride) $(SN)_x$ and the enhancement of conductivity in doped Shirakawa polyacetylene of the order of 10^3 S/cm, the polymeric materials, most commonly known as 'plastics', were considered as insulators. During the past fifteen years, a significant improvement in the methods of processing polyconjugated systems has led to a reduction in the structural and morphological disorder, bringing forth a new generation of conductive polymers with considerably high values of conductivity and excellent environmental stability. In particular, conductivities on the order of 10^4 S/cm were observed at 1987 in iodine-doped Naarman polyacetylene, $(CH)_x$, and further studies [1] have reported conductivity values higher by one order of magnitude, which is comparable to those of traditional metals. Although the majority of conjugated polymers do not show such high conductivity values, their study can provide an understanding of the physical properties for this class of materials. The wide range of conductivity values of the last generation of conducting polymers with respect to those of traditional metals and insulators is shown in Figure 1-1.
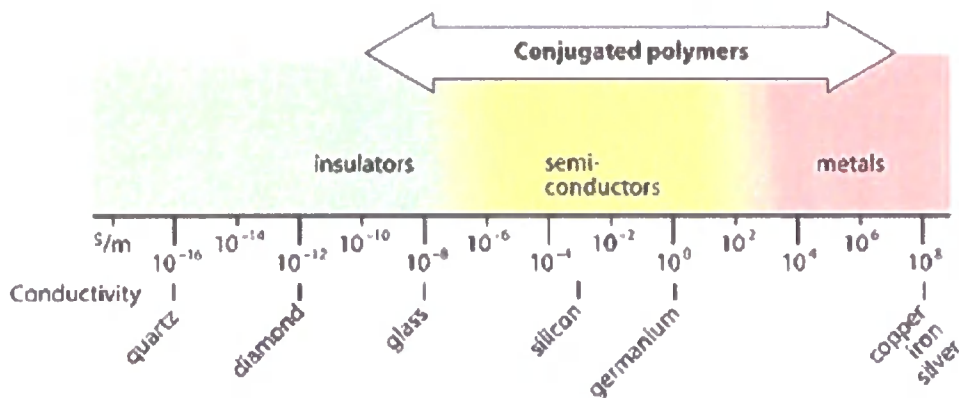
Figure 1-1 A comparison of the conductivities of conducting polymers with those of normal metals and insulators. The graph was taken from The Royal Swedish Academy of Sciences web pages on the occasion of the 2000 Nobel prize award in Chemistry to A. J. Heeger, A. G. MacDiarmid and H. Shirakawa for 'the discovery and development of conducting polymers'.
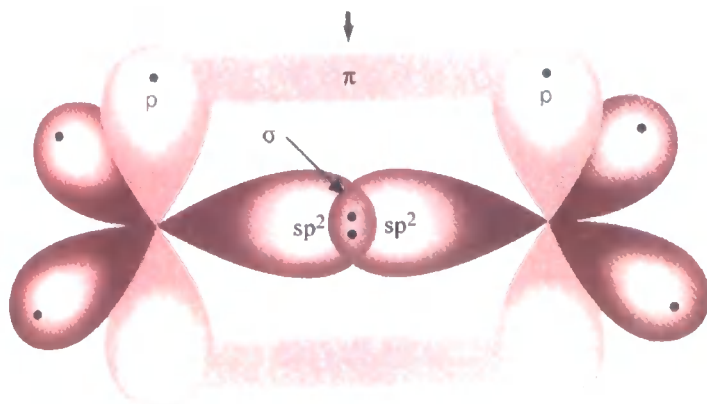
Figure 1-2 The σ and π bonds between two sp^2 hybridized carbon atoms forming an ethylene molecule.

A key feature of conducting polymers is the existence of conjugated double bonds along the polymer backbone. Conjugation is the alternation of double and single bonds among the carbon atoms. This double bond consists of a localized, strong bond, the σ ('sigma') bond, and a weaker, less localized bond, the π ('pi') bond. In π bonding, the carbon orbitals are in the sp^2p_z configuration in which the orbitals of successive carbon atoms along the backbone overlap resulting in the delocalization of the single unpaired electron per carbon atom. Throughout the polymer chain the double bond alternates with the single, σ, bond. Figure 1-2 shows the σ and π bonds of the planar ethylene (C_2H_4) molecule [2].

Conjugation is a necessary, but not sufficient condition for a polymer to become conductive. A common feature of all conductive polymers is the fact that they are insulators in their pure (pristine) form, and only after doping (protonation) do they become conductive. The increase in conductivity induced by doping can be ten orders of magnitude or more, indicating the suitability of conjugated polymers for a systematic study of the metal-insulator transition. The key role held by the doping in the metal-insulator transition has been widely and unequivocally acknowledged in the field [3-5]. Nevertheless, its effect on the nature of the metallic states is still debated as many different models have been proposed.

The doping process in conducting polymers is entirely different from that in semiconductors since the dopants are not substitutional, but interstitial. The dopants are inserted between the chains rather than replacing host atoms, and, dependent on the redox process, can either oxidize to create a positive charge on the chain or reduce and create a negative charge. Alternatively, conjugated polymers can be doped by a non-redox doping process -the protonic acid doping- where there is no change in the number of electrons associated with the polymer backbone, but instead a redistribution of electronic energy levels takes place. The charge carriers generated by doping

are, due to the quasi one-dimensional nature of polymer chains, stored in nonlinear excitation states such as solitons, polarons and bipolarons [6, 7].

When an electron is added to a perfect polymer chain, it causes a chain deformation within fractions of a picosecond. A characteristic pattern of bond deformation is then created which, along with the electron, constitute a polaron. Along with the chain deformation there is a change in the energy level structure. A bipolaron is simply a union of two polarons having the same sign, while a soliton is a collective nonlinear excitation involving both the distortion of the bond alternation and the accompanying electronic states [6, 8, 9]. These quasi-particles are formed initially due to charge transfer from the dopant. Doping polymers with a non-degenerate ground state leads to polarons or bipolarons, whereas in degenerate ground state polymers like trans-polyacetylene, solitons are energetically favoured [7]. The formation energy of a quasi-particle determines whether it can be created or not. One of the significant differences between the soliton and the polaron/bipolaron is that the soliton states are situated at the bandgap, while the polaron/bipolaron states are located symmetric to the band edges [10]. These excitations can travel along a chain as an entity forcing the atoms in its path to change their positions allowing the deformation to travel with the electron or hole. Their role, however, in charge transport and whether they are mobile charge carriers is far from been understood [5, 10] despite certain studies [9, 11-13] indicating that the metallic state in some conducting polymers is a polaron lattice [14]. Such lattices can be formed when the polarons, which are self-localized at low doping concentrations, begin to interact at high doping concentrations sufficiently enough so that a continuum of energy levels is formed because of the overlap of their wavefunctions.

Whether these excitations can behave as free carriers or not is determined by the interchain interaction, the carrier density, the extent of disorder and whether the polymer has a degenerate ground state (e.g. polyacetylene) or a non-degenerate one (polyaniline, polypyrrole etc.). Despite considerable experimental and theoretical work done regarding the nature of those nonlinear excitations, the relation between intrinsic excitations and charge transport is an issue that remains puzzlingly unresolved. The fact that the nature of those primary excitations is determined by a multiplicity of factors such as interchain interaction, Coulomb interaction, screening, electron-phonon interaction, charge delocalization, quantum lattice fluctuations, lattice stiffness, extent of disorder, extent of conjugation length etc., makes theoretical mod-

elling attempts even more confounding, let alone their dependence upon extrinsic factors such as the nature and quality of the samples [10]. Therefore, the nature of the charge carriers is still a widely open issue.

Polymers are intrinsically disordered materials. Although far from being indisputably accepted, the general consensus in the field is that the metal-insulator transition in conducting polymers can be understood within the context of an extended version of the Anderson-Mott localization model, which has successfully explained many properties of disordered systems. A critical parameter in this framework is the correlation/localization length, L_C, that characterises the extent of the electronic wave functions and determines whether the disorder can be considered homogeneous or inhomogeneous. The localization length decreases, as disorder increases, whereas it diverges when the electronic states become delocalized. Considering the fact that polymers exhibit complex morphology by displaying partially amorphous and partially crystalline regions, if L_C is greater than the averaged-over structural coherence length that characterises the size of the crystalline regions, disorder can be considered homogeneous, i.e. the system sees an average of the random fluctuations of the disorder potentials [3-5]. On the contrary, if L_C is less than the structural coherence length, then disorder is considered inhomogeneous and usually this indicates the presence of a strong disorder. In this case, the system is regarded as being similar to a granular metal. The crystalline domains here can be considered as metallic grains of mesoscopic size embedded in amorphous (non-conducting) media [15]. The charge carriers may be able, under certain conditions, to diffuse microscopically between the ordered and the amorphous regions.

Disorder along with interchain interaction and doping level determine the nature of the metal-insulator transition (M-I) in conducting polymers. The relative importance and precise contribution of those factors in the nature of the M-I transition remains controversial. Nevertheless, the metallic behaviour exhibited by some polymers implies that there is a continuous density of states near the Fermi energy, whose extent, characterised by the localization length L_C, decreases as disorder increases.

The metal-insulator transition is one of the most pervading and complex phenomena in solid state physics. It is not an exclusive property of the disordered lattices and the existence of localized states is not a prerequisite. For instance, in a crystalline lattice according to the Bloch-Wilson theory of electrons in crystals, a solid is an insulator if the Fermi energy lies in a filled or an empty band (or in the band gap) and a

metal if the Fermi energy lies within a partly filled band. A metal-insulator transition can occur when, due to a change in the band structure, the Fermi energy moves from the partially filled band to an empty or a filled band, or to the energy gap. All electronic wave functions in both states (metallic and insulating) remain extended and are delocalized throughout the material.

The type of metal-insulator transition that is most relevant to disordered solids is the Anderson transition. In this case the insulating side of the transition corresponds not to extended states, but to localized states. The wave function, whose extent is characterised by the localization length L_C, is limited to a small region in the solid, covering just a few sites. Contrary to the case of doped semiconductors, the localized states in an amorphous solid are intrinsic to the host solid (the perfect crystal without any impurities or defects) and a continuous density of energy states can be defined. As was alluded to above, this is considered to be the case in conjugated polymers. The Anderson metal-insulator transition occurs when the disorder potential exceeds a critical value compared to the bandwidth and induces the Fermi level to fall from the region of the extended states (metallic regime) to the region of localized states (insulating regime) [16]. The energy separating extended from the localized states is called 'the mobility edge', E_C.

Mott extended the Anderson transition for the case of the non-independent electron approximation. It illuminates a regime where the independent picture approximation, innate to both Bloch and Anderson pictures, fails due to electron-electron (e-e) interaction. A transition from an extended state to a localized one occurs when the correlation energy exceeds a critical value compared to the bandwidth. The main concept in the Mott-transition is that the correlation energy can, under certain conditions, cause a solid to have an insulating ground state when the independent electron approximation picture would incorrectly classify it as a metal [16].

Needless to say that in realistic disordered system, let alone conjugating polymers, the M-I transition is neither a pure Anderson nor a pure Mott transition. Such a transition cannot occur by a single mechanism alone, but may arise from a variety of competing or complementary mechanisms involving a close interplay those two main mechanisms: the (e-e) interactions and the weak localization (or disorder). The most recent model trying to combine those two factors and provide a framework for the understanding of their effect on the transport and optical properties is the localization-interaction model [17, 18].

This thesis will deal with the transport (Chapters 2 and 3) and optical properties of polyaniline (Chapter 4), analyzed from the perspective of the localization-interaction model. Polyaniline is one of the most prominent conducting polymers and has been so far the subject of numerous studies. The main reason for the large interest in it is its low cost and relatively easy processibility and its simple protonic acid (non-redox doping) that enables a variety of samples on both sides of the M-I transition to be obtained, making in an excellent system for the study of this transition. Polyaniline's conducting forms are stable, which is prerequisite for this kind of study. Additionally, its potential industrial applications cannot be overlooked [19]. Possible uses include electromagnetic shielding, microwave absorbing or replacing copper in braided parts of a coaxial cable.

A unified understanding of the transport and optical properties of polyaniline within the framework of the localization-interaction model will be attempted in order to examine its consistency, the limits of its validity and any moot points, inadequacies or deficiencies and whether it can provide any substantial information about the nature of the metallic state of polyaniline or, consequently, about the conducting polymers in general. The main theoretical aspects of the model that are related to each experiment will be concisely presented in each chapter. Such a presentation method has the modest objective of underlying the joint importance of theory and experiment for the understanding of any physical phenomena.

2 Conductivity Measurements of Polyaniline Films

2.1 Introduction

The drastic improvement on the quality of conjugating polymers that has been achieved within the last fifteen years has made possible the investigation of materials at every regime (insulating, critical and metallic) of a disorder induced Metal-Insulator (M-I) transition. Samples with varying disorder levels that result in different transport properties can be obtained by the details of the preparation process. The resulting disorder is introduced and controlled by the doping process, making doped conducting polymers exceptionally flexible systems for a comprehensive study of the metal insulator transition.

Temperature dependent conductivity measurements have always been the starting point for a primary classification of a non-crystalline material in terms of the degree of its disorder. Disorder is interlinked with the existence of localized states and their ratio to the extended states, if any, in the system. Since conductivity measurements, being directly related to quantities like the mean free path and the carrier density, are sensitive to the presence of both extended and localized states, they can provide a useful and sensitive probe into the charge transport properties of a disordered material.

A primary classification of the materials in terms of their conductivity values over a wide temperature range is rather straightforward. For instance, a system in the metallic regime has a finite dc conductivity at $T{\rightarrow}0$ K and shows, if it is purely metallic, a positive temperature coefficient of resistivity (TCR)[1] over the entire temperature range. Additional characterization criteria such as the reduced activation energy plots $W(T) = d(\ln\sigma)/d(\ln T)$ for systems with a weak TCR at low temperatures have been well established in the field [5]. However, such methods refer to macroscopically obtained quantities and do not reveal sufficient information about the microscopic mechanisms such as the weak localization, the electron-electron (e-e) interactions and other scattering processes that govern the carrier transport at low temperatures. Nor do they provide any information about the microscopic length scales involved in the conductivity of a disordered system, such as the correlation length on the metallic side, localization length on the insulating side, e-e interaction length, thermal diffusion length and the inelastic scattering length that determine the scattering and relaxation mechanisms in the charge transport [10]. A connection between microscopic and

---

[1] Although in the whole chapter we will be dealing exclusively with conductivity plots and values, the term 'temperature coefficient of resistivity' will be retained in compliance with the current literature.

macroscopic quantities can be established, as usual, by the application of an appropriate model. Many different models purporting to an understanding of the transport properties of conjugated polymers have been proposed, however, none so far has been able to explain all the observed features in a consistent manner [3]. The importance of conductivity measurements as a first step for a mainly qualitative grasp of the charge transport processes occurring in such materials remains, however, undisputed.

In this chapter, the preparation procedure and the results of temperature dependent conductivity measurements on polyaniline films doped with two different acids at various doping levels will be presented. They will be preceded by a concise overview of the phenomenological parameters that enable a qualitative characterisation of the materials in terms of their transport behaviour, followed by a discussion on some of the most widely used models. The emphasis given on the sample preparation is not incidental; the final structural order and therefore the electronic properties of conductive polymers are sensitive to the preparation method.

2.2 Theoretical Background

2.2.1 Transport in crystalline systems

All the important information about the charge transport in crystals is included in the distribution function $f(\vec{r},\vec{k},t)$ which describes the occupancy of the allowed energy states involved in the transport processes. The total time rate of change of the distribution function is given by the *Boltzmann* equation, which in its most general form is [20]

$$\frac{df(\vec{r},\vec{k},t)}{dt} = \frac{\partial f}{\partial t}\bigg|_{\substack{external \\ field}} + \frac{\partial f}{\partial t}\bigg|_{diffusion} + \frac{\partial f}{\partial t}\bigg|_{scattering} + \frac{\partial f}{\partial t}$$

From Liouville's theorem $df / dt = 0$ and consequently

$$-\frac{\partial f}{\partial t} = \vec{v}\cdot\nabla_{\vec{r}}f + \frac{1}{\hbar}\vec{F}\cdot\nabla_{\vec{k}}f + \frac{\partial f}{\partial t}\bigg|_{scattering} \qquad (2.1)$$

where $\vec{F} = \hbar\dot{\vec{k}}$ is the external force acting on the electron and $\vec{v} = \frac{1}{\hbar}\nabla_{\vec{k}}E(\vec{k})$ its velocity. For a time-independent field, the only situation under consideration is the *steady-state* where $\partial f / \partial t = 0$ and (2.1) becomes

$$\frac{\partial f}{\partial t}\bigg|_{scattering} = \vec{v} \cdot \nabla_{\vec{r}} f + \frac{1}{\hbar} \vec{F} \cdot \nabla_{\vec{k}} f \qquad (2.2)$$

The nature of each scattering process determines the first term of (2.2). The distribution function can be written in the general form

$$f(\vec{r},\vec{k}) = f_0(\vec{r},\vec{k}) + f'(\vec{r},\vec{k}) \qquad (2.3)$$

and it is convenient to write

$$f'(\vec{r},\vec{k}) = -\varphi(\vec{r},\vec{k})\frac{\partial f_0}{\partial E} \qquad (2.4)$$

Expression (2.4) is valid when the applied field is weak enough so that the deviation of the steady-state distribution from the equilibrium distribution $f_0(\vec{r},\vec{k})$ is rather small [21]. This is, for example, the case of Ohm's law where the linear relationship between current and electric field shows that in the solution of Boltzmann's equation, only terms linear in f' need be retained. Deviations from Ohm's law can be observed solely in semiconductors subjected to strong electric fields. The function $\varphi(\vec{r},\vec{k})$ is the solution of the Boltzmann equation.

The scattering term can generally be expressed by resorting to complicated statistical methods. In many cases, however, a very convenient approximation called *the relaxation time approximation* is used where the scattering effects can be defined in terms of a relaxation time τ, defined as

$$\tau(\vec{k}) \equiv \varphi(\vec{k})\frac{(\partial f_0 / \partial E)}{(\partial f / \partial E)_{scattering}} \qquad (2.5)$$

or alternatively

$$\frac{\partial f}{\partial t}\bigg|_{scattering} = -\frac{f(\vec{r},\vec{k}) - f_0(\vec{r},\vec{k})}{\tau} = -\frac{f'(\vec{r},\vec{k})}{\tau} \qquad (2.6)$$

The main assumptions underlying the relaxation time approximations are the existence of *elastic scattering*, the assumption that τ is independent of the strength and type of perturbation causing f to depart from f_0 and that the energy surfaces are spherical [22].

Within the relaxation time approximation, the solution of the Boltzmann equation under the presence of an electric field only can easily be found to be given by

$$\varphi(\vec{r},\vec{k}) = \tau e \vec{E} \cdot \vec{v} \qquad (2.7)$$

and consequently the distribution function is

$$f(\vec{r},\vec{k}) = f_0(\vec{r},\vec{k}) - \tau e \vec{E} \cdot \vec{v} \frac{\partial f_0}{\partial E} \qquad (2.8)$$

The knowledge of $f(\vec{r},\vec{k})$ can provide all the transport coefficients of the material. For instance by taking $\vec{E} = E_x \hat{u}_x$, the current density generally defined as

$$\vec{j}(\vec{r}) = -e \int f(\vec{r},\vec{v}) \vec{v} d^3\vec{v} = -\frac{e}{4\pi^3} \int f(\vec{r},\vec{k}) \vec{v} d^3\vec{k} \qquad (2.9)$$

is now finally found to be given by the expression

$$j_x = \frac{ne^2 E_x}{m^*} < \tau(E) > \qquad (2.10)$$

where n and m^* are the electron density and the effective mass respectively, while $<\tau(E)>$ is the average value of the relaxation time over the distribution of electron energies E, whose definition is derived analytically after expanding (2.9). The electrical conductivity σ_B, also known as the Boltzmann conductivity, is consequently given by definition from the expression

$$\sigma_B = \frac{ne^2}{m^*} < \tau(E) > \qquad (2.11)$$

or alternatively in terms of the mobility $\mu_e = \frac{e}{m_e^*} < \tau(E) >$,

$$\sigma_B = ne\mu_e \qquad (2.12)$$

It should be once again emphasised that all of the above derivations are valid only for spherical equal energy surfaces. Within this framework, the underlying physics of the (elastic) scattering processes is included in the average value of the relaxation time $<\tau(E)>$.

In metals, the relaxation time approximation is valid for temperatures greater than the Debye temperature, θ_D, where the scattering of the free electrons at the Fermi surface by the acoustic phonons is large angle scattering and therefore elastic. Assuming that only electrons at the Fermi surface contribute to the conductivity, (2.11) becomes [20]

$$\sigma_B = \frac{ne^2}{m^*} \tau(E_F) \qquad (2.13)$$

Typical values of σ_B for metals are of the order 10^6 S/cm, while in semiconductors cover a range of 15 to 20 orders of magnitude below this value.

Without entering into details involving the relation, for the elastic scattering case, between the relaxation time and the average lattice energy, the various contributions to the resistivity of a metal and for each temperature range, can be summarised as follows [23, 24]

$$\rho(T) = \rho(0) + CT^p \qquad (2.14)$$

where $\rho(0)$ is the residual resistivity due to impurity and defect scattering, $C>0$ as it is always experimentally observed and the exponent p depends on the details of the scattering mechanism according to the temperature ranges and each mechanism in the following way

a) $T \geq \theta_D$, elastic thermal scattering by phonons, $p=1$

b) $T < \theta_D$, inelastic scattering by phonons (small angle), $p=2 \sim 5$

c) electron-electron scattering, $p=2$

d) impurity and defect scattering, $p=0$

2.2.2 Transport in non-crystalline systems

As it has been discussed in the introduction, randomised disorder, due to the Anderson localization, causes the energy states to become localized. Although localized states per se are not unique to non-crystalline systems since they occur in any crystal with imperfections, their extent and its effect on the transport properties is determined by the magnitude of the disorder, which is considerable only in non-crystalline materials. When in the cases of strong disorder the whole energy band is localized, the system is an insulator. If, on the other hand, the disorder is below a critical value, the localized states[2] coexist in the band with the extended states and they are separated by the mobility edge, E_C, below which all the states are localized [25]. Such a generalized picture is shown in Figure 2-1.

---

[2] It should be reminded that a continuous density of states for the localized states can be defined in a similar manner to the extended states.
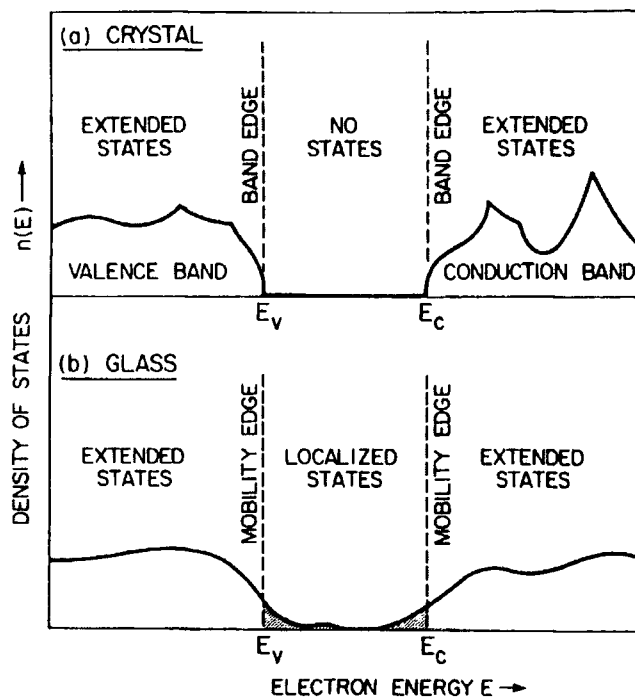
Figure 2-1 A schematic density of states diagram for a crystalline (top) and a non-crystalline semiconductor (bottom). The states at the band edges are the most susceptible to localization. The figure was taken from the book by Zallen [16], page 235.

A simple but very useful criterion for the existence of localized states was introduced in 1960 by Ioffe-Regel [26] and has been widely used thenceforth. It is based on the simple suggestion that since the mean free path, λ, is the distance over which the electron wave function loses phase coherence and the wavelength is the distance over which the phase changes by 2π, it does not make sense to have a wavelength which is substantially more than the mean free path. The Ioffe-Regel criterion, therefore, is $k_F\lambda > 1$. When this criterion is violated the states are localized, however this is not a sufficient condition for the existence of extended states[3]. Based on this criterion Mott proposed in 1973 [27] that the M-I transition which occurs as $E_F{\to}E_C$ (from the metallic side) is discontinuous and introduced the concept of a minimum metallic conductivity σ_{min}. The existence of σ_{min} was disputed throughout the scaling model of localization which demonstrated that the M-I transition is continuous in 3 dimensions. However, the concept of σ_{min} still survives as a qualitative measure of the importance

---

[3] This is due to the fact that although this criterion is satisfied in one dimension for weak disorder, the states are localized.

of localization phenomena: systems with $\sigma \sim \sigma_{min}$ should be considered as being near to the M-I transition.

The Ioffe-Regel criterion is the order parameter for the disorder induced M-I transition. Thus for $k_F \lambda \sim 1$, $\sigma \sim \sigma_{min}$ and the material is near the M-I transition while for $k_F \lambda \ll 1$ the material is in the insulating (Fermi glass regime). In the metallic regime, as mentioned above, $k_F \lambda > 1$ and $\sigma > \sigma_{min}$. Usually $\sigma_{min} \sim 100$ S/cm [28, 29], dependent upon the system under investigation.

The transport properties for a system in the weak disorder limit are apparently contingent on the relative position of the Fermi level E_F in respect to the mobility edge E_C. In general, there are different conduction mechanisms involved for extended and localized states [30]. The contribution of the extended states to the conductivity is always dominant when the states are occupied by a sufficient number of charge carriers; this is the case when E_F lies above the mobility edge (e.g. amorphous metals or alloys) or, as in the case of amorphous semiconductors, within a few $k_B T$ of this limit and the conductivity is then thermally activated with an activation energy corresponding to the distance between E_C and E_F, viz. $\sigma \propto \exp[-(E_C - E_F)/k_B T]$.[4] The conduction in the localized states is done by *phonon assisted hopping*. Each transport regime will be separately examined.

METALLIC REGIME

If E_F is in the region of the extended states, the system is then on the *metallic* regime of charge transport. In order to obtain an expression for the electrical conductivity similar to (2.13), the multiple scattering of the electrons by the disorder potential must be taken into account. The Boltzmann formulation ceases to be valid when the mean free path becomes comparable to the lattice constant. This is the case for narrow bands, for lattice inhomogeneities and for strong electron-phonon coupling. The alternative method for dealing with the transport phenomena in those cases has led to the Kubo-Greenwood formula [30]. Extended calculations applying multiple scattering theory and the Kubo-Greenwood formula [31, 32] have resulted in the following expression for σ

---

[4] The pre-exponential proportionality factor is close to the value of σ_{min}.

$$\sigma = \sigma_B \left[1 - \frac{1}{(k_F \lambda)^2} \right]$$ (2.15)

where σ_B is the conductivity of a normal metal as given by (2.13). In the bottom limit of the Ioffe-Regel rule, $k_F \lambda \sim 1$, and the electrical conductivity becomes zero, showing that the E_F is at the mobility edge. This indicates that a transition from metallic to insulating behaviour has occurred. Such a M-I transition is called the *Anderson transition*. For a typical metal like copper $k_F\lambda=500$ and (2.15) gives $\sigma \approx \sigma_B$, showing that deviations from the Boltzmann conductivity occur for small values of $k_F\lambda$, i.e. in the mobility edge region. It is therefore apparent that $k_F\lambda$ can be used as an order parameter of the system and its knowledge permits us, as we will see in chapter 4, to classify the samples in terms of their disorder degree.

According to Mott [33, 34], equation (2.15) should be generalised to the form

$$\sigma = \sigma_B \left[1 - \frac{C}{(k_F \lambda)^2} \left(1 - \frac{\lambda}{L} \right) \right]$$ (2.16)

where L is either the size of the sample or the inelastic diffusion length L_i, which represents the distance an electron will diffuse before an inelastic collision. The inelastic diffusion length is defined by the equation $L_i \equiv (D\tau_i)^{1/2}$, where τ_i is the inelastic scattering time and D is the diffusion coefficient. The surprising point according to equation (2.16) is that inelastic scattering, such as scattering by phonons, can increase the conductivity. This is attributed to the fact that constructive interference between the scattering waves, which reduces the conductivity, is reduced if the volume available (L^3 or L_i^3) is small [28, 35, 36].

INSULATING REGIME

When the disorder exceeds the critical limit, the Fermi level falls below the mobility edge and the system behaves like an insulator. Since the states at the Fermi level are now localized, the conductivity at zero temperature vanishes. This does not necessarily mean that there is an energy gap with E_F in the mid-gap so that the density of

states $N(E_F)$=0 [27].[5] An insulating material with a finite density of localized states at the Fermi energy can exist and it is called 'Fermi glass'.

There are two main kinds of conduction mechanisms in an insulator [28].

1. By excitation to the mobility edge. Electrons get thermally excited to the mobility edge where the conduction takes place in the extended states and is given by the formula

$$\sigma = \sigma_0 \exp[-(E_c - E_F)/k_B T] \qquad (2.17)$$

where the pre-exponential factor σ_0 is identical to the conductivity when E_F lies at the mobility edge and its value, as given by Mott [31, 34, 37, 38], is

$$\sigma_0 = 0.03 e^2 / \hbar a \qquad (2.18)$$

where a is the interatomic distance. This value of σ_0 is the minimum metallic conductivity, σ_{min}, mentioned above. In the vicinity of σ_{min}, apparently $k_F \lambda \approx 1$. Mott initially argued that the conductivity at absolute zero would reach this value as the disorder increased so that $E_F \rightarrow E_C$ and then fall continuously to zero. This was disproved by the scaling theory of localization, as put forward by Abrahams et al. [39], which demonstrated that the M-I transition is continuous (second order phase transition) in 3D, so that σ_{min} does not have any clear significance for solids and σ_0 just represents a pre-exponential factor related to the activation energy [29]. However, a recent study [40] has provided evidence for the existence of Mott's minimum metallic conductivity by studying the M-I transition in amorphous $Si_{1-x}Ni_x$ films, contributing to the pervasive confusion on this issue.

2. By thermally activated hopping. In this process an electron in an occupied localized state hops to a higher energetically state after receiving energy from a phonon. When the electrons hop among neighbour states, it is call *nearest-neighbour hopping* or fixed range hopping. The temperature dependence of σ_h is given by [28]

$$\sigma_h = \sigma_{h0} \exp[-\bar{W}/k_B T] \qquad (2.19)$$

---

[5] It should be mentioned that according to the Bloch picture for a crystalline solid, an insulator is defined as the material for which an energy gap occurs between a completely filled lower band, the valence band, and a higher, empty, band, the conduction band, with the lower band being lower in energy than the conduction band for all $\bar{k}$ values. In this picture, the electronic wavefunctions of an insulator are still delocalized throughout the crystal, but no conduction is possible due to the unavailability of energy states above the filled band.

where σ_{h0} is a constant $\bar{W}$ is the mean hopping energy. At low temperatures, Mott first pointed out that the most probable hopping process among the localized states near the Fermi energy would not be to a nearest neighbour, but hops of different distances will follow one another. This process is called *variable range hopping* and it can be represented by the general equation

$$\sigma = A\exp[-B/T^x] \qquad (2.20)$$

where A, B are taken to be constants (A has, however, a weak temperature dependence) with somehow different values ascribed to them by some groups due to diverse calculations, while the constant γ is related to the dimensionality d of the system through the expression $x=1/(1+d)$ [10]. For three dimensional hopping of non-interacting carriers $x=1/4$ (Mott's law), while in the Efros-Shklovskii limit (ES) [41], where the interactions between localized electrons play an important role in the hopping transport, $x=1/2$. At high temperatures the variable range hopping is replaced by the fixed range hopping which competes with the activated conductivity in the extended states, as described by equation (2.17).

CRITICAL REGIME

The critical regime of conducting polymers, unlike the well established studies of the metallic and insulating regimes, has only relatively recently been studied in detail [3, 42]. For a three dimensional system on the metallic regime, but very close to the boundary of an M-I transition, the conductivity is not activated, but rather follows a power law dependence on the temperature, as shown by Larkin and Khmelnitskii [43]

$$\sigma(T) \propto T^\beta \qquad (2.21)$$

where the predicted range of validity for β is $0.3 < \beta < 1$.

2.2.3 Identification of transport regimes via conductivity measurements.

The only unambiguous discrimination between metallic and insulating regimes is based on the zero temperature limit [44]. The fundamental property of the metallic behaviour is the existence of a finite conductivity value at $T \to 0$ K. This implies the presence of delocalized states at the Fermi level. On the contrary, if $\sigma \to 0$ as $T \to 0$ K,

the sample is an insulator. This simple definition unfortunately cannot be used directly since measurements at absolute zero are untenable making one strongly dependent upon the sometimes intractable zero temperature extrapolation techniques. Therefore one should resort to other phenomenological criteria related to the electrical conductivity in order to characterise the system in terms of its transport behaviour.

According to (2.14), the metallic resistivity shows a positive temperature coefficient throughout the whole temperature range. Such consistency is certainly difficult to be observed in a disordered metal, although a positive TCR over a specific temperature range can be construed as an indication of a transport mechanism similar to that of a clean metal. The detailed study of disordered metallic systems has, however, shown that even systems with a weakly negative TCR can be metallic [10]. In this case, Zabrodskii and Zeninova [45] from their study of $\sigma(T)$ in disordered semiconductors have shown that the temperature dependence of $\sigma(T)$ is better understood by using the reduced activation energy W, defined as

$$W(T) = \frac{d(\ln \sigma)}{d(\ln T)} = \frac{T}{\sigma}\frac{d\sigma}{dT}$$ (2.22)

For a metallic sample, according to (2.22), $W(T)$ vanishes as $T{\rightarrow}0$. The activation energy W, being far more sensitive than the conductivity itself [46], can be used to analyze the temperature dependence of conductivity for samples showing a weak negative TCR and identifying the characteristic transport regimes in the following way [10]:

1. If $W(T)$ has a positive temperature coefficient at low temperatures, then the system is on the metallic side of a M-I transition, ensuring that there is a finite conductivity at $T{\rightarrow}0$.

2. If $W(T)$ is temperature independent for a wide range of temperature, then the system is on the critical regime of an M-I transition.

3. If $W(T)$ has a negative temperature coefficient at low temperatures, the system is on the insulating side of the M-I transition.

It must not be overlooked that a sample with a positive TCR, like a clean metal, has a negative value of W. The above criterion does not, therefore, apply for this category of samples, but only to samples with a weakly negative value of the TCR at low temperatures. The precise extent of this 'low temperature' range is usually determined in practise, as the measurement section will reveal. It is understandable, nevertheless,

that the lower the temperature range, the more accurate results an application of this criterion will give.

The activation energy criterion is frequently [3, 4] used in conjunction with another, albeit less robust and reliable, empirical parameter, the resistivity ratio, which is defined as $p_r = \rho(T_1) / \rho(T_2)$, where $T_1 < T_2$ with T_1 referring to the lowest accessible temperature and T_2 usually referring to the room temperature. By its definition, it is apparent that the lower the values of p_r, the more metallic-like the system's behaviour. The value range of p_r that corresponds to each transport regime is usually determined case by case and it, undoubtedly, does not provide a rigorous classification parameter of the system's transport behaviour. It can provide, even in this offhand manner, however, an immediate estimate of the transport regime, especially considering the fact that as p_r increases, the temperature dependence of W gradually moves from a positive (metallic) to a negative (insulating) temperature coefficient at low temperatures [5].

2.3 Sample Preparation

2.3.1 Polyaniline

Polyaniline is a prominent member of the family of intrinsically conducting polymers, or most commonly known as 'synthetic metals', which refers to the kinds of polymers whose electrical conductivity is no longer due to additives but to their chemical and crystalline structure or morphology [47]. Its base form has the generalised composition [48-50]

which consists of alternating reduced and oxidized
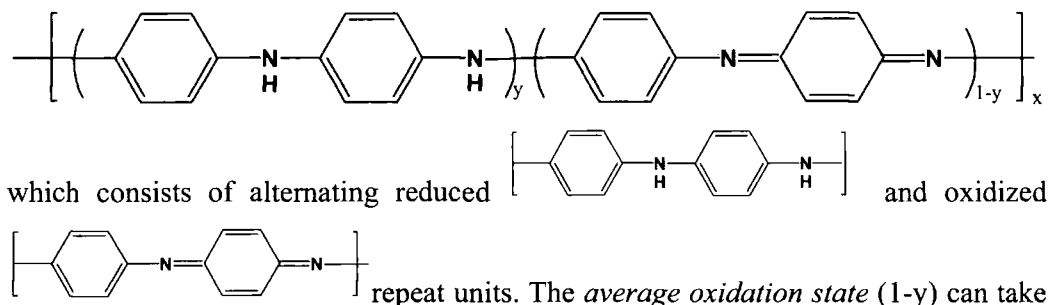
 repeat units. The *average oxidation state* (1-y) can take three distinct values 0, 0.5 and 1, leading respectively to leucoemeraldine (fully reduced), emeraldine (half-oxidized) and pernigraniline (fully oxidized) base forms shown in Figure 2-2.

Emeraldine Base

Pernigraniline Base

Leucoemeraldine Base
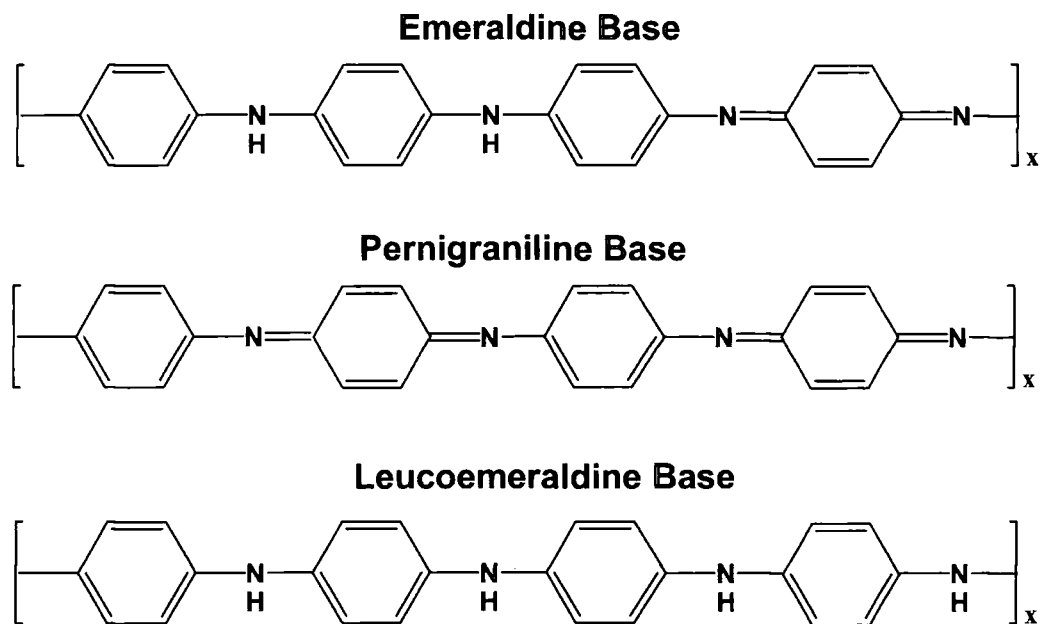
Figure 2-2 Schematic form of the three different base forms, one for each oxidation state, of polyaniline.

Polyaniline, like all conjugated polymers, is an electrical insulator in its base form. It can only become conducting through the process of doping. In principle there are various types of doping, we will refer, however, to the two main mechanisms that are particularly related with polyaniline. The *redox doping* that involves the partial addition (reduction) or removal (oxidation) of electrons to or from the π-system of the polymer backbone and the *protonic acid doping* during which the number of electrons associated with the polymer backbone does not change [50]. Both types of doping result in the formation of a polymeric salt. The resulting salt, as shown in Figure 2-3, has quasi-quinoid structure with two delocalized charge carriers per base unit that leads to conjugation and finally to conductivity. The main idea used to describe protonation is that it removes one of the imine nitrogens lone pair electrons to form the N-H bond, while the remained, unpaired, electron gets delocalized in the backbone, giving rise to conductivity. In this picture, the carriers responsible for the conductivity are the electrons. Protonation can also cause the imine rings to change their geometry which alters bond lengths and, additionally, causes them to rotate to a more planar configuration, increasing the wave function overlap to yield a highly conductive state [51].

The protonic acid doping makes polyaniline unique among the conducting polymers since the transition from an insulator to a conductor is done without the addition

or the removal of charge carriers, but only with a rearrangement of the electronic energy levels after protonation. Through protonic acid doping, the conductivity of polyaniline can change by 9~10 orders of magnitude, making polyaniline ideal for the study of the insulator-metal transition. Variations of the doping level can induce considerable differences in the transport properties of the deduced PANI salts, providing us with a variety of systems on both sides of a M-I transition for investigation.

2.3.2 Solution processing of PANI salts

Like most intrinsically conducting polymers, polyaniline salts are formed from various solution casting techniques. The choice of the solvent depends on the protonic acid used and factors such as the solution concentration, the doping level, the base chosen etc. A judicious choice of all these factors can enhance the electrical and mechanical properties of the final material and considerable research is ongoing in the field [52]. The emeraldine base (half-oxidized) form of PANI was found to give conducting salts, unlike the fully oxidized form (pernigraniline base) which contrary to other polyconjugated systems is not conducting upon protonation. The preparation technique is described hereafter.

The emeraldine base form of PANI with high molecular weight (M_w ~2×10^5g mol^{-1}, synthesized in Durham at 248K [53, 54], was used as our starting material. Two categories of PANI free standing films were obtained in the following way: EB and the doping acid (either CSA or AMPSA) were mixed in an agate mortar and pestle at various molar ratios and added to the appropriate solvent (m-cresol for PANI-CSA and dichloroacetic acid for PANI-AMPSA sample) to obtain a 2% w/w solution concentration. The solution was homogenized until complete dissolution, poured onto silicon wafers and left to dry in an oven at 353 K for 24 h . The free standing films (emeraldine salts) were pealed from the silicon wafers and labelled according to the molar ratio of the dopant to the EB. For instance, a 50% doping level means that all the imine nitrogens in a four ring EB repeat unit (half oxidized form) are protonated. The thicknesses of the films ranged from 30-100 µm and they were considered isotropic since this method of preparation does not favour any particular anisotropy. The structures for the EB form of PANI along with CSA and AMPSA are shown in Figure 2-3.

Factors such as the solution concentration [55], the solvent evaporation rate, the evaporation temperature and duration and other random elements incurred through the

preparation procedure, have an effect on the degree of the disorder present on the sample [56-58], however, a variety of measurements performed on samples with the same characteristics has demonstrated a considerable repeatability that makes it feasible to discuss of certain distinctive physical tendencies in the samples. In order to minimise the effect of any residual solvent left in the conductivity of the sample [58], the films were left under high vacuum (~10^{-5} mbar) for over 2 days so that any further evaporation of the residual solvent would be entirely minimal. Similar arguments can be made regarding the ageing effect on conductivity [59, 60], which in our case was hardly noticeable (~2%). In any case however, the usual sample ageing concerns only the absolute value of the conductivity and we are mostly interested not in the value itself, but on its temperature dependence which is not affected by it.
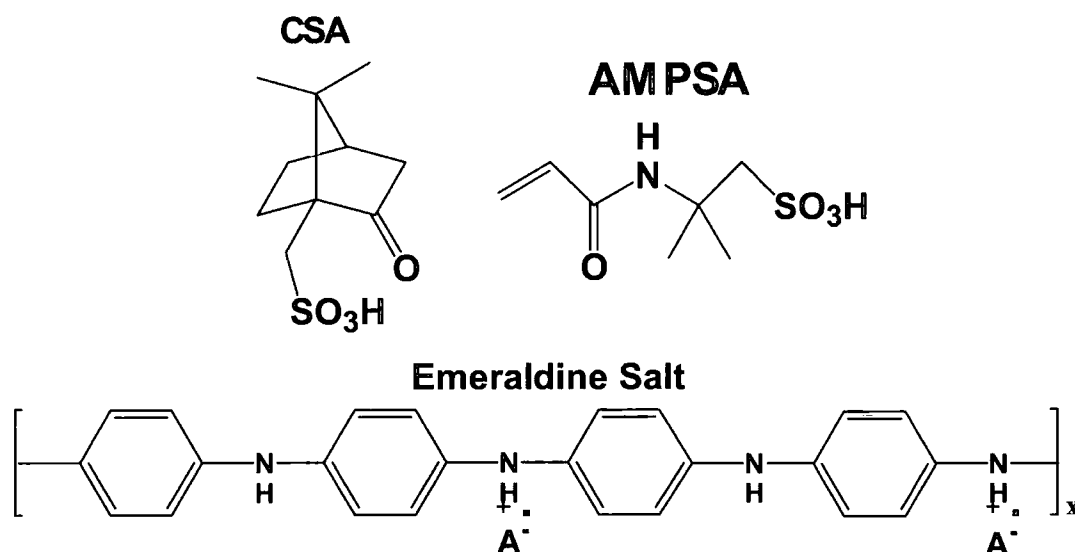
Figure 2-3 Structures for the emeraldine salt (ES) as formed after doping emeraldine base with either 2-acrylamido-2-methyl-1-propanesuplhonic (AMPSA) or 10-camphorsuplhonic acid (CSA). The two protonated nitrogen atoms become electron deficient with one of their electrons being delocalized across the polymer backbone.

2.4 Experimental setup

Temperature dependent conductivity measurements were performed inside a closed-loop helium cryostat under dynamic vacuum (~10^{-4} mbar). The temperature range was 10-295 K. Four gold strips were evaporated on the sample surface to provide the best possible contacts between the four in-line electrodes formed on a printed circuit board, and the sample. The four in line technique mainly consists of applying a constant current, I, through the two outer electrodes and measuring the potential drop, V, between the inner electrodes.

Figure 2-4 Two different printed circuit boards used for conductivity measurements.

Then, by definition, the conductivity is given by the Ohm's law $\sigma = lI/(Vdw)$, where l,d,w are respectively the length, the thickness and the width of the sample between the two inner electrodes. Two different printed circuit boards were designed for this type of measurement. One with point contacts between electrodes and the sample (Figure 2-4, left) and one with line contacts (Figure 2-4, right). Both configuration gave, expectedly, similar values of conductivity, however the point contacts board gave slightly better signal/noise ratio. The sample was afterwards securely mounted on the cryostat's cold finger in a way that the pressure exerted on the sample surface was constant and homogeneous. The whole configuration aims to minimize the contact resistance between the sample and the electrodes so that the conductivity values are as accurate as possible.

Before data acquisition, the linear response of the samples as defined by the current-voltage curves was confirmed so that Ohm's law holds. For each voltage measurement, the applied current was 1mA so that the dissipated power into the sample did not exceed 1 µW. The measurements were made when a constant temperature throughout had been achieved, ensuring that the sample was in thermal equilibrium with its surroundings. At each temperature, 100 voltage measurements were taken and averaged for increased precision. Finally, the conductivity values were obtained using Ohm's law after having accurately measured the dimensions of the sample.

2.5 Results and discussion

Temperature dependent conductivity measurements are widely used as a simple tool for an initial classification of a system in respect to its transport properties [5, 10, 56, 61]. They can provide a qualitative sense of the extent of the disorder present in the sample, since the conductivity is dependent upon the relaxation time, which, since it is controlled by the scattering processes occurring in the material, is sensitive to the presence of any disorder in the system. In order to achieve this, the activation energy $W = d(\ln\sigma)/d(\ln T)$, being far more sensitive than the conductivity itself [46] can be used as analyzed in 2.2.3, when the sample shows a weekly negative TCR, at temperatures usually below 40 K. W has a positive temperature coefficient for a sample in the metallic regime, it is temperature independent for a sample in the critical regime and has a negative temperature coefficient for a sample at the insulating side of the I-M transition. In conjunction with the activation energy, a less robust empirical parameter, the resistivity ratio $\rho_r = \sigma(295K)/\sigma(10K)$ is used for a quick estimate of the sample quality. According to previous studies [62, 63], for PANI samples in the metallic regime $\rho_r<2$, while the corresponding limits for critical and insulating behaviour are $2< \rho_r<5$ and $10<\rho_r$ respectively.

Table 2-1 The room temperature conductivity, the peak conductivity with its respective temperature and the resistivity ratio ρ_r for all the samples examined in Figure 2-5 and Figure 2-6.

Sample	σ_{dc} (295 K)	$T (\sigma_{dc}^{peak})$	σ_{dc}^{peak}	ρ_r
	S/cm	(K)	S/cm	
PANI-AMPSA 30% (A1)	60	230	61	1.140
PANI-AMPSA 40% (A2)	87	125	93	0.969
PANI-AMPSA 50% (A3)	110	80	122	0.920
PANI-AMPSA 60% (A4)	68	150	74	0.963
PANI-CSA 30% (C1)	35	245	35	1.337
PANI-CSA 40% (C2)	73	290	73	1.405
PANI-CSA 50% (C3)	178	160	189	1.034
PANI-CSA 60% (C4)	202	120	216	0.956

In order to investigate the effect of the doping on the transport properties of PANI, conductivity measurements on a series of samples were performed and are

shown in Figure 2-5 and in Figure 2-6 .[6] The samples were labelled accordingly, and the room temperature conductivity, the peak conductivity with its respective temperature and the resistivity ratio are listed in Table 2-1. The values are consistent with previous studies [64, 65]. Despite the fact that measurements at temperatures below 10 K were unattainable inhibiting a more accurate determination of the resistivity ratio, from the low values of ρ_r and the weak temperature dependence of σ demonstrated in the conductivity plots, it can be surmised that all the samples are on the metallic side of the I-M transition. The most metallic samples, (A3) and (C4), have the onset of a positive TCR (i.e. $d\sigma / dT < 0$) at lower temperatures, signifying a decrease in the disorder-induced localization in the system. Samples C2 and C3 seem to have the tendency of a positive TCR at temperatures below 10 K, however, due to the lack of data points in this region and considering the fact that small fluctuations like these observed are within the experimental error, conclusions about the existence of positive TCR at very low temperatures, like the one observed in ion-implanted PANI [66], cannot be made.

It is observed that the highest conductivity values in the case of PANI-CSA samples occur for a 60% doping level. This is contrary to the fact that 50% is theoretically enough to fully protonate the EB, as can be seen in PANI-AMPSA samples. This indicates that doping with CSA is less successful than with AMPSA, requiring a higher CSA/EB molar ratio for complete protonation. This requirement can be attributed to the fact that CSA, as Figure 2-3 shows, is structurally a bigger and more complex molecule than AMPSA, something that adversely affects its doping efficiency. In the case of PANI-AMPSA samples, any doping level greater than 50% seems to inhibit carrier transport, as Figure 2-5 demonstrates.

Further evidence of the sample's metallic behaviour is provided by the activation energy plots W as a function of temperature, as shown in Figure 2-7. The positive slope of W is more pronounced for the PANI-CSA samples, whose conductivity shows slightly stronger temperature dependence than the PANI-AMPSA samples. The W plots indicate that the samples are on the metallic side of an I-M transition; some being closer to the critical regime than others according to their doping level. The most conductive samples, A3 and C4, show a rather more erratic behaviour in their W plots than the rest of the samples. This can be related to the fact the crossover from

---

[6] The glitch observed at approximately 42 K is a consistent and repeatable experimental artefact, constituting a systematic error.

negative TCR to positive TCR occurs at considerably lower temperatures, indicating that the electron-phonon scattering increasingly contributes to the transport properties against the interplay of other factors like disorder, screening and interactions. The extent of the importance of each of those factors and its contribution to the charge transport is impossible to be assessed from the conductivity data by itself and therefore other measurements, such as magnetoconductance, are necessary for clarifying the situation any further. Magnetoconductance measurements will follow in the next chapter.

It should be mentioned, however, that the activation energy plots are more accurate and reliable at lower temperatures than the ones employed here. This will be made clear in the next chapter, where temperatures as low as 1.5 K were reached for the conductivity measurements. Similar arguments apply to the resistivity ratio and to its value range.
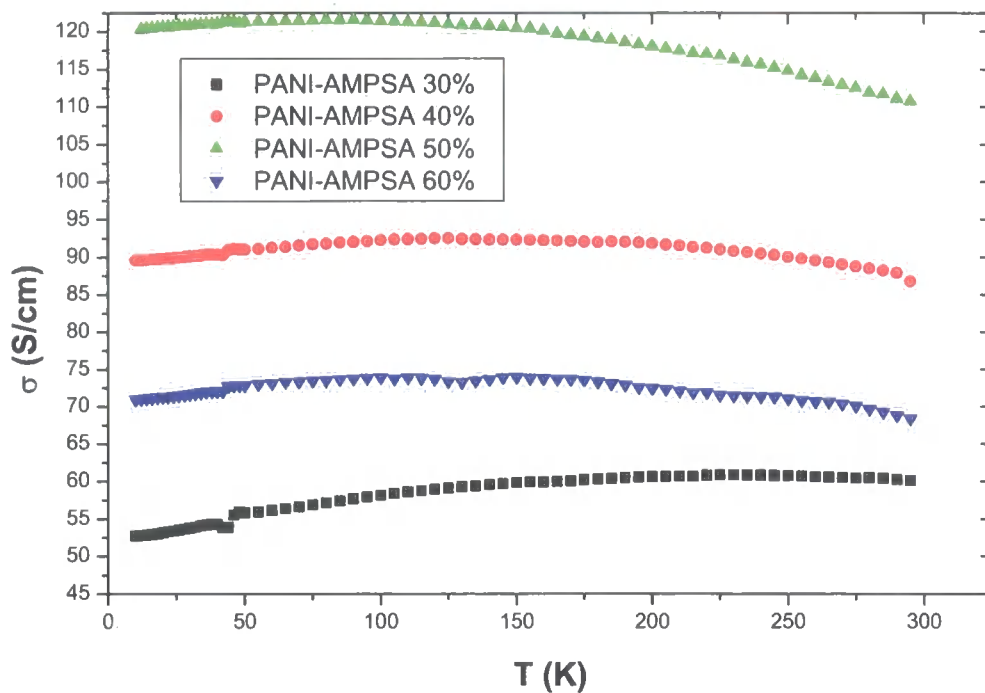
Figure 2-5 Temperature dependent dc conductivity for PANI-AMPSA samples.
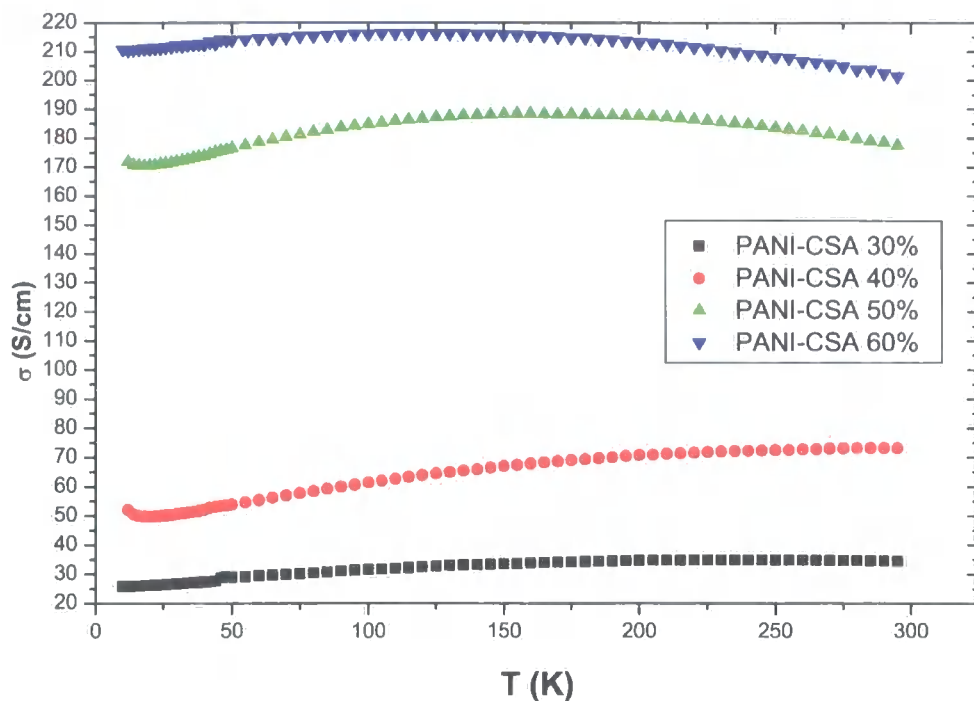
Figure 2-6 Temperature dependent dc conductivity for PANI-CSA samples.
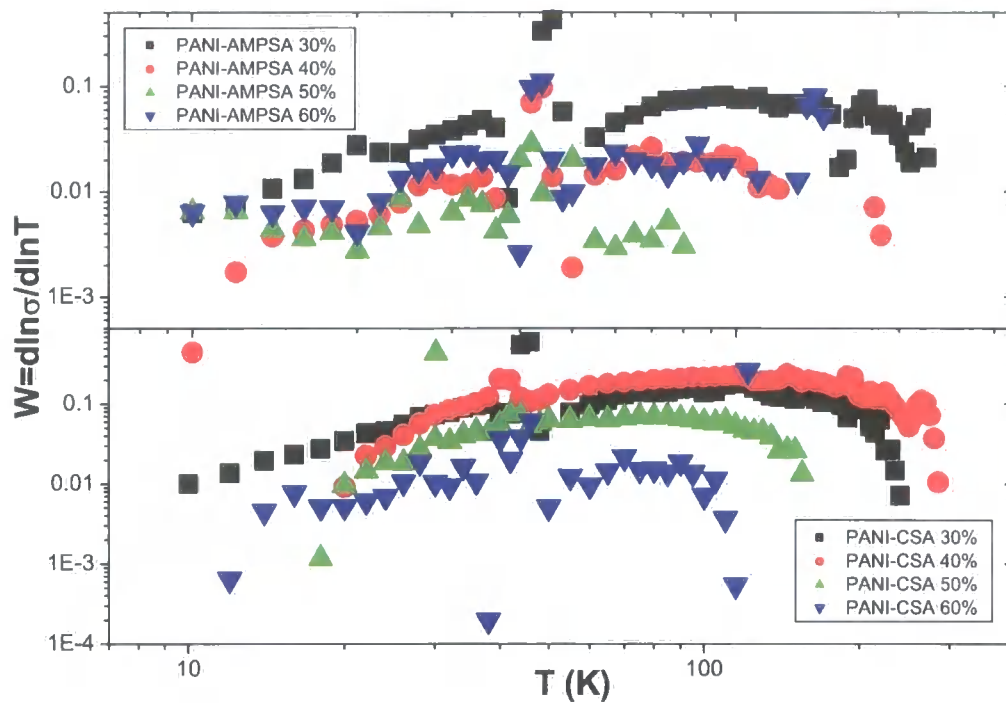
Figure 2-7 Log-log plots of the activation energy W against temperature for PANI-AMPSA (top) and PANI-CSA (bottom). Both sets of curves show a prevailing positive slopes, even though the PANI-AMPSA curves are considerably more erratic.

2.6 Summary

The basic theoretical framework for the understanding of the transport properties of conjugated polymers has been concisely presented. The key concept is the disorder induced metal-insulator transition which is examined in the context of an Anderson-Mott transition. Conducting polyaniline samples were prepared after protonation of the emeraldine base. Temperature dependent conductivity measurements on two different PANI systems and at various degrees of doping were performed. The intrinsically metallic characteristics of PANI were confirmed after applying the phenomenological criteria, related to conductivity measurements, used for identifying samples at either regime in the boundary of a metal-insulator transition.

3 Magnetoconductance studies of Polyaniline Films.

3.1 Introduction

The measurements of various physical quantities under the presence of a static and homogeneous magnetic field have always been of significant interest. The magnetic field profoundly affects the transport properties and through the observation of the phenomena it induces, important information and a greater insight can be obtained about the electronic structure of solids. The presence of a magnetic field, due to the variety of effects it generates, is a very large topic to be studied extensively. This chapter, therefore, will be solely focused on its effect on the transport properties of selected PANI films, which were investigated in the preceding chapter, complementing and extending, in part, the relevant conclusions.

The chapter is rather conventionally structured: after providing a concise overview of the theoretical concepts concerned with the transport phenomena under a magnetic field in a crystalline and a disordered material, the results of magnetoconductance measurements under a magnetic field will be presented and analysed. Such a course purports to shed some light into the complex scattering processes that occur in a disordered metallic system such as PANI and to attest the suitability of the localization-interaction model [17] for a quantitative understanding of transport processes occurring in conducting polymers.

3.2 Theoretical Background

The systematic study of magnetic field effect on a solid's transport properties dates back to 1879, when E. H. Hall was conducting measurements of the magnetic force exerted on a current carrying wire [67]. He expected the current to be drawn to one side of the wire and, consequently, an increase in the experienced resistance, without, however, managing to determine this extra resistance. His own statements reveal that he did not regard this result as final: 'The magnet may *tend* to deflect the current without being able to do so. It is evident that in this case there would exist a state of stress in the conductor, the electricity pressing, as it were, toward one side of the wire.' The 'state of stress' is known today as Hall voltage and its understanding comes readily from the magneto-transport theory that follows.

3.2.1 Elementary theory of conduction under a magnetic field.

A principal distinction for the study of the magnetic field effects is that of the *weak* and *strong field* limits [20]. Such a classification is defined in terms of a basic parameter called the *cyclotron frequency* ω_c, which is the angular frequency of the circular orbit perpendicular to the magnetic field $\vec{H}$ and is obtained by equating the centrifugal and the magnetic force exerted on the electron. It is, thus, given by the expression

$$\omega_c = \frac{eH}{m^* c} \qquad (3.1)$$

The *weak* field limit corresponds to the situation where the electrons mean free path is smaller than the circumference of its cyclotron orbit, viz. $\omega_c \tau \ll 1$, where τ is the relaxation time of the dominant scattering mechanism. In this case, the electron will be scattered while making only a small fraction of an orbit (a small arc) before it suffers a collision and starts a new orbit. The magnetic field can be treated as a small perturbation giving rise to the Lorentz force and the relaxation time solution to the Boltzmann equation, developed in the previous chapter, may be appropriate [20, 21]. This will be the approximation used in the forthcoming theoretical treatment.

In the *high* field limit $\omega_c \tau \gg 1$. The electron has enough time to complete many circular orbits before being scattered or, alternatively, its mean free path is longer than the circumference of its orbit. In this case the magnetic field cannot be treated as a small perturbation and quantum effects due to magnetic field occur prompting the use of a quantum-mechanical approach that takes full account of the magnetic field by abolishing the semi-classical notions about carrier motion in a well defined orbit for quantized motion.

Using the free electron mass, it is obtained from (3.1) that $\omega_c = 1.759 \times 10^7$ sec^{-1}/Oe. Hence, for the weak field limit $H \ll 5.685 \times 10^{-8}/\tau$ Oe, and for $\tau \sim 10^{-14}$ sec, as in typical metals, $H \ll 5.685 \times 10^6$ Oe [7], i.e. a colossal field value far greater than the

---

[7] It must be noted that in the Gaussian system of units (unrationalized CGS) all the field vectors $\vec{E}$, $\vec{D}$, $\vec{B}$, $\vec{H}$, $\vec{P}$ and $\vec{M}$ have the same dimensions, although people have been giving different names to the units. Usually $\vec{B}$ is expressed in gauss and $\vec{H}$ in oersted, however this is not binding and $\vec{H}$ can be expressed in gauss and subsequently converted to Tesla (1 T=10^4 gauss). This is a common practise in the current research literature of magnetoconductance studies. A detailed discussion regarding the system of units in electromagnetism can be found in reference [68].

largest steady state magnet in a laboratory ($\sim 30 \times 10^4$ Oe). Thus, the weak field limit approximation is in the case of typical metals entirely justified at room temperatures.[8]

SOLUTION OF THE BOLTZMANN EQUATION

As discussed in 2.2.1, the governing equation of transport is the *Boltzmann equation*. Since at the weak field limit the relaxation time approximation is valid, the general solution with the inclusion of the magnetic field term [20] can be expressed as

$$\varphi(\vec{r}, \vec{k}) = \vec{k} \cdot \vec{\theta}(E, \vec{E}, \vec{H}) \tag{3.2}$$

where $\vec{\theta}$ is not a function of $\vec{k}$. The equation for $\vec{\theta}$ is

$$\vec{\theta} = \frac{\tau \hbar}{m^*} \left(e\vec{E} \right) - \frac{e\tau}{cm^*} \left(\vec{H} \times \vec{\theta} \right) \tag{3.3}$$

which has the solution

$$\vec{\theta} = \frac{(\hbar/m^*)\tau \left[e\vec{E} - (e\tau/m^*c)\vec{H} \times e\vec{E} + (e\tau/m^*c)^2 \vec{H}(\vec{H} \cdot e\vec{E}) \right]}{1 + (e\tau H/m^*c)^2} \tag{3.4}$$

For $\vec{H} = H\hat{z}$ and $\vec{E} = E_x \hat{x} + E_y \hat{y}$, using (3.1) we obtain

$$\theta_x = \frac{\hbar \tau e}{m^*} \frac{E_x + \omega_c \tau E_y}{1 + (\omega_c \tau)^2} \tag{3.5}$$

$$\theta_y = \frac{\hbar \tau e}{m^*} \frac{E_y - \omega_c \tau E_x}{1 + (\omega_c \tau)^2} \tag{3.6}$$

Since the distribution function can be written in the general form

$$f(\vec{r}, \vec{k}) = f_0(\vec{r}, \vec{k}) + f'(\vec{r}, \vec{k}) \tag{3.7}$$

where

$$f'(\vec{r}, \vec{k}) = -\varphi(\vec{r}, \vec{k}) \frac{\partial f_0}{\partial E} = -\vec{k} \cdot \vec{\theta} \frac{\partial f_0}{\partial E} \tag{3.8}$$

The current density is generally defined by

$$\vec{j}(\vec{r}) = -e \int f(\vec{r}, \vec{v}) \vec{v} d^3 \vec{v} = -\frac{e}{4\pi^3} \int f(\vec{r}, \vec{k}) \vec{v} d^3 \vec{k} \tag{3.9}$$

---

[8] The same conclusion can be reached by considering the fact that in the high field limit $\hbar \omega_c > k_B T$ so that thermal motion is not dominant and the change in the energy of the carrier upon scattering is greater than its thermal energy. From the above expression the typical values of H should satisfy the inequality $H > 7.442 \times 10^4$ Oe/K. At room temperature (300 K) $H > 223 \times 10^4$ Oe, but at 1K $H > 0.744 \times 10^4$ Oe. Hence, the high field limit drastically changes at low temperatures.

and by using equations (3.7) and (3.8), we obtain

$$\vec{j} = -\frac{e}{4\pi^2} \int (\vec{k} \cdot \vec{\theta}) \vec{v} \frac{\partial f_0}{\partial E} d^3\vec{k}$$ (3.10)

since the integration over the equilibrium distribution $f_0(\vec{r}, \vec{k})$ is zero. After some lengthy calculations, the x and y components of the current density can be derived. The results are [20]

$$j_x = \frac{ne^2}{m^*} \left(\frac{\tau E_x}{1 + \omega_c^2 \tau^2} - \frac{\omega_c \tau^2 E_y}{1 + \omega_c^2 \tau^2} \right)$$ (3.11)

$$j_y = \frac{ne^2}{m^*} \left(\frac{\tau E_y}{1 + \omega_c^2 \tau^2} + \frac{\omega_c \tau^2 E_x}{1 + \omega_c^2 \tau^2} \right)$$ (3.12)

It must be pointed out that the above general expressions are valid for spherical energy surfaces in the energy-independent relaxation time approximation, where the perturbed distribution function is given by (3.4) and (3.8).

INTERPRETATION OF THE HALL EFFECT

A straightforward application of equations (3.11) and (3.12) is the interpretation of the Hall effect shown in Figure 3-1. After experiencing the Lorentz force $-\frac{e}{c} \vec{v} \times \vec{H}$, the electrons begin to accumulate at the side of the wire in the negative y direction. This results in the appearance of a transverse electric field E_y that opposes the motion of the electrons until the attainment of equilibrium where $j_y = 0$. From (3.12), the expression for the Hall field can be obtained

$$E_y = -\omega_c \tau E_x = -\frac{eH}{mc} \tau E_x$$ (3.13)

and by substituting this value in (3.11), the current density j_x is given by

$$j_x = \frac{ne^2}{m^*} eE_x = ne\mu E_x = \sigma E_x$$ (3.14)

The Hall coefficient R_H is given by definition

$$R_H \equiv \frac{E_y}{j_x H} = \frac{-\omega_c \tau E_x}{\frac{ne^2 \tau}{m} E_x H} = -\frac{1}{nec}$$ (3.15)

Equation (3.14) is identical to that of the electron motion under the sole presence of an electric field. Therefore, in the particular case of spherical equal-energy surfaces and with a relaxation time independent of energy, the transverse magnetoresistance is predicted to be zero, confirming Hall's initial observation. This certainly is not true as latter experiments have revealed measurable changes, occasionally very large, in the resistance of real metals.[9] This is due to the complex energy surfaces of real metals as subsequent evidence from the quantum theory of solids shows [21].
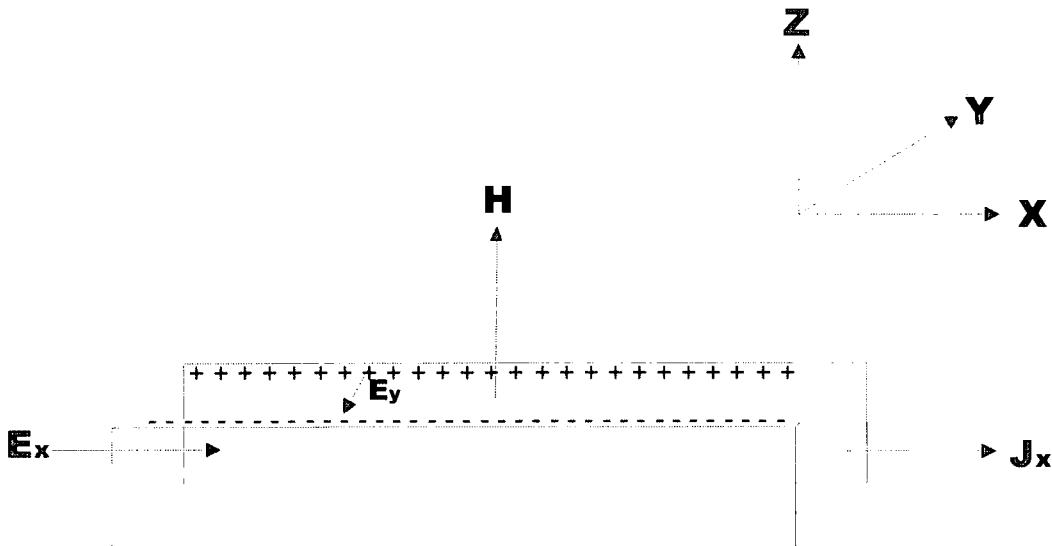
Figure 3-1 A schematic representation of the Hall effect. The electrons gather in the $-y$ director as shown leading to the creation of the transverse field E_y (or the Hall field) that balances the Lorentz force.

3.2.2 Magnetoresistance

In practise, due mainly to deviations from a spherical Fermi surface, the resistance of a metal changes after the application of a magnetic field. The change in resistance, R, of a material under an applied magnetic field H is called *magnetoresistance* (MR). It is usually defined as [70]

$$\frac{\Delta \rho}{\rho_0} = \frac{R(H,T) - R(0,T)}{R(0,T)} \tag{3.16}$$

Alternatively the expression for *magnetoconductance* (MC) is also commonly used

---

[9] It should be mentioned that although in the case of one-carrier conductivity systems that satisfy the aforementioned conditions no magnetic field effects on conductivity are predicted, this is no longer true in the case of two or more charge carrier conductivity since the Hall field cannot cancel j_y for all the carriers resulting to magnetoresistance effects.

$$\frac{\Delta\sigma}{\sigma_0} = \frac{\sigma(H,T) - \sigma(0,T)}{\sigma(0,T)} \qquad (3.17)$$

and the relation between MR and MC is easily found to be

$$\frac{\Delta\sigma}{\sigma_0} = -\frac{\Delta\rho}{\rho(H,T)} \qquad (3.18)$$

The magnetoresistance of a material is not a simple scalar quantity [71]. Dependent upon the relative orientation of the magnetic field and the current, it can be separated into *transverse* MR, where the current is perpendicular to the magnetic field, and in *longitudinal* MR, where current and magnetic field are parallel[10]. Both these effects are of about the same order of magnitude in metals, although the transverse effect is usually the larger [71].

Magnetoresistance calculations tend to be quite complicated, however, there seems to be a general rule which appears to hold quite accurately in nearly every instance. According to that rule, which is called Kohler's rule, the MR of a metal can be represented in the form

$$\frac{\Delta\rho}{\rho_0} = F\left(\frac{H}{\rho_0}\right) \qquad (3.19)$$

where F is a function depending only on the metal and its geometrical configuration. It can be directly derived from implications concerning the solution to the Boltzmann equation discussed in 3.2.1. Equation (3.19) indicates that magnetoresistance measurements are best performed at low temperatures, where ρ_0 is as small as possible, in order that the effect of the magnetic field to be more significant, i.e. greater values of $\Delta\rho$. Such practice was duly followed in the MR experiments conducted on PANI samples. Another general fact about metals and semiconductors, despite some deviations at high field, is that the magnetoresistance is proportional to H^2 [20, 72, 73].

3.2.3 Magnetoresistance of disordered materials

Considering the aforementioned difficulties for formulating a general model for magneto-transport in traditional metals, the situation for a disordered material is expected to be even more confounding. There have been significant attempts in the early part of the decade 1980-1990, however, for the development of a theory that

---

[10] In this case the Lorentz force $-\frac{e}{c}\vec{v} \times \vec{H}$ is zero, however effects are measured due to distortions of the spherical Fermi surface.

could describe the effects of Anderson localization [32, 39, 74, 75] and the effects of electron-electron interactions [76-80] on the transport properties for disordered electronic systems. The scaling theory of localization [39] has lead to the localization-interaction model [17] that, as numerous studies from different groups have shown [10, 61-63, 66, 81-86], describes with considerable success the observed transport properties of homogeneously disordered metallic systems close to the metal-insulator transition.

The localization-interaction model predicts behaviours different from those of periodic systems and provides quantum mechanical corrections to the semiclassical Boltzmann conductivity which arise in sufficiently disordered metals at low temperatures [87]. These corrections are the self-explanatory electron-electron interaction and the weak localization that tends to localize the electron wavefunction due to quantum interference. According to the localization-interaction model, the conductivity in the disordered metallic regime at low temperatures is expressed by [17]

$$\sigma(T) = \sigma(0) + m'T^{1/2} + BT^{p/2} \qquad (3.20)$$

where the second term arises from electron-electron interactions, while the last term is the correction to the zero-temperature conductivity due to localization effects [85]. The value of p is determined by the temperature dependence of the scattering rate, $\tau_{in}^{-1} \propto T^p$, of the dominant dephasing mechanism. Reported values of p are: p=2.5-3 for electron-phonon scattering, p=2 for inelastic electron-electron scattering (clean limit) or p=3/2 (dirty limit) [10]. The calculations by Belitz and Wysokinski [88] give p=1 close to the metal-insulator transition. The parameter m' is given by the expression [76, 85]

$$m' = a\left[\frac{4}{3} - \gamma\left(\frac{3F_\sigma}{2}\right)\right] \qquad (3.21)$$

where $a \propto D^{-1/2}$ with D being the diffusion coefficient, γ is a parameter dependent on details of the electronic structure and F_σ the interaction parameter, which is a complicated but monotonic function of the Thomas-Fermi screening wave vector K. It is related to the Fermi-liquid parameter F, which is the screened electron-electron interactions averaged over the Fermi surface by the expression (Hartree interaction) [85]

$$F_\sigma = -\frac{32}{3F}\left[1 - 3F/4 - (1 - F/2)^{3/2}\right] \qquad (3.22)$$

where the Hartree factor F can be written as

$$F = (1/x)\ln(1+x) \tag{3.23}$$

with $x = (2k_F / K)^2$. The screening length K^{-1} becomes very large near the transition whereby F varies between 0 and 1, decreasing while the transition is approached. The parameter F_σ (always positive) follows the decrease of F, causing the parameter m' to change sign from negative to positive when $\gamma F_\sigma < 8/9$. Since $a \propto D^{-1/2}$ with D being the diffusion coefficient, $a \propto \sigma_0^{-1/2}$, and therefore a gives a contribution to m' in (3.21) that increases in magnitude as the metal-insulator transition is approached[11]. Deep in the metallic regime, m' is negative since F_σ is large, increasing as the transition is approached and changing sign when K^{-1} diverges at the metal-insulator transition.

In the framework of the localization-interaction model, the primary distinction between high and low magnetic field limits is made by comparing the Zeeman splitting energy of the electron (the energy quanta of a quantum-mechanical transition) $g\mu_B H$, where g is the electron gyromagnetic ratio (*g-factor*) which is approximately equal to 2, to the thermal energy $k_B T$. Hence the *high* field limit condition is $g\mu_B H \gg kT$ and the *low* field is $g\mu_B H \ll kT$. The high magnetic field condition after numerical substitution becomes $H/T \gg k_B/g\mu_B = 0.744 \times 10^4$ Oe/K.

ELECTRON-ELECTRON INTERACTIONS

The quantum corrections to the magnetoconductance, due to e-e interactions, defined as

$$\Delta\sigma_1(H,T) = \sigma_1(H,T) - \sigma_1(0,T) \tag{3.24}$$

are given from the following expressions [10, 84]

$$\Delta\sigma_1(H,T) = -0.041 a(g\mu_B / k_B)^2 \gamma F_\sigma T^{-3/2} H^2$$
$$\text{For } g\mu_B H \ll kT \tag{3.25}$$

$$\Delta\sigma_1(H,T) = a\gamma F_\sigma T^{1/2} - 0.77 a(g\mu_B / k_B)^{1/2} \gamma F_\sigma H^{1/2}$$
$$\text{For } g\mu_B H \gg kT \tag{3.26}$$

---

[11] Whenever it is mentioned that a metal-insulator transition is approached, it is implied that the direction is from the metallic to the insulating side.

From the above equations it is apparent that the magnetoconductance[12] due to e-e interactions is expected to behave as $H^{1/2}$ at very high and as H^2 at very low fields. Also the contribution of the e-e interactions to the magnetoconductance is always *negative*, arising from Zeeman splitting of the spin-up and spin-down bands.

An expression similar to (3.20) for the conductivity at low temperatures under the presence of a strong magnetic field, but due to e-e interactions only, can be obtained from the following procedure:

Equations (3.24) and (3.26) give

$$\sigma_1(H,T) = \Delta\sigma_1(H,T) + \sigma_1(0,T) \tag{3.27}$$

where $\sigma_1(0,T) = \sigma_1(T)$ and it is given by (cf. (3.20))

$$\sigma_1(T) = \sigma_1(0) + m'T^{1/2} \tag{3.28}$$

Therefore

$$\sigma_1(H,T) = \Delta\sigma_1(H,T) + \sigma_1(0) + m'T^{1/2} \tag{3.29}$$

and

$$\sigma_1(H,0) = \Delta\sigma_1(H,0) + \sigma_1(0) = \sigma_1(0) - 0.77\alpha(g\mu_B/k_B)^{1/2}\gamma F_\sigma H^{1/2} \tag{3.30}$$

By combining equation (3.29) with (3.26) and (3.30), after using (3.21), we obtain

$$\sigma_1(H,T) = \sigma_1(H,0) + m_H T^{1/2} \tag{3.31}$$

where the coefficient m_H is given by

$$m_H = a\left[\frac{4}{3} - \gamma\left(\frac{F_\sigma}{2}\right)\right] \tag{3.32}$$

The parameters present in (3.32) are identical to the ones of (3.21) since the equations were derived under the fundamental assumption that a,γ and F_σ are independent of the magnetic field. Since $\gamma F_\sigma = (m_H - m')/a$ and $,\gamma F_\sigma$ is always positive, $m_H > m'$ with m_H having a positive range of values. As disorder increases, γF_σ decreases, causing m' to become negative when $\gamma F_\sigma > 8/9$. The application of a high magnetic field can, therefore, cause a change in the conductivity slope whenever $m'<0$, namely in the samples for which $\gamma F_\sigma > 8/9$.

---

[12] If we want to be pedantic and consistent with the definition given by (3.17), the term "change in conductivity" should, instead of "magnetoconductance", have been used for $\Delta\sigma_1$. However, such discrepancy is a common practise in research literature and it has been kept mostly for practical purposes since the precise meaning can easily be derived from context.

Values of m' and m_H, obtained from the magnetoconductance data, can characterise the extent of the disorder present in the sample and its relative position in an imaginary metal-insulator transition scale via the value of γF_σ, which, as mentioned before, decreases until zero as the sample goes from the metallic to the insulating side of the transition. Thus, from the magnetoconductance measurements, interesting parameters, unavailable from the conductivity data alone, that provide extra information about the sample properties can be deduced. Such procedure will be followed in the experimental section.

WEAK LOCALIZATION

The primary distinction that must be made concerning the weak localization term is whether the spin-orbit effects are important or not. Studies [35, 72, 89] of disordered metallic films and doped semiconductors [84-86] where the spin-orbit coupling was strong have revealed a negative magnetoconductance. It appears that weak localization under the presence of strong spin-orbit effects changes to weak antilocalization due to destructive backscattering. Theoretical issues in the case of strong spin-orbits effects are yet to be decided. In conducting polymers, however, due to the dominance of atoms with relatively low atomic number, it should be expected the spin-orbit effects to be weak. This conjecture will, rather justifiably, be followed in the forthcoming analysis.

In the presence of weak spin-orbit effects, the magnetoconductance due to the weak localization term defined as

$$\Delta\sigma_L(H,T) = \sigma_L(H,T) - \sigma_L(0,T) \qquad (3.33)$$

can be expressed by the following equations [74, 87, 90]

$$\Delta\sigma_L(H,T) = (1/12\pi^2)(e/c\hbar)^2 G_0 l_{in}^3 H^2$$
$$\text{For } g\mu_B H \ll kT \qquad (3.34)$$

$$\Delta\sigma_L(H,T) = B_{WL} H^{1/2}$$
$$\text{For } g\mu_B H \gg kT \qquad (3.35)$$

where l_{in} is the inelastic scattering length, $G_0 = (e^2/\hbar)$ and B_{WL} is a constant with an estimated value for an isotropic material of the order of magnitude of 0.01 S cm^{-1} Oe$^{-1/2}$ [91] and having a maximum value of 0.0435 S cm^{-1} Oe$^{-1/2}$ [92]. According to (3.34) and (3.35), weak localization gives *positive* magnetoconductance.

Therefore, the effect of the magnetic field is to suppress the localization effect. The high and low field behaviour of the magnetoconductance is identical to that due to e-e interactions, i.e. behaviour proportional to $H^{1/2}$ at very high and to H^2 at very low fields.

TOTAL CORRECTIONS

The corrections to magnetoconductance due to e-e interactions and weak localization are additive, providing the following expression for the total magnetoconductance

$$\Delta\sigma(H,T) = \sigma(H,T) - \sigma(0,T) = \Delta\sigma_I(H,T) + \Delta\sigma_L(H,T) \qquad (3.36)$$

The contribution of the quantum mechanical corrections to the magnetoresistance can be schematically represented by the diagram of Figure 3-2. It has been surmised by various studies [84, 90] that despite the importance of the interplay between those two interactions for the extent of the disorder present in the system, the e-e interactions are more dominant at lower temperatures and higher fields, while the weak localization effects are more dominant at higher temperatures and lower fields. The validity of such remarks will be explored during the analysis of the magnetoconductance data taken from PANI films.

Low Magnetic field limit
$g\mu_B H \ll kT$

e-e interactions

$\Delta\sigma_1(H,T) = -0.041a(g\mu_B/k_B)^2 \gamma F_\sigma T^{-3/2} H^2$

Negative magnetoconductance

Weak Localization

$\Delta\sigma_L(H,T) = (1/12\pi^2)(e/ch)^2 G_0 l_{in}^3 H^2$

Positive magnetoconductance

Total magnetoconductance

$\Delta\sigma(H,T) = -0.041a(g\mu_B/k_B)^2 \gamma F_\sigma T^{-3/2} H^2 + (1/12\pi^2)(e/ch)^2 G_0 l_{in}^3 H^2$

High Magnetic field limit
$g\mu_B H \gg kT$

e-e interactions

$\Delta\sigma_1(H,T) = a\gamma F_\sigma T^{1/2} - 0.77a(g\mu_B/k_B)^{1/2} \gamma F_\sigma H^{1/2}$

Negative magnetoconductance

Weak Localization

$\Delta\sigma_L(H,T) = B_{WL} H^{1/2}$

Positive magnetoconductance

Total magnetoconductance

$\Delta\sigma(H,T) = a\gamma F_\sigma T^{1/2} - 0.77a(g\mu_B/k_B)^{1/2} \gamma F_\sigma H^{1/2} + B_{WL} H^{1/2}$

Figure 3-2 A diagram representing the contributions to the total magnetoconductance by the e-e interactions and the weak localization at the weak and strong field limits. It must be noted that the absence of strong spin-orbit effects has been assumed (otherwise the weak localization contributions could be negative).

3.3 Experimental setup

Conductivity and MC measurements were carried out in a helium cryostat with a superconducting magnet that enabled magnetic fields up to 14×10^4 Oe and temperatures ranging from room temperature to 1.5 K to be reached. The temperature was monitored with either Pt resistance thermometer (for $T > 50$ K) or a carbon glass thermometer (for $T < 50$ K).

The conductivity of the samples was measured using the 'four-in-line technique' that was described, along with the sample preparation, in the Chapter 2. This time, instead of using a printed circuit board, the electrical contacts were made by placing four thin copper wires with conductive graphite adhesive onto the gold strips of the samples, as Figure 3-3 shows. The linear response in the current-voltage curve was once again confirmed and in order to avoid any additional sample heating, the dissipated power onto the sample did not exceed 1 μW. The magnetoconductance measurements were conducted with the magnetic field *perpendicular* to the film surface and, thus, to the current direction.
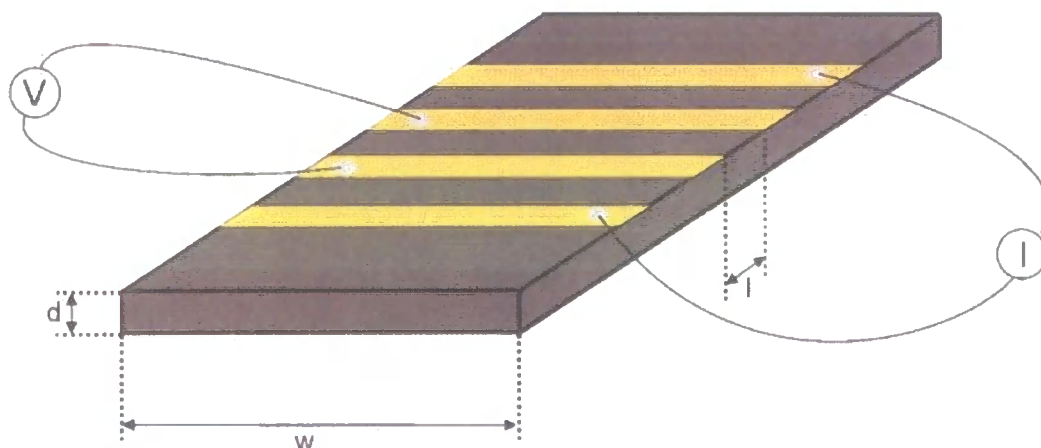
Figure 3-3 The sample configuration used for magnetoconductance measurements. The contacts between the gold strips and the copper wires were made using conductive graphite adhesive.

3.4 Results and Discussion.

3.4.1 Temperature dependence of conductivity.

Low temperature ($T < 10$ K) dependent conductivity measurements initially without an external magnetic field and, afterwards under a magnetic field $H = 13.09 \times 10^4$ Oe were performed on PANI-CSA and PANI-AMPSA samples. The results from each

sample category will be presented separately for clarity purposes, whereas the conclusions will be charted collectively.

PANI-CSA FILMS

According to the conductivity results of the previous chapter, PANI-CSA 60% and PANI-CSA 30% are, respectively, the most metallic and least metallic of all the PANI-CSA films studied thereby. Due to the availability of conductivity values at 1.5 K, their resistivity ratio can now be more accurately defined as $\rho_r = \sigma(295 \text{ K})/\sigma(1.5 \text{ K})$ and its values are included in Table 3-1, page 57. From these values, it is surmised that PANI-CSA 60% is in the metallic regime ($\rho_r < 2$), whereas PANI-CSA 30% is in the insulating regime ($10 < \rho_r$) of a disorder induced metal-insulator (M-I) transition [56].[13] Such classification is corroborated by the activation energy $W = d(\ln\sigma)/d(\ln T)$ plots of Figure 3-5. Sample PANI-CSA 30% shows a negative temperature coefficient at low temperatures, while PANI-CSA 60% a positive one, indicating the former is on the insulating side of the M-I transition whereas the latter is on the metallic. The activation energy criterion was applicable since the samples, as the conductivity plots of Figure 3-4 testified, showed a negative temperature coefficient of resistivity (TCR) at the low temperature regime. The agreement between the $W(T)$ plots and the resistivity ratio (defined this time at 1.5 K), confirms the importance of these two factors for the precise identification of the metallic, critical and insulating regimes in conducting polymers.

According to the localization-interaction, the conductivity of disordered system in the *metallic* regime is given by expression (3.20).[14] At very low temperatures ($T < 4$ K), the e-e interaction dominates over the weak-localization contribution to the conductivity [81, 85, 93] and the conductivity is given by

$$\sigma_1(T) = \sigma_1(0) + m'T^{1/2} \tag{3.37}$$

---

[13] Apparently the PANI-CSA 30% sample studied here is more disordered than the one studied in the previous chapter. Such difference can be once more attributed to subtle variations in the disorder due to random factors occurring in the film preparation such as the solvent evaporation rate, solution concentration etc. The differences among PANI-AMPSA samples of the same characteristics are considerable smaller, suggesting that in PANI-AMPSA systems the random disorder introduced through the preparation process is less significant.

[14] Attempts to fit this equation to the data were abandoned due to problems of overparametrization.

while under the presence of a strong magnetic field[15] (H>8x10^4 Oe), as explained in 3.2.3, the corresponding expression is

$$\sigma_1(H,T) = \sigma_1(H,0) + m_H T^{1/2} \qquad (3.38)$$

Equations (3.37) and (3.38) were successfully fitted to the PANI-CSA 60% low temperature conductivity data, as Figure 3-6 demonstrates. The values of the fitting parameters $\sigma_1(0)$, m', $\sigma_1(H,0)$ and m_H are summarised in Table 3-1. Both samples showed negative magnetoconductance after the application of the magnetic field.

Such fitting procedure is obviously not possible for a sample in the insulating regime such as PANI-CSA 30%. Figure 3-7 demonstrates the unsuitability of the metallic regime expression for the low temperature conductivity, supporting, thus, its validity. For samples in the insulating regime, the conductivity follows the activated temperature dependence of Variable Range Hoping (VRH) among localized states below the mobility edge [27, 28]. In this case, $\sigma(T)$ becomes exponential and is given by the general expression

$$\sigma(T) = \sigma_0 \exp\left[-\left(\frac{T_0}{T}\right)^x \right] \qquad (3.39)$$

where σ_0 is a constant, $x=1/(1+d)$ (d the dimensionality of the system) and, for three-dimensional systems, $T_0 = const / k_B N(E_F) L^3$ (L being the localization length). For three dimensional hopping of non-interacting carriers $x=1/4$ (Mott's law), while in the Efros-Shklovskii limit (ES) [41], where the interactions between localized electrons play an important role in the hopping transport, $x=1/2$. By substituting (3.39) in the expression for the activation energy $W = d(\ln \sigma) / d(\ln T)$, we find that

$$W = x T_0^x T^{-x} \qquad (3.40)$$

or

$$\ln W = \ln(x T_0^x) - x \ln T \qquad (3.41)$$

The VRH parameters can, therefore, be determined from the slopes of the W versus T plots of Figure 3-5. The values obtained for PANI-CSA 30% sample are x=0.345 and T_0=60 K, which are in the value range reported by other groups on similar (but not identical systems) [4, 42]. The exponent x grows as the samples become more insulat-

---

[15] The magnetic field should exceed the limit for Zeeman splitting, $g\mu_B H > k_B T$, i.e. $H/T >> k_B/g\mu_B$=0.744x10^4 Oe/K. This condition is satisfied in the measured temperature range since H=13.09x10^4 Oe and T<4 K.

ing and the charge transport becomes more characteristic of hopping on isolated chains with reduced dimensionality. In the current case, $d=1.9$ indicating a quasi-2D transport mechanism. It must be noted, however, that obtaining the VRH parameters from the $W(T)$ plots is not an entirely precise procedure since the $W(T)$ plots themselves are deduced by differentiating the measured conductivity data and it is well known in the field of numerical analysis that numerical differentiation is a high-risk technique that poses complicated problems, not always malleable, for an error-free application. The standard errors in the $W(T)$ plots can, therefore, become quite large (e.g. relative error greater than 50%) depending on the differentiation technique used. However, since the plots have more comparative than absolute value and considering the fact the same differentiation technique was used for every sample, we would expect the relative errors to be similar from sample to sample and that the general trends in the plots will remain distinguishable.
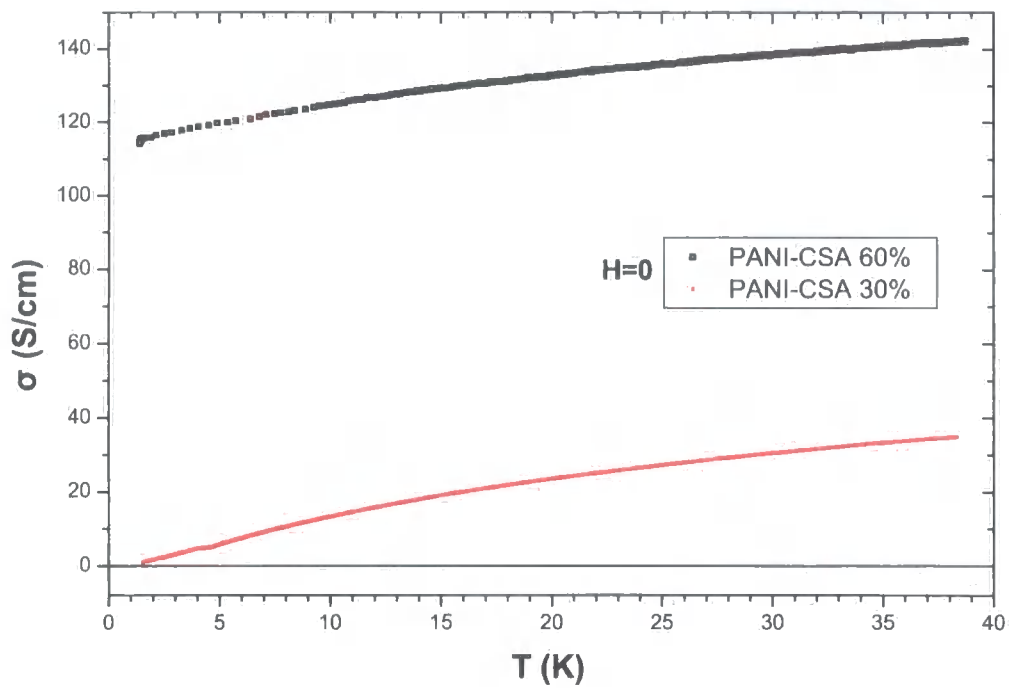
Figure 3-4 The low temperature dependence of the dc conductivity for PANI-CSA samples.
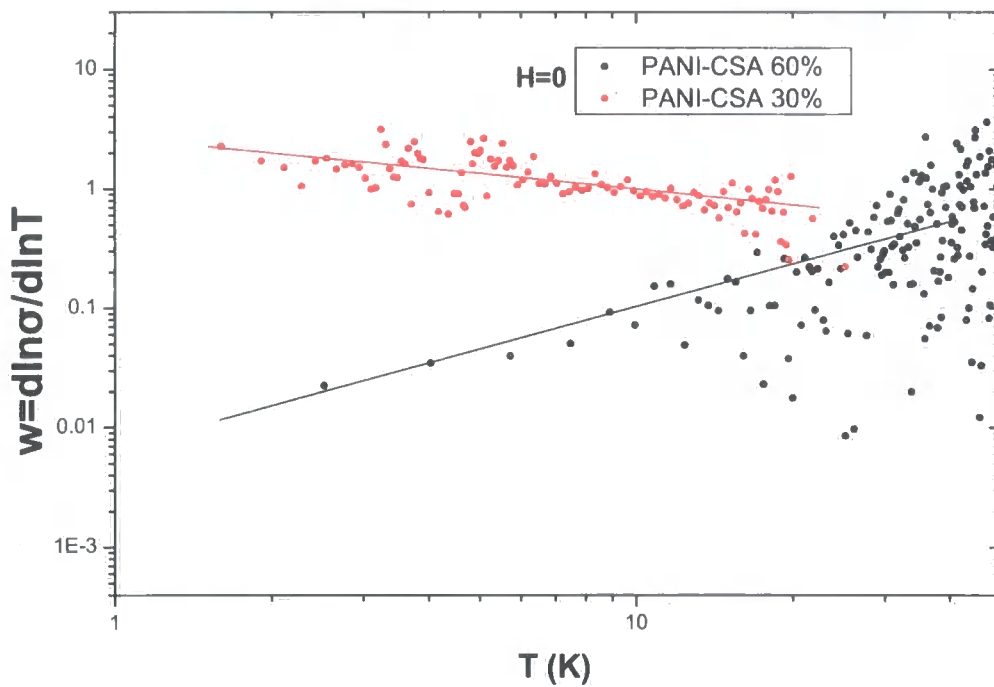
Figure 3-5 Log-Log plots of the activation energy W against temperature for the PANI-CSA samples shown in Figure 3-4. At low temperatures, ($T<20$ K), where the criterion is applicable, the PANI-CSA 60% film shows a positive slope (metallic regime), whereas PANI-CSA 30% a negative slope (insulating regime).
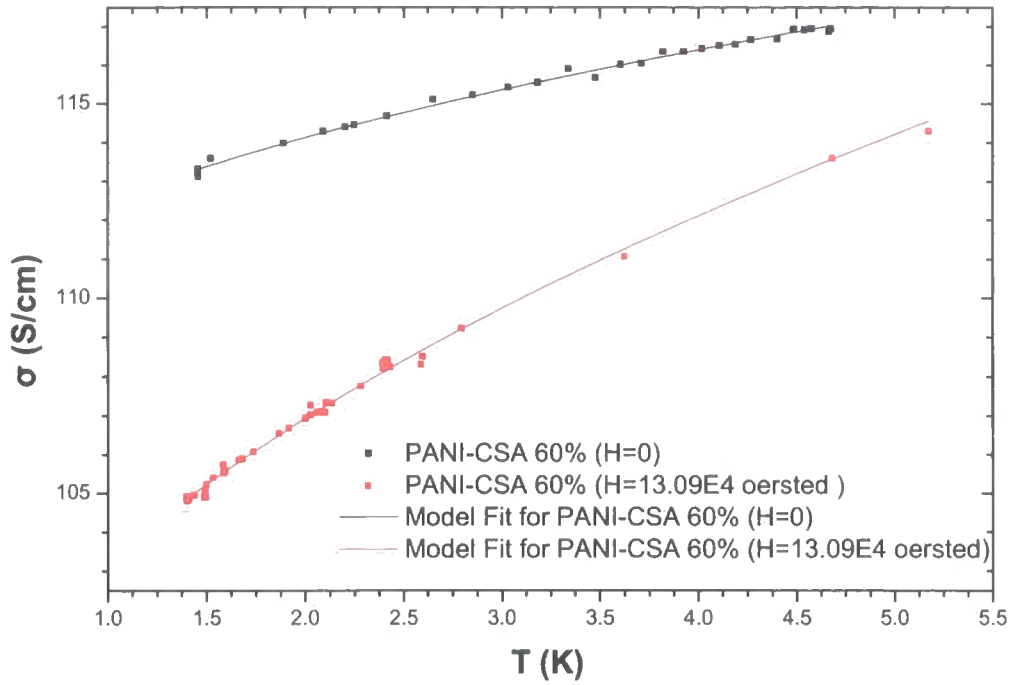
Figure 3-6 Temperature dependence of the conductivity for PANI-CSA 60% sample with and without the presence of an external magnetic field. Model fits were performed in the context of the localization-interaction model for samples in the metallic regime.
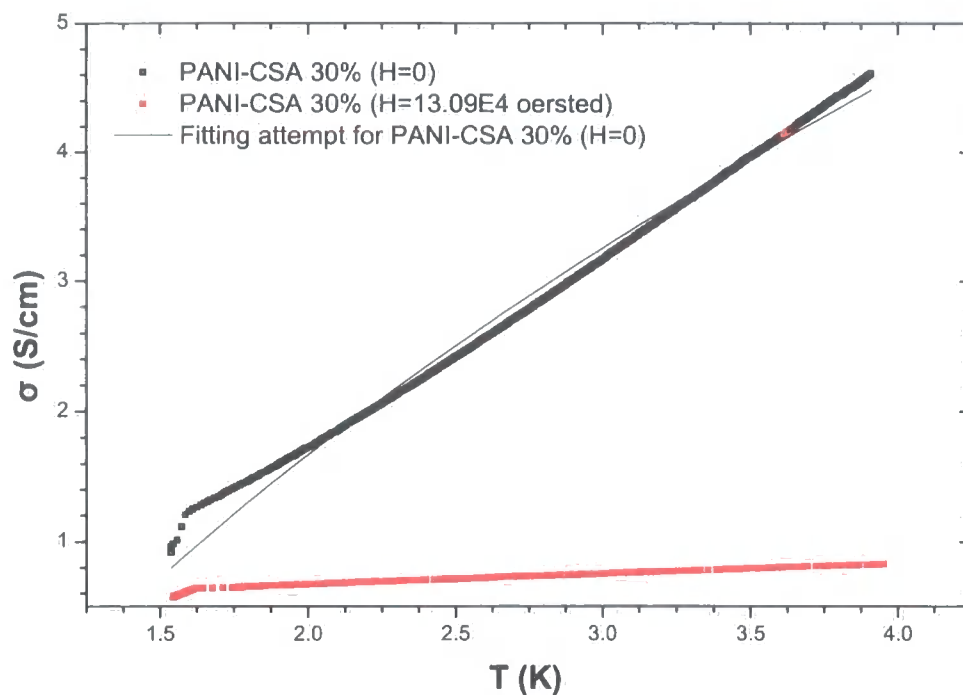
Figure 3-7 Temperature dependence of the conductivity for PANI-CSA 30% sample with and without the presence of an external magnetic field. Since the sample is in the insulating regime, attempts to fit the same model, described by (3.37), as in the case of PANI-CSA 60% sample have failed.

PANI-AMPSA 50% FILM

Figure 3-8 shows the low temperature conductivity data of the PANI-AMPSA 50% sample. It is observed that, contrary to PANI-CSA samples, the magnetoconductance increases after the application of a strong external magnetic field, $H=13.09 \times 10^4$ Oe. This observation will be discussed in detail in the magnetoconductance section that follows. The resistivity ratio and the slightly positive slope of the $W(T)$ curve indicate that the sample is on the metallic side, albeit closer to the transition that PANI-CSA 60%. Furthermore, the activation energy values of PANI-AMPSA film are greater than those of PANI-CSA 60% (metallic regime) and smaller than those of PANI-CSA 30% (insulating regime), suggesting that, since the reduced activation energy increases as the samples becomes more insulating, the film is on an intermediate position in an imaginary M-I transition diagram. Following the same

procedure with PANI-CSA 60%, the model curve fits are plotted in Figure 3-9 and the fitting parameters are listed in Table 3-1.
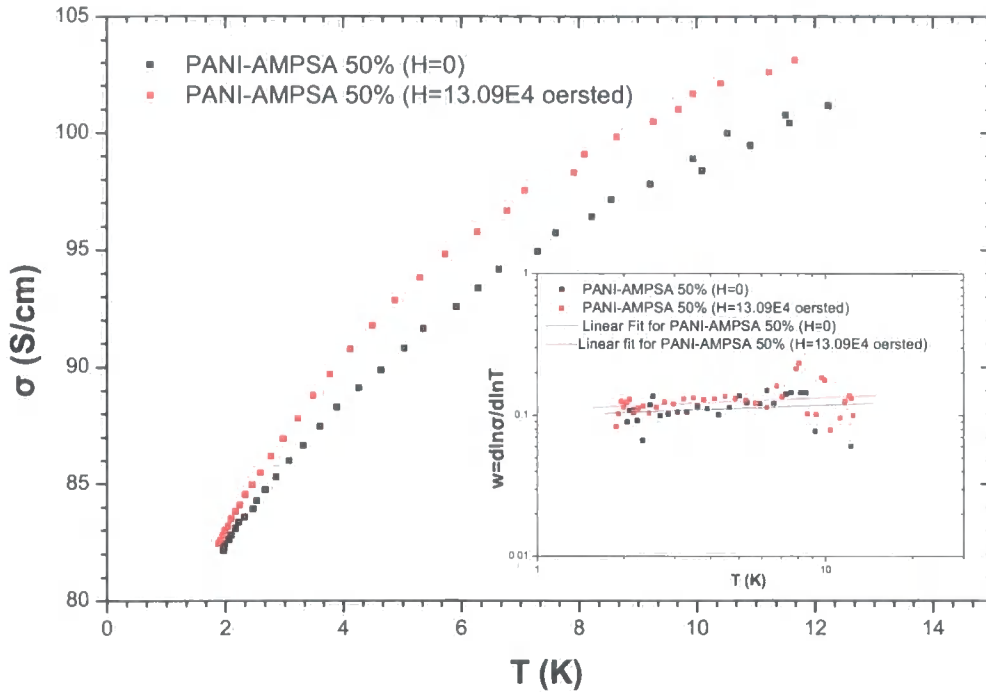
Figure 3-8 The low temperature dependence of conductivity for PANI-AMPSA 50% sample with and without the presence of an external magnetic field. The corresponding activation energy curves are logarithmically plotted in the inset.
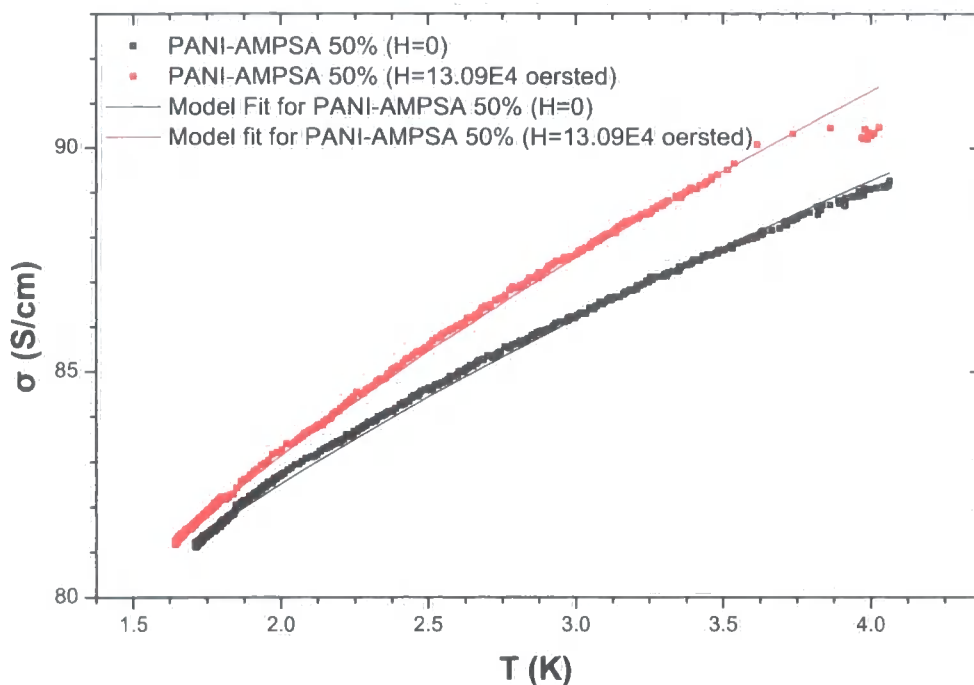
Figure 3-9 The low temperature conductivity curves along with the localization-interaction model fits for the PANI-AMPSA 50% sample.

COLLECTIVE RESULTS

The results of all the samples studied are listed in Table 3-1. According to the localization-interaction model, $m_H > m'$, something that is confirmed by the current results. As explained in 3.2.3, the value of m' increases in magnitude as the M-I transition is approached, viz. the more insulating samples have larger values of m'. This was found to be the case for the samples under investigation since the primary classification done by the resistivity ratio and the reduced activation energy plots is consistent with the values of m' that were derived by applying the localization-interaction model on the low temperature conductivity data.

Table 3-1 The reference conductivity values for the samples under investigation along with the fitting parameters of the localization-interaction model for a sample in the metallic regime of an M-I transition. The MC percentage is calculated for $H=13.09 \times 10^4$ Oe and $T=1.5$ K. The relative errors of the fitting parameters are approximately 0.1%.

Sample	$\sigma(295)$ (S/cm)	ρ_r	$\sigma_1(0)$ (S/cm)	m' $(\Omega\ m\ K^{1/2})^{-1}$	$\sigma_1(H,0)$ (S/cm)	m_H $(\Omega\ cm\ K^{1/2})^{-1}$	MC (%)
PANI-CSA 30%	52	57	-	-	-	-	-40
PANI-CSA 60%	120	1.06	108.63	3.88	94.40	8.86	-7
PANI-AMPSA 50%	100	1.22	66.04	11.51	63.55	13.86	0.7

From the values of m_H and m', the parameters a and γF_σ can be determined, after solving equations (3.21) and (3.32), by the expressions

$$a = \frac{3}{8}(3m_H - m')$$
(3.42)

$$\gamma F_\sigma = \frac{m_H - m'}{a}$$
(3.43)

The values of a and γF_σ are plotted in Figure 3-10. In accordance with the theory, a (γF_σ) increases (decreases) as the sample moves from the metallic to the insulating side of the M-I transition. These values are similar to the ones found by other groups from studies on other conducting polymers close to the M-I transition [56, 81, 93]. Since for both samples $\gamma F_\sigma < 8/9$, m' is positive showing that the samples are not deep in the metallic regime, where m' is negative, but rather they are close, on the metallic side, to the boundary of an M-I transition. It is apparent that ρ_r, a and γF_σ, as Figure 3-10 shows, along with m' can provide a consistent classification of a sample in respect to its degree of disorder and the position in a virtual M-I transition diagram. This is achieved without any knowledge of microscopic quantities that determine the charge transport such as carrier density, relaxation time, drawing a line between conducting polymers and inorganic semiconductors [84-86] where such quantities are either known or can be precisely measured.
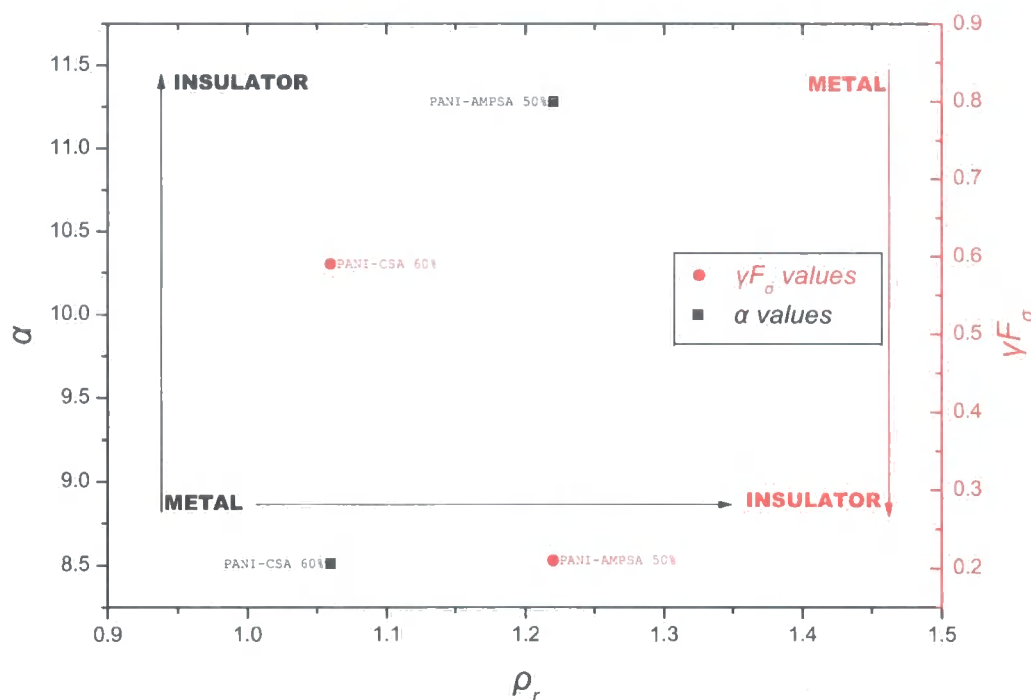
Figure 3-10 The values of a (black) and γF_σ (red) against the resistivity ratio of each sample. The correspondence between the value change of each parameter and the direction of the M-I transition is schematically shown.

Before proceeding with the magnetoconductance data, an important subtle point regarding the applicability of expressions (3.37) and (3.38) for the case of a sample in the metallic regime, but with *positive* magnetoconductance, must be made. According to theory of 3.2.3, the above expressions were derived under the fundamental assumption that the low temperature conductivity is determined only by the e-e interaction. Since the e-e interaction leads always to negative magnetoconductance, the application of those expressions in the case of positive magnetoconductance, like in the case of PANI-AMPSA 50% sample, seems, at first, questionable. However, in the case of a strong magnetic field $H=13.09 \times 10^4$ Oe, the inequality $H/T >> k_B/g\mu_B = 0.744 \times 10^4$ Oe/K is satisfied for the whole temperature range that the fits were performed. This implies that the weak-localization contribution to the magnetoconductance is given by the expression (3.35), which is repeated here

$$\Delta\sigma_L(H,T) = B_{WL} H^{1/2} \tag{3.44}$$

According to (3.44), the weak-localization contribution to the conductivity at high fields and low temperatures is *temperature independent* (since B_{WL} is constant). Therefore for $H=13.09 \times 10^4$ Oe, $\Delta\sigma_L$ is constant and therefore can be incorporated in

the constant $\sigma_1(H,0)$ of equation (3.38).[16] Hence, the application of the localization-interaction model for a sample marginally in the metallic regime of a M-I transition like PANI-AMPSA 50%, is formally justified.

3.4.2 Field dependency of magnetoconductance

Complementary information regarding the charge dynamics under a magnetic field can be obtained by measuring the magnetoconductance as a function of the applied field at different temperatures. This procedure has been followed on all the samples investigated in the previous section.

PANI-CSA 60%
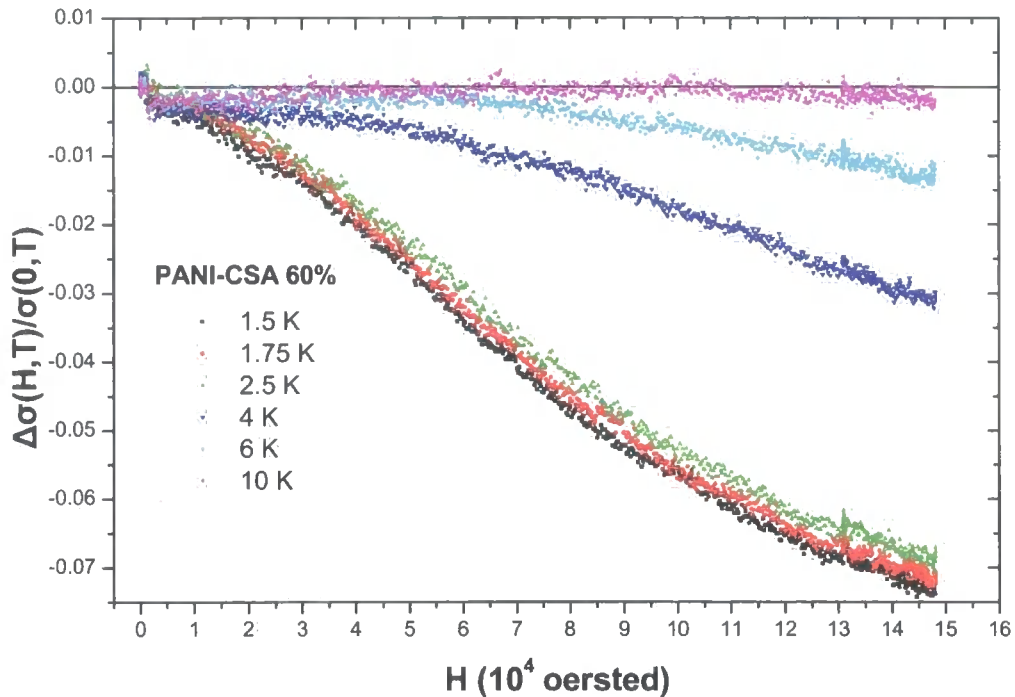
Figure 3-11 Magnetoconductance as a function of the applied magnetic field for the PANI-CSA 60% at different temperatures.

Figure 3-11 shows the magnetoconductance of the sample, as principally defined by (3.17), under an applied magnetic field ranging from 0 to 14.8×10^4 Oe. The measurements were performed at various temperatures. The experimental values are simi-

---

[16] The formal proof is similar to the of the theory section, but beginning with the expression for the total magnetoconductance, (3.36).

lar to the ones reported by other studies on similar systems [3, 4]. The maximum value of the MC is observed at $T=1.5$ K and is approximately 7.3%. The MC decreases with the increase of temperature and becomes almost negligible around 10 K. This is consistent with Kohler's law mentioned in 3.2.2, but not exactly for the same reason (conductivity values). The decrease of the MC with increasing temperature can be attributed to the dominance of other scattering, both elastic and inelastic, mechanisms such as electron-phonon scattering that are temperature activated over the relatively weak localization and e-e interaction effects that constitute the sample's MC. The sample is not metallic enough (although it is in the metallic regime as discussed previously) to observe any considerably positive MC as in the case of weakly disordered metal.

According to Figure 3-2, the total change in conductivity is given in the high field limit by the expression

$$\Delta\sigma(H,T) = a\gamma F_\sigma T^{1/2} - 0.77a(g\mu_B / k_B)^{1/2}\gamma F_\sigma H^{1/2} + B_{WL}H^{1/2} \qquad (3.45)$$

Assuming once again that in the high magnetic field limit the weak localization contribution is small in comparison with the e-e interaction term and, thus, can be omitted, equation (3.45) can be approximated by

$$\Delta\sigma(H,T) = a\gamma F_\sigma T^{1/2} - 0.89a\gamma F_\sigma H^{1/2} \qquad (3.46)$$

Equation (3.46) has been fitted to the MC data at different temperatures with $a\gamma F_\sigma$ as a fitting parameter giving similar results at each temperature. Figure 3-12 shows such a fit at 1.5 K. The obtained value for $a\gamma F_\sigma$ is 3.94 which is comparable with the values obtained in the previous section (Figure 3-10) give that $a\gamma F_\sigma=5.02$. The discrepancy can at first sight be attributed to the small influence of the WL in the measured curves and to other random errors that inhibit the accuracy of the fitting process. Another potential reason is that the parameter a as given by equation (3.42) may be temperature independent. Whether such case is valid here is a moot point, revealing that certain issues concerning the localization-interaction model remain unresolved. Nevertheless, the agreement is quite acceptable, suggesting an internal coherency in the model.

Ahlskog et al. [90, 91] have tried calculating the e-e contribution without omitting the WL term of (3.45) since such omission is indeed valid only under approximation. After assuming correctly that since the WL contribution B_{WL} is temperature independent, it can be cancelled out by subtracting the values of $\Delta\sigma$ at two different temperatures, satisfying the condition $H/T>>k_B/g\mu_B=0.744\times10^4$ Oe/K, they calculated the e-e

coefficient $B_{EE} = -0.77a(g\mu_B / k_B)^{1/2}\gamma F_\sigma H^{1/2}$ from the resulting values of

$\Delta\sigma(H,T_1) - \Delta\sigma(H,T_2)$. They, however, did not provide any further information re-

garding their calculation of B_{EE}. The aforementioned subtraction actually gives

$$\Delta\sigma(H,T_1) - \Delta\sigma(H,T_2) = a\gamma F_\sigma(T_1^{1/2} - T_2^{1/2}) + (B_{EE}^{T_1} - B_{EE}^{T_2})H^{1/2} \qquad (3.47)$$

and by considering that the e-e interaction is temperature independent as well, the

value of $a\gamma F_\sigma$ can be obtained. By trying different pairs of temperatures, a set of simi-

lar values of $a\gamma F_\sigma$ mostly greater than 5 was obtained, however such a method is sen-

sitive to millikelvin temperature fluctuations leading, occasionally, to large dispersion

when it is applied over a random set of temperature pairs. Hence, it should be applied

with care. Nevertheless, the fact that the values of $a\gamma F_\sigma$ are greater than the value ob-

tained from the $T^{1/2}$ dependence of $\sigma(T)$, demonstrates that in the first case the omis-

sion of the WL (positive contribution) has lead to an undervaluation of the absolute

value of B_{EE} or, in other words, to the underestimation of the contribution of the e-e

interaction to the magnetoconductance. The above procedure provides us with further

insight regarding recognition and quantification of the interplay of those two factors

dominating the charge transport mechanism of a conducting polymer at low tempera-

tures.[17]

---

[17] Low temperatures here refer to the temperature where the effect of other scattering processes to the charge transport in the material is negligible.
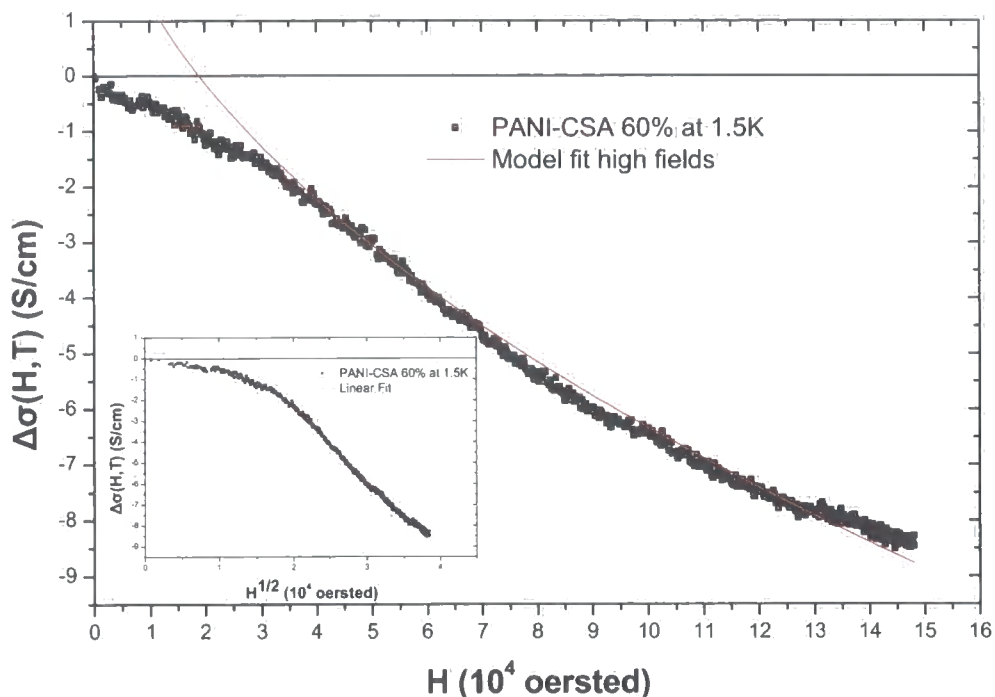
Figure 3-12 The change in conductivity under a magnetic field of PANI-CSA 60% at 1.5 K and the high field fit of the localization-interaction model given by equation (3.46). The inset plots $\Delta\sigma$ against $H^{1/2}$ to elucidate the suitability of (3.46) in the high-field region.

PANI-CSA 30%

The magnetic field dependence of the conductivity for sample PANI-CSA 30% at various temperatures is shown in Figure 3-13. The MC values displayed are significantly larger than the previous sample, exceeding 40% at 1.5 K. The dramatic increase of the negative MC as the sample crossed from the metallic (60% doping level) to the insulating regime (30%) is something typical for samples in the insulating regime of a M-I transition [5, 56, 62]. The largely negative values of MC in the insulating regime can be attributed to the reduction of the overlap of the localized wave functions under the influence of the magnetic fields and the field's effect on the hopping transport among the localized states. The proportional relation among MC and the extent of disorder can be used in order to classify the systems according to their degree of disorder and their relative position on the insulating regime on a virtual M-I transition diagram.
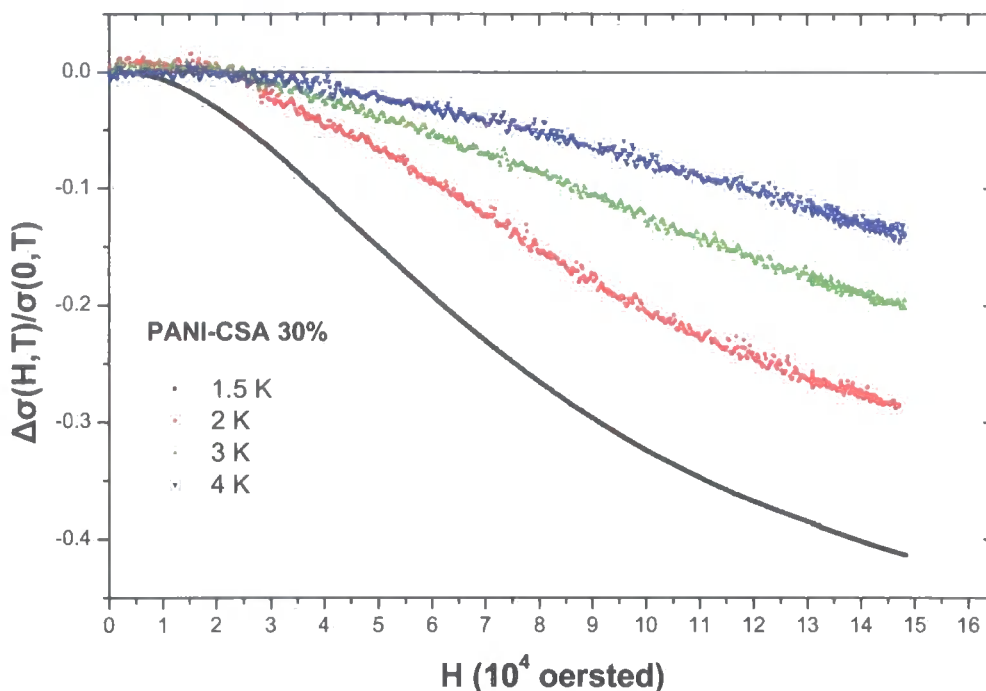
Figure 3-13 Magnetoconductance as a function of the applied magnetic field for the PANI-CSA 30% at different temperatures.

PANI-AMPSA 50%

Figure 3-14 plots the magnetoconductance of PANI-AMPSA 50% as a function of the magnetic field at different temperatures. The data are significantly different to the ones of the PANI-CSA samples, more resembling the magnetoconductance data of certain highly conducting polyacetylene samples as published by Nogami et al. [92]. The positive contribution to the MC increases with increasing temperature and field. The existence of a local minimum for the MC curve at approximately 7.5×10^4 Oe for temperatures below 2 K cannot be explained in the context of the localization-interaction model for any choice of the parameters $a\gamma F_\sigma$ and B_{WL} of equation (3.45). At higher temperatures the MC becomes overwhelmingly positive and such rapid switch from negative to positive MC cannot be explained with the assumption that $a\gamma F_\sigma$ and B_{WL} are temperature independent since it is obvious that such increase requires modification of the coefficients in each of the three terms of (3.45). Hence, the 3D localization theory is not suitable for interpreting the present case.

The inadequacy of the localization-interaction model is not, however, terminal. One of its main theoretical assumptions was that it is valid only for samples in the metallic regime and it is by no means clear that the theory is applicable very near to the transition (always on the metallic regime). The sample PANI-AMPSA 50% was found to be, from the activation energy plots and its resistivity ratio value, in the metallic regime, but closer to the transition in comparison to PANI-CSA 60% where the application of the model was found to be successful (cf. Figure 3-10). Another factor that could explain such insufficiency is the fact that, as Figure 3-14 shows, the maximum MC measured is approximately 1.8%, a value that is strikingly smaller than almost any reported value on conjugated polymers [3, 93]. Such small changes in the conductivity could be affected or even induced by the temperature fluctuations of the sample which are of the order of a tenth of a Kelvin. A quick look at the plots of Figure 3-14 reveals a greater degree of dispersion than other samples. However, such dispersion cannot be an excuse for an altogether dismissal of the current plots since the existence of a certain tendency is traceable enough to be attributed to random factors occurred during the measurement session. The only safe conclusion that can currently be made is that the magneto-transport properties of the PANI-AMPSA 50% cannot be entirely understood within the present theoretical context.
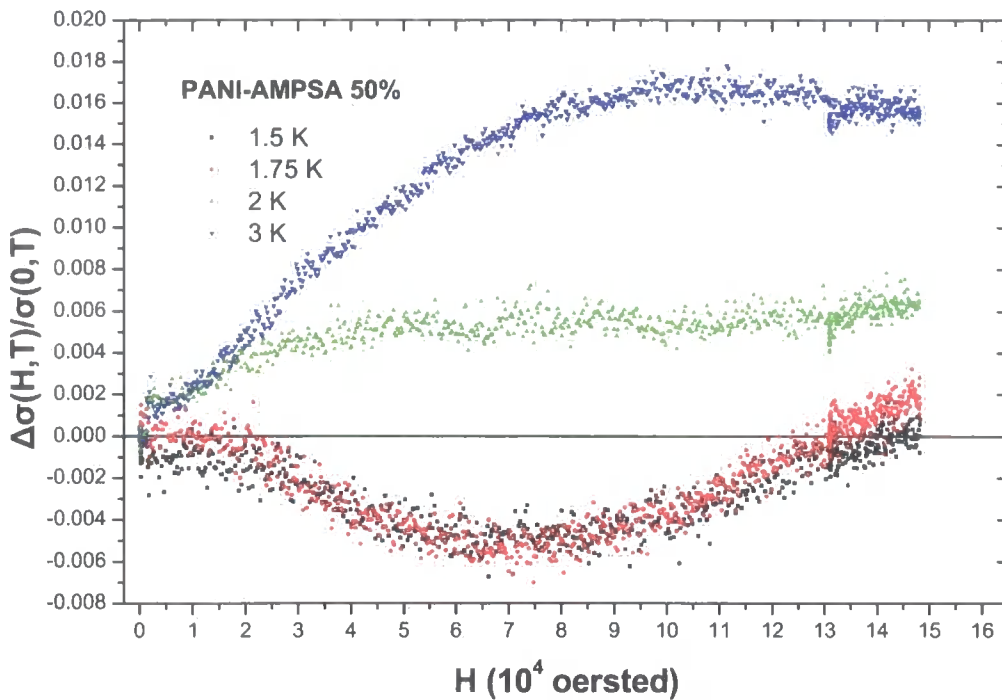
Figure 3-14 Magnetoconductance as a function of the applied magnetic field for the PANI-AMPSA 50% at different temperatures.

3.5 Summary

Low temperature magnetoconductance measurements were performed on three different polyaniline systems. The low temperature conductivity measurements enabled a primary classification of the materials in respect to the extent of the disorder present in their system that determined their position on a virtual metal-insulator transition diagram. More rigid evidence was provided by studying the effect of a varying magnetic field on the charge transport and attempting to interpret it in the context of the 3D localization-interaction model which is valid for samples in the disordered metallic regime of the M-I transition. The model, despite certain shortcomings, can consistently interpret the charge transport properties of a sample being on the metallic side of the transition. An estimate of the competitive contribution of the e-e interaction and weak-localization was obtained. However, the model is found to be inadequate for samples being on the metallic side but close to the transition, whereas in the insulating regime the charge transport occurs through variable-range hopping among localized states. The importance of MC measurements for a sensitive investigation of

the microscopic charge transport mechanism in conducting polymers remains undisputed, although there are still unresolved theoretical issues, prompting the need for an improvement of the available models.

4 Optical Properties of Polyaniline films.

4.1 Introduction.

The interaction with light is one of the most common and informative ways of illuminating the inner workings of solids. A wide range of information about the electronic and vibrational structure of different types of materials, through an immense range of length and time scales, can be obtained from a combination of optical experiments with an appropriate theoretical framework. Due to the vastness of the length and energy scales involved in the interaction of an electromagnetic field with matter, a single theory which provides a satisfactory description of the observed phenomena is almost impossible to be found. Instead, a set of relatively simple ideas and concepts, mostly phenomenological, is frequently used in order to understand most experiments. The optical properties of a material can be determined and analysed as a result of that approach.

This chapter is divided into two discrete, but inseparable parts. Firstly, all the necessary theoretical concepts dealing with electromagnetic wave transport in solids will be concisely presented, elaborating the ideas and physical quantities that will enable the discussion of the experimental results presented in the second part of the chapter. The main aim of this approach is to attempt to understand the observed optical behaviour of Polyaniline in terms of some well established, firmly defined concepts.

Part A. Theoretical Framework.

4.2 Macroscopic Electrodynamics.

4.2.1 Maxwell's Equations

Maxwell's equations remain at the origin of any attempt to describe the interaction of the electromagnetic field with matter and the latter's consequent optical characterization. Because of their classical nature, they are only valid in the limit where the number of photons is very large. Thus they are adequate for explaining the behaviour of a sample under a beam of light, but are unable to predict processes involving a small number of photons, where the wave particle duality should be considered, as with spontaneous emission of photons.

There are two versions of Maxwell's equations commonly used. The microscopic form where the fundamental interactions of charged particles are expressed and the macroscopic form wherein, while retaining the form of microscopic equations, the collective properties of a vast number of individual particles can be sufficiently explained through spatial averaging of their microscopic counterparts.[18]

Maxwell's equations in the *microscopic* form, in standard notation, are

$$\vec{\nabla} \cdot \vec{E} = 4\pi \rho^{micro} \qquad \vec{\nabla} \cdot \vec{B} = 0$$
$$\vec{\nabla} \times \vec{E} = -\frac{1}{c}\frac{\partial \vec{B}}{\partial t} \qquad \vec{\nabla} \times \vec{B} = \frac{4\pi \vec{J}^{micro}}{c} + \frac{1}{c}\frac{\partial \vec{E}}{\partial t} \qquad (4.1)$$

Averaging the microscopic electric and magnetic fields, as well as the microscopic current and charge densities, while retaining the same notation, the *macroscopic* form of Maxwell's equations is obtained:

$$\vec{\nabla} \cdot \vec{E} = 4\pi \rho^{total} \qquad \vec{\nabla} \cdot \vec{B} = 0$$
$$\vec{\nabla} \times \vec{E} = -\frac{1}{c}\frac{\partial \vec{B}}{\partial t} \qquad \vec{\nabla} \times \vec{B} = \frac{4\pi \vec{J}^{total}}{c} + \frac{1}{c}\frac{\partial \vec{E}}{\partial t} \qquad (4.2)$$

We see that the only difference between equations (4.1) and (4.2) is that the microscopic charge and current densities have been replaced by their average values on the small volume ΔV,[19] and the fact that the fields present in (4.2) are the total macroscopic fields.

Introducing the dielectric displacement $\vec{D}$ and the magnetic field vector $\vec{H}$ through the expressions

$$\vec{D} \equiv \vec{E} + 4\pi \vec{P} \qquad (4.3)$$

$$\vec{H} \equiv \vec{B} - 4\pi \vec{M} \qquad (4.4)$$

we can see clearly how external and total fields as well as external and total charge densities are related by obtaining a very common form of Maxwell's equations:

$$\vec{\nabla} \cdot \vec{D} = 4\pi \rho^{ext} \qquad \vec{\nabla} \cdot \vec{B} = 0 \qquad (4.5)$$

---

[18] Such averaging is only valid when the wavelength of the incident light is larger than the volume element ΔV, where the averaging takes place. Generally speaking, the macroscopic form can be used for wavelengths up to the X-ray region.

[19] A general expression of the average of a microscopic quantity $\vec{a}(\vec{r})$ over a small volume ΔV is

$$\vec{A}(\vec{r}) = \langle \vec{a}(\vec{r}) \rangle = (1/\Delta V) \int_{\Delta V} \vec{a}(\vec{r} + \vec{\xi}) d\vec{\xi}, \text{ where } \int d\vec{\xi} \text{ symbolizes } \int dx dy dz. \text{ The volume } \Delta V$$

should satisfy the double inequality $V_i \ll \Delta V \ll \lambda^3$, where V_i is the volume per atom and λ the spatial variation length of the *macroscopic quantity* $\vec{A}$.

$$\vec{\nabla} \times \vec{E} = -\frac{1}{c} \frac{\partial \vec{B}}{\partial t} \qquad \vec{\nabla} \times \vec{H} = \frac{1}{c} \frac{\partial \vec{D}}{\partial t} + \frac{4\pi}{c} \vec{J}^{free} \qquad (4.6)$$

In order to emphasize the physics of the various processes that take place in the material, charge and current are usually divided into two groups: bound and free. A summary of all the possible divisions, which are not fundamental but rather conventional, especially in the case of time varying external fields, is as follows [94]

$$\vec{J}^{total} = \begin{cases} \vec{J}^{bound} = \begin{cases} \vec{J}^{pol} = \dfrac{\partial \vec{P}}{\partial t} \\ + \\ \vec{J}^{mag} = c\vec{\nabla} \times \vec{M} \end{cases} \\ + \\ \vec{J}^{free} = \begin{cases} \vec{J}^{cond} \\ + \\ \vec{J}^{ext} \end{cases} \end{cases} \qquad \rho^{total} = \begin{cases} \rho^{bound} = \rho^{pol} = -\vec{\nabla} \cdot \vec{P} \\ + \\ \rho^{ext} \end{cases}$$

It is apparent that what is meant by free current density does not correspond to the movement of free charge density since current flow in a metal is a result of electron movement, but there is no net charge density since the electronic charge is exactly balanced by the positive nuclei charge.

In the case of time varying fields the distinction between bound electrons and conduction electrons is rendered meaningless, since both type of carriers are participating in oscillatory motion. Thus, the current density $\vec{J} = \vec{J}^{bound} + \vec{J}^{cond}$ now describes the motion of all the types of charges and is related to the polarization $\vec{P}$, which now describes the displacement of all charges, by definition through the expression

$$\vec{J} \equiv \frac{\partial \vec{P}}{\partial t} \qquad (4.7)$$

Now combining Eqs. (4.3) and (4.7), Maxwell's equations (4.6) can be rewritten with only the external current (i.e. introduced into the system from an external source) present

$$\vec{\nabla} \times \vec{E} = -\frac{1}{c} \frac{\partial \vec{B}}{\partial t} \qquad \vec{\nabla} \times \vec{H} = \frac{1}{c} \frac{\partial \vec{D}}{\partial t} + \frac{4\pi}{c} \vec{J}^{ext} \qquad (4.8)$$

4.2.2 Material Equations

Maxwell's equations (4.5) and (4.6) connect the five basic quantities $\vec{E}$, $\vec{H}$, $\vec{B}$, $\vec{D}$ and $\vec{J}$. To allow a unique determination of the field vectors from a given distribution of currents and charges, these equations must be supplemented by relations that describe the response of the material to the applied field. These relations are known as *material equations* (or *constitutive relations*) and in general they are rather complicated. However for a linear, homogeneous and isotropic (l.h.i.) material, they take the relatively simple form

$$\vec{J} = \sigma\vec{E} \tag{4.9}$$

$$\vec{D} = \varepsilon\vec{E} \tag{4.10}$$

$$\vec{P} = \chi\vec{E} \tag{4.11}$$

$$\vec{B} = \mu\vec{H} \tag{4.12}$$

where σ is the *conductivity*, ε the *dielectric constant* (or permittivity) while χ and μ are respectively the *electric susceptibility and magnetic permeability* (μ is equal to one for nonmagnetic samples, like the samples under investigation and henceforth would not be considered) and since the fields under consideration are time-varying, all these physical quantities will be complex.[20]

In general, the time variation of the fields is considered of the form $\exp(-i\omega t)$ so from Eqs. (4.7), (4.3), (4.11) and (4.10)

$$\vec{J} = -i\omega\vec{P} = -i\omega\frac{\varepsilon-1}{4\pi}\vec{E} = -i\omega\chi\vec{E}$$

and consequently σ, χ and ε are related by

$$\varepsilon(\omega) = 1 + \frac{4\pi i}{\omega}\sigma(\omega) \tag{4.13}$$

$$\varepsilon(\omega) = 1 + 4\pi\chi(\omega) \tag{4.14}$$

$$\sigma(\omega) = -i\omega\chi(\omega) \tag{4.15}$$

From Eqs. (4.13) and (4.15) we obtain the expressions relating the real and imaginary parts of the optical quantities:

$$\sigma_1 = \omega\chi_2 \qquad \sigma_2 = -\omega\chi_1 \tag{4.16}$$

$$\sigma_1 = \omega\varepsilon_2 / 4\pi \qquad \sigma_2 = -\omega(\varepsilon_1 - 1) / 4\pi \tag{4.17}$$

---

[20] It should be mentioned that equation (4.9) refers to the total current density $\vec{J} = \vec{J}^{bound} + \vec{J}^{cond}$, being in consistency with equation (4.7).

From Eqs. (4.16) and (4.17) becomes apparent that the knowledge of either a complex dielectric constant, a complex conductivity or a real dielectric constant and a real conductivity is enough for the determination of all the optical constants. In most of the optical studies in the current literature, the real and the imaginary parts of the dielectric constant $\varepsilon = \varepsilon_1 + i\varepsilon_2$ along with the real part of the conductivity are used, i.e. ε_1, ε_2 and σ_1 respectively.

4.2.3 Electromagnetic wave propagation

Considering a l.i.h. medium without the presence of any external sources, or currents, combining Maxwell's equations (4.8) and (4.5) with Eqs. (4.10) and (4.12) and using the vector identity $\vec{\nabla} \times (\vec{\nabla} \times \vec{E}) = \vec{\nabla}(\vec{\nabla} \cdot \vec{E}) - \vec{\nabla}^2 \vec{E}$, the wave equation can be obtained

$$\vec{\nabla}^2 \vec{E} = \frac{\varepsilon \mu}{c^2} \frac{\partial^2 \vec{E}}{\partial t^2} \tag{4.18}$$

Assuming that the material is non-magnetic (μ=1), for a plane wave solution with a complex wave vector[21] $\vec{q} = \vec{q}_1 + i\vec{q}_2$ of the form

$$\vec{E} = \vec{E}_0 e^{i(\vec{q} \cdot \vec{r} - \omega t)} \tag{4.19}$$

the *dispersion relation* can be obtained

$$q^2 = \left(\frac{\omega}{c}\right)^2 \varepsilon \tag{4.20}$$

By defining a complex refractive index through the expression

$$n = n_1 + in_2 \equiv \left(\frac{c}{\omega}\right)q \tag{4.21}$$

and taking z as the propagation direction, with no loss of generality, equation (4.19) becomes

$$\vec{E} = \vec{E}_0 \exp\left[-\frac{\omega}{c}n_2 z\right]\exp\left[i\frac{\omega}{c}n_1 z\right]\exp\left[-i\omega t\right] \tag{4.22}$$

It becomes apparent that the plane wave solutions of (4.18) are attenuated with distance and this attenuation is described by the imaginary part n_2 of the refractive index. The real part n_1 of the refractive index is the usual index of refraction in regions where the material is non-absorbing and it determines the phase velocity through the

---

[21] Since $\vec{q}$ is complex, its magnitude q will be complex as well, with $q^2 = (q_1{}^2 - q_2{}^2 + 2i\vec{q}_1 \cdot \vec{q}_2)$

expression $Re(\omega/q)=c/n_1$. The fractional decrease of the wave intensity with distance is described be the *absorption coefficient* that is defined as

$$\alpha = -\frac{1}{I}\frac{dI}{dz} \quad \text{or} \quad I(z) = I(0)e^{-\alpha z} \tag{4.23}$$

where I is the intensity. Since the intensity is proportional to the square of the fields, from Eqs. (4.22) and (4.23) we find that

$$\alpha = \frac{2\omega n_2}{c} = \frac{4\pi n_2}{\lambda} \tag{4.24}$$

Another useful set of relations are those between the refractive index and the dielectric constant. The dispersion relation (4.20) and the definition (4.21) give

$$\varepsilon = n^2 \tag{4.25}$$

and consequently the real and imaginary parts are related through

$$\varepsilon_1 = n_1^2 - n_2^2 \quad \varepsilon_2 = 2n_1 n_2 \tag{4.26}$$

or

$$n_1 = \left[\frac{1}{2}\left(\sqrt{\varepsilon_1^2 + \varepsilon_2^2} + \varepsilon_1\right)\right]^{1/2} \quad n_2 = \left[\frac{1}{2}\left(\sqrt{\varepsilon_1^2 + \varepsilon_2^2} - \varepsilon_1\right)\right]^{1/2} \tag{4.27}$$

It is apparent that both parts of the refractive index are always positive. It should be explicitly mentioned that all the above quantities are functions of ω only and do no depend on wave vector $\vec{q}$. This assumption is valid for wavelengths larger than the lattice constants, but for other wavelengths the dielectric functions is also a function of $\vec{q}$, i.e. there is spatial dispersion of $\varepsilon(\vec{q},\omega)$ because of the non-local response of the material to the electric field. Excitons in semiconductors and the anomalous skin-effect in metals are examples of spatial dispersion and non-locality.

4.2.4 Optical reflectance

One of the most useful experimental methods to determine the frequency dependence of the optical constants is to measure the reflectivity of the sample as a function of frequency. The *reflectivity coefficient* $r(\omega)$ is a complex function defined as:

$$r(\omega) = \frac{E^r}{E^i} \equiv \rho(\omega)\exp[i\theta(\omega)] \tag{4.28}$$

where E^r and E^i are the amplitudes of the incident and reflected electric fields. In the case of a *normally* incident plane wave, Fresnel's equations [69] give[22]

$$r(\omega) = \frac{n-1}{n+1} = \frac{n_1 + in_2 - 1}{n_1 + in_2 + 1} \qquad (4.29)$$

The quantity measured experimentally is the *reflectance R* [23] which depends on the measured intensities

$$R = \frac{|E^r|^2}{|E^i|^2} = r^*r = |r|^2 = \frac{(n_1 - 1)^2 + n_2^2}{(n_1 + 1)^2 + n_2^2} \qquad (4.30)$$

In principle, it is necessary to measure both the normal-incidence reflectance $R(\omega)$ and the absorption coefficient a in order to calculate from equations (4.24) and (4.30) the refractive index and hence the dielectric function $\varepsilon(\omega)$. In practise, it is sufficient to simply measure $R(\omega)$ over a wide range of frequencies and then deduce the other quantities by using the *Kramers-Kronig* dispersion relations.

4.2.5 Kramers-Kronig Dispersion Relations

A dispersion relation is an integral formula relating a dispersive process to an absorption process, for instance n_1 to the extinction coefficient n_2 [94]. The dispersion relations follow rigorously from the requirement of causality [95]. Causality means that there can be no effect before the cause such as absorption or reflectance before the arrival of the primary light wave. The dispersion relations for linear systems subject to causality are quite general and very useful since they can be used for the calculation of the optical constants of the material by having solely the experimental reflectivity data as a starting point.

The Kramers-Kronig (KK) relations or the *dispersion* relations, show that the real and imaginary parts of a linear response function $G(\omega) = G_1(\omega) + iG_2(\omega)$ are not independent, but satisfy the expressions

$$G_1(\omega) = \frac{2}{\pi} P \int_0^\infty \frac{sG_2(\omega)}{s^2 - \omega^2} ds \qquad (4.31)$$

---

[22] Under the assumption that the incident medium is air whose refraction index is unity. Generally: $r(\omega) = \dfrac{n_c - n_a}{n_c + n_a}$, where n_c and n_a are, respectively, the indices of refraction of the reflective medium ($n_c = n_1 + in_2$) and of the medium in which the incident and reflected waves are measured (usually air).

[23] In the literature the terms reflectivity and reflectance are indiscriminately used for the coefficient R, a practise that will be followed here as well.

and

$$G_2(\omega) = -\frac{2\omega}{\pi} P \int_0^{\infty} \frac{G_1(\omega)}{s^2 - \omega^2} ds \qquad (4.32)$$

where P means the principal value of the integral[24]. A linear response function, such as $\chi(\omega)$ or $\varepsilon(\omega)$, describes the response of a system to an external stimulus and equations (4.31) and (4.32) are quite general since they rely only on causality and spatial locality of the response[25]. Hence, spatial dispersion is neglected and this local approximation is usually valid for wavelengths greater than the lattice constants, as it was mentioned in 4.2.3. However, it must be noted that causality does not presume locality in time and consequently the response may be delayed in time with respect to the stimulus.

According to equation (4.28) $r(\omega)$ is the response function between the incident and reflected waves and therefore (4.31) and (4.32) can be applied to

$$\ln r(\omega) = \ln R^{1/2}(\omega) + i\theta(\omega) \qquad (4.33)$$

since from (4.30) $R(\omega) = \rho^2(\omega)$, to obtain

$$\ln R(\omega) = \frac{4}{\pi} P \int_0^{\infty} \frac{s\theta(\omega)}{s^2 - \omega^2} ds \qquad (4.34)$$

and

$$\theta(\omega) = -\frac{\omega}{\pi} P \int_0^{\infty} \frac{\ln R(\omega)}{s^2 - \omega^2} ds \qquad (4.35)$$

Hence, from the experimentally measured reflectivity $R(\omega)$, the phase $\theta(\omega)$ can be obtained and the real and imaginary parts of the refractive index are subsequently determined from $\rho(\omega)$ and $\theta(\omega)$ by the relations [97]

$$n_1 = (1 - \rho^2)/(1 + \rho^2 - 2\rho\cos\theta) \qquad (4.36)$$

$$n_2 = 2\rho\sin\theta/(1 + \rho^2 - 2\rho\cos\theta) \qquad (4.37)$$

---

[24] The *Cauchy principal value* of a definite integral $\int_A^B f(x)dx$ whose integrand becomes infinite at a point α in the interval of integration, i.e. $\lim_{x \to \alpha} |f(x)| = \infty$, is defined as

$$P \int_A^B f(x)dx = \lim_{\varepsilon \to 0} \left[\int_A^{\alpha - \varepsilon} f(x)dx + \int_{\alpha + \varepsilon}^B f(x)dx \right]$$

In many cases, the principal value exists even when the integral itself has no meaning [96].

[25] If spatial dispersion, i.e. a non local response, is included the Kramers-Kronig become more complicated and will not be examined here.

which are direct consequences of (4.29). Therefore $\rho(\omega)$ and $\theta(\omega)$ specify completely the optical constants and from their knowledge, all the optical quantities (e.g. refractive index, dielectric function etc.) mentioned in 4.2.2 can be determined. However, since it is impossible to measure the reflectivity $R(\omega)$ from zero to infinite frequency to evaluate the integral (4.35), it becomes necessary to use extrapolations to both low and high frequencies. This issue will be examined in the experimental section.

4.3 The Dielectric Function.

Among the aforementioned optical functions, probably the most important one is the dielectric function $\varepsilon(\omega)$, which for an isotropic material relates $\vec{D}(\omega)$ with $\vec{E}(\omega)$ through $\vec{D}(\omega) = \varepsilon(\omega)\vec{E}(\omega)$. The importance of the dielectric function rests in the fact that the knowledge of its frequency dependence could in principle enable the classification of the material in the two main categories, i.e. conductor and insulator. Furthermore, as discussed in 4.2.3, a wide range of physical quantities could be expressed through it, while the microscopic behaviour of the material is reflected on its dependence from ω. Hence, by applying an appropriate model, the dielectric function can act as a bridge between microscopic and macroscopic properties.

4.3.1 Mechanical Oscillators as Dielectric Function

This is a phenomenological and classical model that describes elementary electromagnetic interactions with matter, but a quantum mechanical analogue also exists. It is based on the Lorentz and Drude classical theory of absorption and dispersion of light and it is often called the *Lorentz oscillator* model. The basic assumption is that the electrons are bound to their cores by harmonic forces and divided into groups where each of them contains f_i electrons per unit volume. Obviously,

$$\sum_i f_i = n \tag{4.38}$$

where n is the electron density. Under the presence of a field (external and induced at the same time) $\vec{E}(\omega)$ the motion of an electron I is given by

$$m\ddot{\vec{r}}_i + m\gamma_i\dot{\vec{r}}_i + m\omega_i^2\vec{r}_i = -e\vec{E} \tag{4.39}$$

where m and e are the mass and charge of the bound electron, ω_i is the natural oscillator frequency, γ_i is the damping constant of the velocity dependent damping term. Up to the ultraviolet frequency region, the applied field can safely be written in the form

$$\vec{E}(\vec{r},t) = \vec{E}(\omega)\exp[-i\omega t] \tag{4.40}$$

and the solution of (4.39) is

$$\vec{r}_i(\omega) = \frac{-e\vec{E}/m}{(\omega_i^2 - \omega^2) - i\gamma\omega} \tag{4.41}$$

Hence the electron velocity is $\vec{v}_i = \dot{\vec{r}}_i = -i\omega\vec{r}_i$ and the current $\vec{j}_i = -ef_i\vec{v}_i$. Therefore the conductivity $\sigma = \vec{j}/\vec{E} = (\sum_i \vec{j}_i)/\vec{E}$ is equal to

$$\sigma(\omega) = \sum_i \frac{-i\omega f_i e^2}{m(\omega_i^2 - \omega^2 - i\gamma_i\omega)} \tag{4.42}$$

and consequently from (4.13), the dielectric function is given by

$$\varepsilon(\omega) = 1 + \frac{4\pi e^2}{m} \sum_i \frac{f_i}{(\omega_i^2 - \omega^2) - i\gamma_i\omega} \tag{4.43}$$

We see that, according to (4.43), each group of oscillating electrons contributes to the dielectric function according to f_i. The parameter f_i is called the oscillator strength and quantum mechanically is a measure, after the necessary normalization, of the relative probability of a quantum mechanical transition [98].

Equation (4.43) can describe, for a suitable choice of the constants f_i, ω_i and γ_i, quite successfully the behaviour of the dielectric function $\varepsilon(\omega)$ of a wide range of materials. The frequencies ω_i can be estimated quite easily since they often represent characteristic eigenfrequencies of the system. Following a similar methodology, the ionic contribution, which arises from the displacement of a charged ion with respect to other ions induced by the applied field, to the dielectric function is given by an expression similar to (4.43) [99]

$$\varepsilon(\omega) = \varepsilon_\infty + \sum_{i=1}^{p} \frac{S_i^2}{(\omega_{0i}^2 - \omega^2) - i\gamma_i\omega} \tag{4.44}$$

where $S_i^2 = 4\pi Q^2 N_i / \mu V$ with Q being the dynamic apparent charge of the ion since a point charge is a poor approximation for deformable atoms, N_i/V is the number of ion pairs per unit volume, μ the reduced mass of the positive-negative ion system, and p is the number of modes with oscillating dipole moments. In (4.44), 1 has been replaced by ε_∞. The physical reason is simple: ε_∞ summarises the dielectric response of all the processes that occur at frequencies higher than those in the lattice vibrational region which are considered in expression (4.44), while the "infinity" subscript denotes the fact that the electronic resonances, described by (4.43), are at very much higher ener-

gies than lattice resonance. Polar molecules also contribute to the dielectric function, but at a very low frequency range (UHF to microwaves) [99, 100]. The various contributions from each one of the aforesaid factors to the real part of the dielectric function over the whole spectrum range are schematically shown in Figure 4-1.
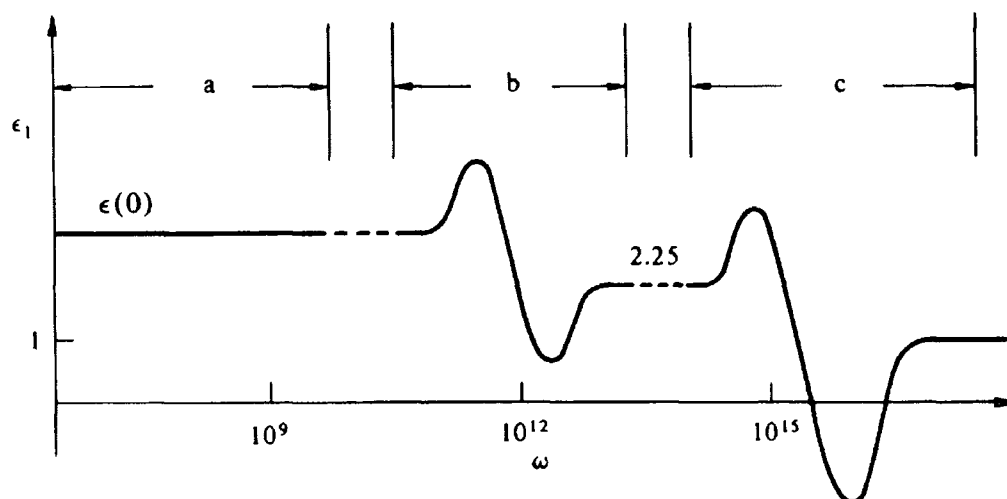
Figure 4-1 A schematic diagram of the real part of the dielectric constant, ε_1, against frequency showing each contribution to the dielectric function per spectral region. Hence, region a) shows the relaxation of the permanent dipoles or perhaps impurities, region b) is due to lattice vibration (ionic polarization) and region c) is due to electronic contribution (from valence and bound electrons). This figure was taken from reference [99], page 459.

Note: An important remark regarding the derivation of equation (4.43) must be made in order to avoid confusion. The electric field $\vec{E}$ used in (4.39) is the *mean* macroscopic field, which has implicitly assumed to be the same as the microscopic field (or local field) $\vec{E}_{loc}$ acting on an individual electron (or ion). However, this is generally not the case since in many cases fluctuations in the value of $\vec{E}_{loc}$ between sites are significant, resulting in $<\vec{E}_{loc}> \neq \vec{E}$ because $<\vec{E}_{loc}>$ is usually an average over atomic sites and not over regions between sites. In this case a relation between $\vec{E}_{loc}$ and $\vec{E}$ should be established and $\vec{E}_{loc}$ must replace $\vec{E}$ in (4.39). This is a problem of considerable complexity, yet the relation is known when certain assumptions have been made. A detailed investigation of this topic can be found in reference [67] (pp. 539-542). This topic will not be pursued further since the mean field assumption that has been made is sufficient to describe the properties of the materials under investigation, at least in a reasonable approximation. The local field correction is mainly

necessary for insulating materials, where the electrons are trapped close to the mole-cule and the local field value $\vec{E}_{loc}$ is very different from the macroscopic value $\vec{E}$, which also includes the regions between the molecules [94].

4.3.2 The Lorentz and Drude Models.

Lorentz model: The general expression of the *Lorentz* electronic oscillator model is immediately elicited from expression (4.43) after a rearrangement of terms and the inclusion, in a somewhat ad hoc manner[26], of the term ε_∞ for reasons already men-tioned. Hence,

$$\varepsilon(\omega) = \varepsilon_\infty + \sum_i \left(\frac{4\pi e^2 N_i}{mV} \right) \frac{1}{(\omega_{0i}^2 - \omega^2) - i\gamma_i \omega} \qquad (4.45)$$

where the sum is over the i different types of oscillating electrons of density N_i/V. For only one group of oscillating electrons, the real and imaginary part of (4.45) take the simple form

$$\varepsilon_1(\omega) = \varepsilon_\infty + \left(\frac{4\pi e^2 N}{mV} \right) \frac{(\omega_0^2 - \omega^2)}{(\omega_0^2 - \omega^2)^2 + \gamma^2 \omega^2}$$

$$\varepsilon_2(\omega) = \left(\frac{4\pi e^2 N}{mV} \right) \frac{\gamma \omega}{(\omega_0^2 - \omega^2)^2 + \gamma^2 \omega^2} \qquad (4.46)$$

Figure 4-2 shows a plot of equations (4.46) for a random choice of parameters. It must be mentioned that neither of the two functions peak exactly at ω_0. The only function that peaks exactly at ω_0 for any value of γ ω_0 is the real part of the optical conductiv-ity $\sigma_1 = \omega \varepsilon_2 / 4\pi$.

Drude model: In the Lorentz oscillator model, the presence of the frequency ω_0 implies that the electron is bound. Therefore, to get the expression for a gas of free electrons with density N/V, it is sufficient to put $\omega_0 = 0$ in (4.45) or (4.46). Hence, the expressions that give the dielectric function of an electron gas are

$$\varepsilon(\omega) = \varepsilon_\infty - \frac{\omega_p^2}{\omega^2 + i\gamma\omega} \qquad (4.47)$$

where

$$\omega_p^2 \equiv \frac{4\pi e^2 N}{mV} \qquad (4.48)$$

---

[26] A more complete theory that includes oscillators at far higher frequencies than the region of ω under study would give this term automatically.

and $\gamma=\tau^{-1}$ with τ being the relaxation time. The quantity ω_p is called the *plasma frequency* and its importance will be discussed afterwards. Table 4-1 shows characteristic values of the above parameters for conventional metals [100]. The Drude model can be applied also for the free carriers that are introduced into semiconductors by doping, behaving in many ways like those in simple metals. However since the dopant concentration is typically less than 10^{20} cm^{-3}, the plasma frequencies of carriers in semiconductors are usually in the infrared range whereas, as Table 4-1 demonstrates, they are in the visible or ultraviolet for metals.

Table 4-1 Typical values of the dc conductivity, the electron concentration, the plasma frequency and the relaxation time for characteristic metals. For a good metal $\omega_p\tau\gg1$ ($10\mathrm{eV}=1.5\times10^{16}$ sec^{-1}), i.e. the damping is very small compared to the plasma frequency.

	σ $(10^5$ S/cm$)$	N/V $(10^{22}$ cm$^{-3})$	ω_p (eV)	τ $(10^{-14}$ sec$)$
Ag	6.21	5.85	8.97	3.7
Cu	5.88	8.45	10.7	2.5
Al	3.65	18.06	15.8	0.71
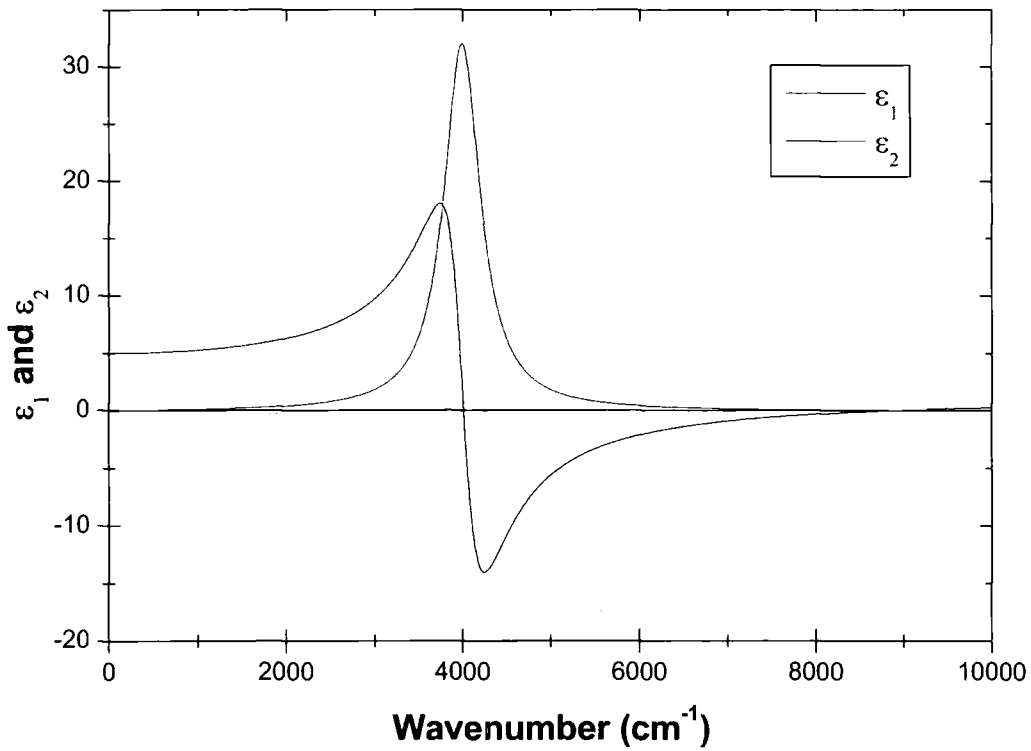
Figure 4-2 Plot of the real and imaginary part of a Lorentz oscillator with one type of oscillating frequency as given by equations (4.46), after taking $\gamma/\omega_0=1/8$ (modestly damped system), $\omega_0=4000$ cm^{-1} and $\varepsilon_\infty = 1$. For $\gamma \rightarrow 0$, ε_1 goes to infinity for frequencies close to ω_0, demonstrating the necessity of the damping term in the model.

From (4.47), the expressions for the real and imaginary part of the dielectric function are obtained

$$\varepsilon_1(\omega) = \varepsilon_\infty - \frac{\omega_p^{\;2}}{\omega^2 + \gamma^2}$$

$$\varepsilon_2(\omega) = \frac{\omega_p^{\;2}\gamma}{\omega(\omega^2 + \gamma^2)}$$

(4.49)

Figure 4-3 shows the behaviour of ε_1 and ε_2 for a typical metal like Ag. Combining (4.17) and (4.49), the expression for the complex optical conductivity is also obtained

$$\sigma = \frac{\sigma_0}{1 - i\omega\tau}$$

(4.50)

where $\sigma_0 \equiv \tau e^2 N / mV$ and the real part is given by

$$\sigma_1 = \frac{\omega_p^{\;2}\tau}{4\pi(1 + \omega^2\tau^2)} = \frac{\omega_p^{\;2}\gamma}{4\pi(\omega^2 + \gamma^2)}$$

(4.51)

Equations (4.50) and (4.51) give the so called *Drude* conductivity.
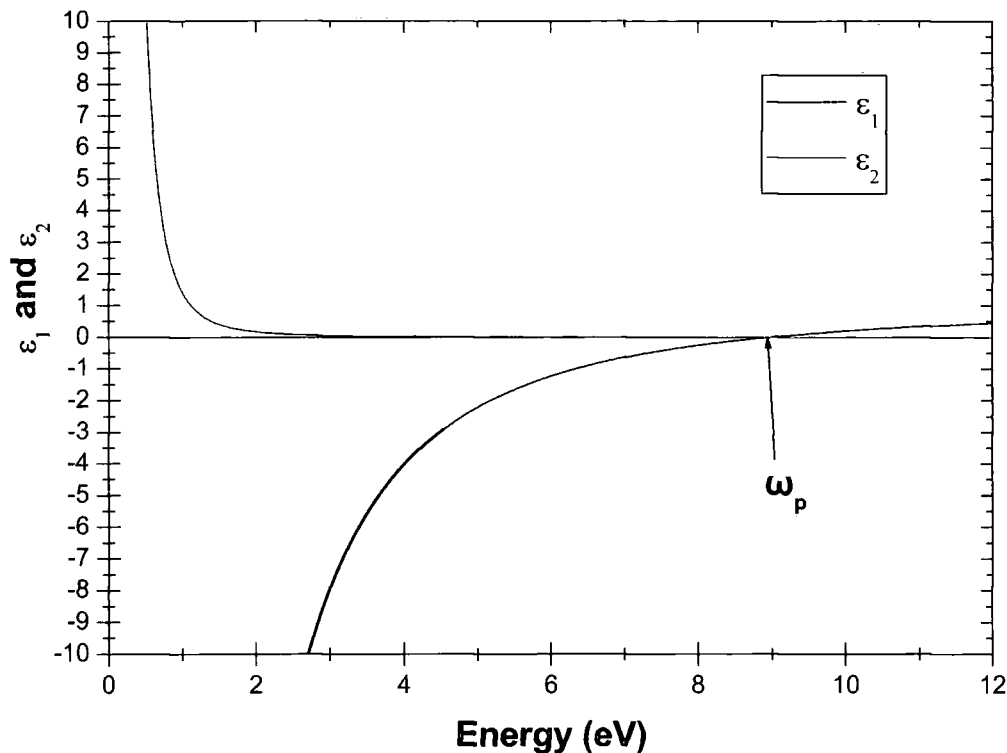
Figure 4-3 Plot of the real and imaginary parts of the dielectric functions as described by the Drude model and given by equations (4.49).The values of Ag from Table 4-1 were used. The zero of the real part of the dielectric function occurs at the plasma frequency ω_p.

4.3.3 Longitudinal oscillations and dielectric function.

During the discussion about electromagnetic wave propagation in 4.2.3, we had considered only transverse wave solutions of the form given by (4.19), where the wave vector $\vec{q}$ is perpendicular to $\vec{E}$ and satisfies the equation

$$\varepsilon(\omega)\vec{q} \cdot \vec{E} = 0 \qquad (4.52)$$

which can be directly obtained by substituting (4.19) onto the Maxwell's equation (4.5). However, more generally $\vec{q}$ (and the atomic displacements) should be decomposed into parts parallel and perpendicular to $\vec{E}$. The parallel or longitudinal part $\vec{q}_{\parallel}$ can also satisfy equation (4.52) for any frequency ω_l provided that

$$\varepsilon(\omega_l) = 0 \qquad (4.53)$$

Therefore *the poles (zeros) of the dielectric constant determine the longitudinal oscillations of the system*. When $\varepsilon=0$, $\vec{E}$ is not necessary zero, even for $\vec{D} = 0$. In fact,

from (4.3) we get that $\vec{E}_l = -4\pi\vec{P}$. This implies that no external causes are required to generate an electric field and consequently the particles of the system partake in a collective oscillation with ω_l being a normal mode of the system. The collective oscillation generates $\vec{E}$ from the polarization induced by the oscillations and $\vec{E}$ afterwards acts as a restoring force to the longitudinal oscillation. Hence, without damping a collective oscillation continues ad infinitum [99, 101].

Now let us consider the free electron oscillations, whose behaviour could be described by the Drude equations (4.49). Such collective longitudinal oscillations are known as *plasma oscillations* and the energy of these oscillations can be quantized into units of $\hbar\Omega_p$. The quantized entities are called plasmons and the frequency Ω_p is the *plasma frequency*, which was referred at the discussion of the Drude model. In practice, a well defined plasma frequency can be observed if $\varepsilon_1(\Omega_p) = 0$ and $\varepsilon_2(\Omega_p) \ll 1$. By introducing the energy loss function

$$\mathrm{Im}(-1/\varepsilon) = \frac{\varepsilon_2^{\,2}}{\varepsilon_1^{\,2} + \varepsilon_2^{\,2}} \qquad (4.54)$$

which gives the energy loss by a charged particle moving in a solid, the plasma frequency can in practice be identified by a peak in $\mathrm{Im}(-1/\varepsilon)$ that occurs at the frequency where $\varepsilon_1(\Omega_p) = 0$. By solving equation (4.49), we get

$$\Omega_p^{\,2} = \frac{\omega_p^{\,2}}{\varepsilon_\infty} - \gamma^2 \qquad (4.55)$$

with $\omega_p^{\,2} \equiv \dfrac{4\pi e^2 N}{mV}$ representing the unscreened plasma frequency defined in the Drude model[27]. For a very good metal $\omega_p\tau \gg 1$ and by ignoring any interband transitions at high frequencies, the distinction between Ω_p and ω_p ceases to exist.

4.4 Applications to real systems.

4.4.1 Summary of experimentally observed structures.

The optical constants are widely used for observing the kinds of structures and identifying the generic types of elementary excitations that are usually used to de-

---

[27] This expression is correct only for free electrons. In the presence of a periodic potential, the plasma frequency is modified. Conventionally, the electron mass m is replaced by an effective mass called the optical mass.

scribe them. Such elementary excitations are intra and interband individual-particle excitations (Drude and Lorentz models respectively) and collective plasma resonances. A summary of some commonly observed structures, as it is reflected on the behaviour of the optical constants, is given schematically in Figure 4-4.

The first two panels of Figure 4-4, a) and b), deal with the free electron region in metals; a) shows the free electron behaviour which usually occurs in the infrared, whereas b) shows the effect off the low energy interband transitions on the free electron behaviour. At the onset of the interband transitions, the reflectance drops and both ε_2 and $Im(-1/\varepsilon)$ increase. The other panels are applicable to both semiconductors and metals. Panel c) shows a region where the interband transitions are dominant. In that region, a peak in the reflectance and $Im(-1/\varepsilon)$ and possibly an oscillator-like behaviour of the real and imaginary part of the dielectric function can be observed. Panel d) deals with a region where the plasma effects determine the behaviour of the optical constants. In that region the reflectance drops precipitously in accord with the fact that the plasma frequency separates the reflecting and transmitting regions in free-electron metals. In addition there is a peak in $Im(-1/\varepsilon)$ and the necessary conditions for a well defined plasma oscillations are satisfied since $\varepsilon_1=0$ and $\varepsilon_2<<1$. While it is in general not possible to distinguish plasma and interband effects from the appearance of the energy loss function $Im(-1/\varepsilon)$ (it peaks in both cases), such a distinction can be made unambiguously if the dielectric function is known precisely so that the given conditions that determine each kind of effect can be inspected. However, this in not always feasible in the case of diffuse structures. Panel e) shows that the effect of the interband transitions to the plasma frequency is to modify the energy at which this actual occurs by lowering the frequency at which ε_1 passes through 0 and consequently the plasma frequency. Finally, panel f) illustrates the phenomenon of excitation from deeper bands that are mostly observed in the far ultra-violet and X-ray region. Since such excitations occur at high energies, the structure in the dielectric constant is rather featureless [102].
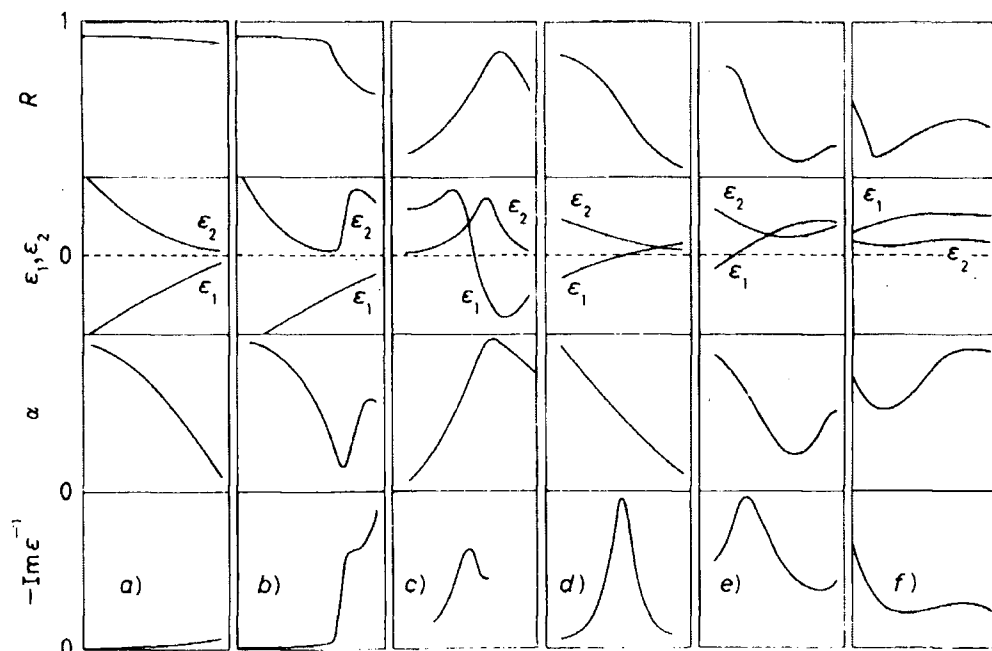
Figure 4-4 Typical behaviour of the optical constants as associated with the various excitation processes that take place in metals and insulators. For metals: a) free electron range as described by the Drude model, b)low-energy interband transitions. For semiconductors or metals: c) interband transitions, d) plasma region, e) plasma region modified by interband transitions, f) excitation of deeper bands above plasma frequency. Figure was taken from reference [102], page 151.

4.4.2 Sum rules.

The basic optical properties of solids despite their great diversity are rigorously limited by nature. These limitations take the form of sum rules and dispersion relations (such as the Kramers-Kronig relations) that reflect the physical laws governing the dynamics of matter and its interaction with light. Sum rules exist for both absorption and dispersive processes. A typical example of the latter is the sum rule

$$\int_0^\infty \left(n_1(\omega) - 1 \right) d\omega = 0 \qquad (4.56)$$

which shows that the real part of the refractive $n = n_1 + in_2$ averaged over all frequencies must be unity [103]. It can be shown that this restriction arises in part from the inertial property of matter. Related rules –with similar physical interpretation- can been applied to the dielectric function and to the loss function. Formally such rules are a consequence of the asymptotic behaviour of the optical functions and the Kramers-Kronig dispersion relations [104]. Hence, they arise physically from causality and

the dynamical laws of motion and may be viewed as a restatement of these laws in frequency space.

The best-known optical sum rule is the f (oscillator strength) sum rule [97, 103, 105], a common form of which is

$$\int_0^\infty \omega\varepsilon_2(\omega)d\omega = \frac{2\pi^2 e^2 N}{Vm} \tag{4.57}$$

where N/V denotes the total electron density. Alternatively, for the real part of the optical conductivity $\sigma_1(\omega)$, we obtain

$$\int_0^\infty \sigma_1(\omega)d\omega = \frac{\pi e^2 N}{2mV} \tag{4.58}$$

Often it is more useful to define the effective density of carriers, $n_{eff}(\omega_0)$ contributing to the optical properties up to an energy ω_0, and the partial sum law can be obtained following (4.58)

$$\int_0^{\omega_0} \sigma(\omega)d\omega = \frac{\pi e^2}{2} \frac{n_{eff}(\omega_0)}{m} \tag{4.59}$$

The application of (4.59) enables us to comprehend sometimes what kind of carriers (free electrons or bound) contribute to the optical properties within the examined frequency region. Clearly for $\omega_0 = \infty$, n_{eff} is equal to the total number of electrons per atom.

Part B. Experimental Results.

4.5 An overview of the techniques used for reflectance measurements.

A general configuration for reflectance measurements is schematically shown in Figure 4-5. The source provides collimated monochromatic light that passes through the entrance optics and through the exit optics before reaching the detector and after having been reflected from the sample surface. The entrance and exit optics measure and analyze the intensity and/or the polarization state of each beam, while the detector may determine absolute or relative intensities and their time dependencies [106].
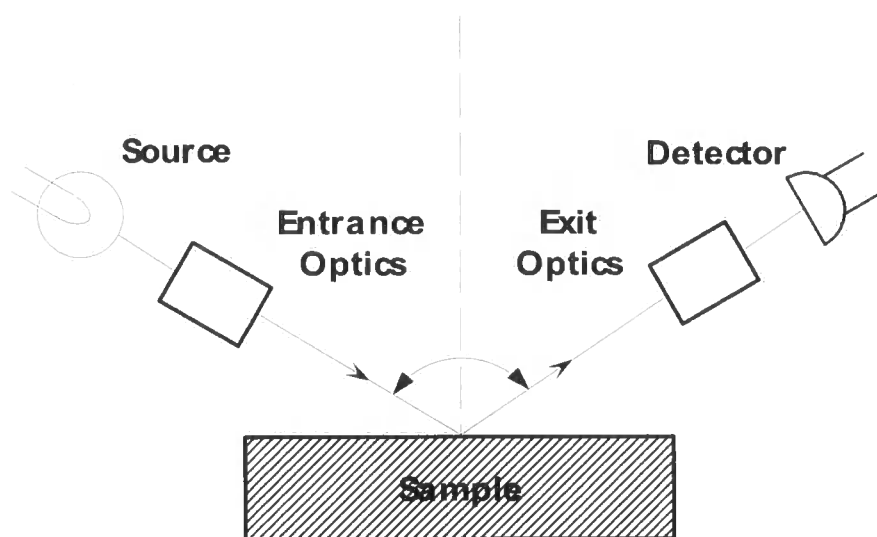
Figure 4-5 A generalised configuration for reflectance studies.

The configuration of Figure 4-5 is applicable for various reflectance methods ranging from ellipsometry to reflectometry. Reflectometry and ellipsometry are two different techniques of deriving information about the sample properties through its interaction with the light beam in a way similar to that portrayed in Figure 4-5. Ellipsometry is, for an isotropic sample, a strictly non-normal incidence technique that deals with intensity independent complex quantities, while reflectometry, since it measures intensities, is fundamentally a power measurement. Ellipsometry is significantly a more powerful method since by virtue a complex quantity such as the dielectric function can be directly obtained without resorting to multiple measurements and Kramers-Kronig transformations. Another big advantage of ellipsometry is its excep-

tional accuracy since ellipsometric measurements are relatively insensitive to any intensity fluctuations of the source, temperature drifts of electronic components and macroscopic roughness [106]. An ellipsometer, however, is a far more complicated instrument than a reflectometer and transmission through various optical elements like polarizers is usually required, limiting its spectral range of applicability since good quality transmitting elements are not available for every frequency range.

Reflectometry is a simpler, less precise, but still very useful technique. Its great advantage is its simplicity. For instance, in the case of a normal-incidence reflectometer, no entrance or exit optics are required. Therefore, with the appropriate combination of light sources and detectors, a wide range spectral range can be covered. The precision of this method can be increased if a double beam configuration is used; however, this is not always feasible. It is generally easier to increase accuracy by reducing or taking account of any macroscopic roughness that scatters the light away from the detector. The special care put on this issue will be emphasized shortly in the description of the experimental configuration used for the measurements on polyaniline films.

4.6 Experimental configuration for infrared reflectivity measurements.

Normal incidence infrared reflectivity measurements between 20 and 9000 cm^{-1} (or 0.002-1.116 eV) were taken using a Bruker IFS66v/S Fourier transform interferometer at NSLS (Beamline U10A) in Brookhaven National Laboratory [107]. The general instrument and beamline characteristics are shown below (as taken from the web page: http://infrared.phy.bnl.gov/u10a.htm):

- Frequency range (cm^{-1}): 20 > 25,000
- Resolution (cm^{-1}): 0.11
- Brightness (relative to 1000K black-body source): 100-1000
- Total angular acceptance (milliradians): 40H x 40V
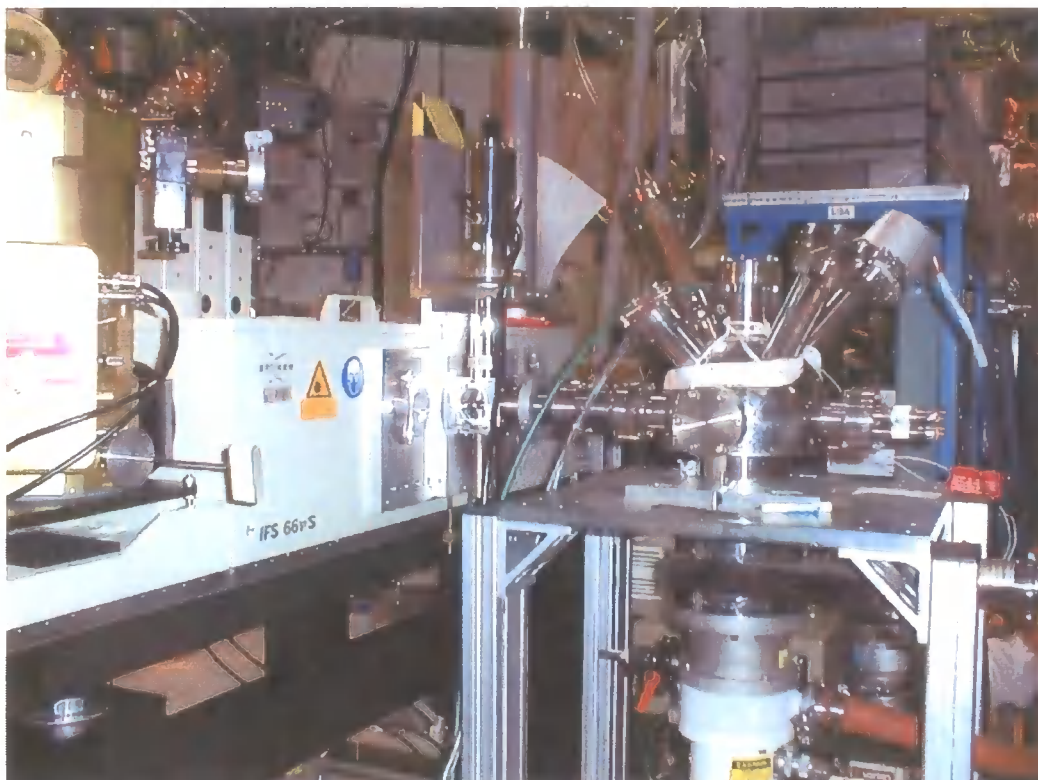
Figure 4-6 A photograph of the Bruker IFS66v/S at the National Synchrotron Light Source (NSLS) in reflectance configuration where the beam is drawn out of the instrument to the reflectance chamber attached on the side.

Figure 4-6 shows a photograph of the entire instrument. The reflectance chamber attached to the side of the instrument contains the sample, the reference mirror and a built in facility for evaporation onto the sample surface. The instrument operates under vacuum for improved perfomance, while the sample chamber is under high vacuum with pressure values being less than 10^{-5} mbar. There are three internal sources in addition to the broad band external synchrotron source. An Arc lamp can be used for the far infrared (10-500 cm^{-1}), a Globar for the mid infrared (100-6000 cm^{-1}) and a Tungsten lamp for the near infrared and the visible regions (3000-25000 cm^{-1}). There is a variety of detectors (e.g. 4.2K Si:B bolometer, room temperature DTGS[28] pyroelectric detectors) and beam splitters for every spectral region of interest. The instrument has an option that enables changing the sources and, to a lesser extent the detector, while it is under vacuum, thus facilitating the overlap between different spectral regions.

---

[28] DTGS stands for deuterated tri-glycine sulfate pyroelectric. These are the most common detectors used in Fourier Transform infrared instruments mainly due to their ease of use, good sensitivity, wide spectral responsivity and excellent linearity.

For the infrared reflectivity measurements, each sample was visually inspected for surface quality sufficient to minimise scattering losses and then mounted as flat as possible inside the vacuum chamber of the spectrometer, where the pressure was less than 10^{-5} mbar, as mentioned above. The reflectivity of the sample with respect to an Al reference mirror was initially measured. Immediately afterwards, without altering the configuration, gold was evaporated on the sample surface using the built-in evaporator chamber. The reflectivity of the gold-coated surface with respect to the Al mirror was used for correcting the reflectance data by taking into consideration surface imperfections. Hence, the absolute reflectivity of the sample was finally obtained after using the absolute Au values from the literature for the final correction[29]. The two aforementioned measurement sessions can be described schematically as:

a) Reflectivity of the sample with respect to reference Al mirror:

$$R_1^{meas} = \frac{I_{sample}}{R_{Al} I_{Incident}}$$

b) Reflectivity of the gold coated sample surface with respect to Al mirror:

$$R_2^{meas} = \frac{I_{Au} R_{Au}}{R_{Al} I_{incident}}$$

Consequently, the measured reflectivity of the sample, which takes into account any surface imperfections, is given by the ratio of R_1 and R_2

$$R_{sample}^{meas} = \frac{I_{sample}}{I_{Au} R_{Au}}$$

and the absolute reflectivity value is obtained by multiplying with R_{Au}, as given in the literature and explained in the footnote below. A variety of light sources, beam splitters and detectors was used in order to cover the whole frequency range; the overlap between the different regions was excellent.

---

[29] This fact can be explained in more detail as follows:
The reflectivity measured is generally defined as

$$R_m = \frac{\text{Reflected Intensity detected}}{\text{Incident Intensity detected}} = \frac{I_{sample}}{R_{ref} I_{incident}}$$

Therefore the corrected reflectivity value is given by the expression:

$R_{correct} = R_m R_{ref} = \dfrac{I_{sample}}{I_{incident}}$, where the reference values R_{ref} are taken from the literature and refer to

the values of the surface used (usually Al or Au) to get the approximate value of the incident intensity.

4.7 Sample preparation.

The sample preparation technique is identical to that described in section 2.3.2. Similar considerations regarding the connection between sample preparation and the degree of disorder apply.

4.8 Optical properties of PANI films. Results and discussion.

In general, optical measurements can provide information about the charge carrier dynamics over a wide energy range, through processes occurring on smaller time scales ($\sim\omega^{-1}$) than transport ones. With the application of an appropriate model, furthermore, they can give further evidence about the extent of the disorder and other significant parameters for the understanding of the I-M transition.

Optical measurements were conducted on a series of PANI-AMPSA films with four different doping levels and on the most and least conductive, according to the transport behaviour discussed in Chapter 2, PANI-CSA samples. Table 4-2 lists all the samples that will be examined along with their previously reported (section 2.5) conductivity values.

Table 4-2 The room temperature conductivity, the peak conductivity with its respective temperature and the resistivity ratio ρ_r for all the samples selected for optical measurements.

Sample	σ_{dc} (295 K) S/cm	$T(\sigma_{dc}^{peak})$ (K)	σ_{dc}^{peak} S/cm	ρ_r
PANI-AMPSA 30% (A1)	60	230	61	1.140
PANI-AMPSA 40% (A2)	87	125	93	0.969
PANI-AMPSA 50% (A3)	110	80	122	0.920
PANI-AMPSA 60% (A4)	68	150	74	0.963
PANI-CSA 30% (C1)	35	245	35	1.337
PANI-CSA 60% (C4)	202	120	216	0.956

4.8.1 Infrared Reflectivity

Figure 4-7 displays the room temperature reflectivity spectra (20-9000 cm^{-1}) of all the samples in Table 4-2. All samples manifest reflectivity values greater than 80% in the far infrared ($\omega \leq 100$ cm^{-1}), exceeding values of 90% for the most conducting samples A3 and C4. The effect of the disorder on the reflectivity values is apparent since the reflectivity, unlike the one of a typical metal (Figure 4-4, first panel), drops monotonically until the onset of interband transitions that occur in the visible spectral range [108]. Obvious phonon features appear between 200-2000 cm^{-1} and, contrary to typical metals, are insufficiently screened by the free electrons.
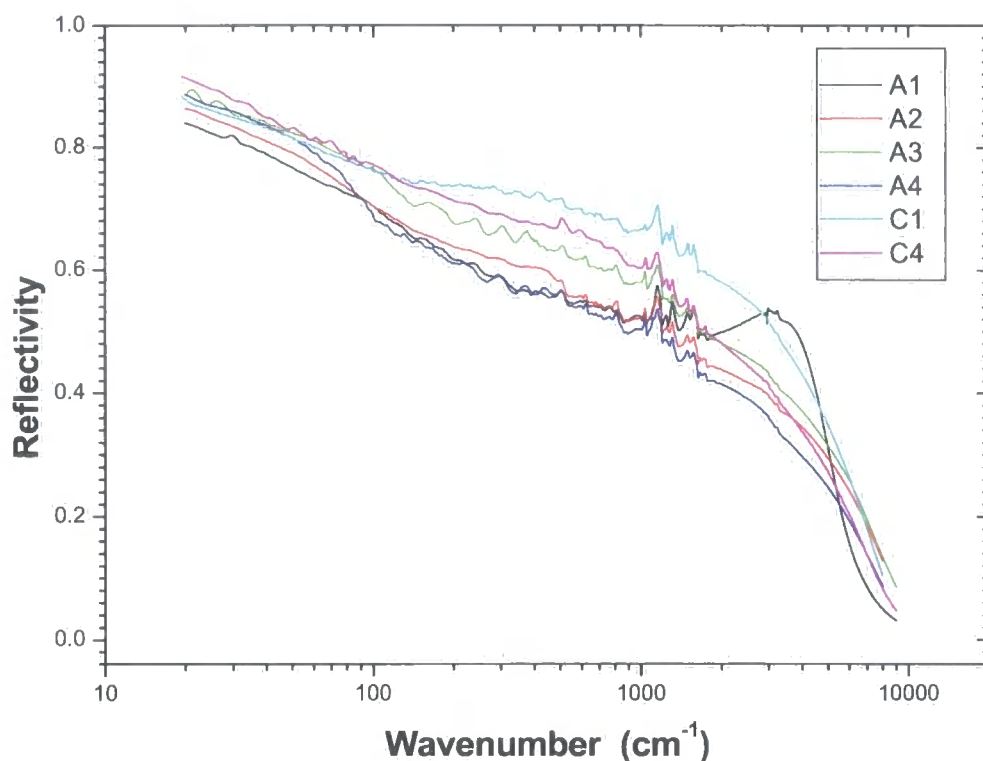
Figure 4-7 Semi log plot of the room temperature reflectivity for the PANI samples listed in Table 4-2.

4.8.2 Kramers-Kronig transformation of the Reflectivity data

The principal purpose of the reflectivity data is the calculation, through the Kramers-Kronig (KK) integral transformations, of the complex dielectric constant, $\varepsilon=\varepsilon_1+i\varepsilon_2$, which describes the optical properties of the system in a more detailed manner. Reflectivity measurements, however, are usually only available over a limited frequency range. Therefore, the use of the dispersion relations explained in 4.2.5 necessitates 'physically reasonable' extrapolations of the reflectivity data outside the measured interval. For the analysis of the reflectivity data taken from polyaniline samples, the following extrapolations were used:

- For the very low frequency region ($\omega<20$ cm^{-1}), metallic behaviour was assumed in accordance with the very high reflectivity values displayed in Figure 4-7 and the reflectivity data were extrapolated according to the *Hagen-Rubens* relation

$$R(\omega)=1-\left(2\omega/\pi\sigma_{dc}\right)^{1/2} \tag{4.60}$$

- For the high frequency behaviour (ω>9000 cm^{-1}), the reflectivity data were assumed to behave according to the *power law*

$$R(\omega) = R_2(\omega_2 / \omega)^p \qquad \omega \geq \omega_2 \qquad (4.61)$$

where R_2 is the measured frequency at ω_2 and p is an empirical parameter chosen to give best agreement with the experimental results for frequencies smaller than the cut-off point [97, 103].

In general, no entirely satisfactory extrapolation procedure with general validity exists because different procedures can give good results in many cases. Both of the aforementioned extrapolations have been used in many studies of the optical properties of solids [108-111].

The computer program used for the numerical evaluation of the KK integrals was courtesy of Professor David Tanner at the Department of Physics of the University of Florida.[30] The results were identical to the ones obtained using a similar program developed by the author; the former was chosen over the latter due to better functionality. The program uses two parameters for controlling the high frequency behaviour of the reflectivity data.[31] The high frequency extrapolation is performed by applying equation (4.61) consecutively for two frequency regions ($\omega_2 \leq \omega \leq \omega_3$ and $\omega_3 \leq \omega$) above the last measured data point ω_2 with each region initially having a different value of p. It is well established [97] that for very high frequencies (ω_3>100,000 cm^{-1}) the reflectivity drops as ω^{-4} (free electron behaviour), hence p=4 in that region. In the interim region p varies and is usually determined by fitting equation (4.61) at the edge of the measured range. The values of the crossover frequency ω_3 and p were provided to the program before performing the KK transformation, allowing in this way precise control of the high frequency extrapolation procedure. Figure 4-8 shows the real part, ε_1, of the dielectric function for sample A1 as calculated from KK transformation of the reflectivity spectrum of Figure 4-7, by taking different values of the high frequency extrapolation parameters ω_3 and p. The overall curve shape remains unchanged for different values of ω_3 and p, while curves with ω_3 differing by one order or magnitude and having the same value of p are almost identical. The zero crossover of ε_1 is, moreover, the same for all the curves. The value of p that most accurately matches the

---

[30] The entire set of the optical analysis programs can be downloaded from the following web address: http://www.phys.ufl.edu/~tanner/

[31] Such control is not possible for the low frequency extrapolation since the Hagen-Rubens relation does not have any adjustable parameters (σ_{dc} is the measured dc conductivity). Yet, good level of agreement with experiment is found for many materials.

extrapolated data with the measured ones is p=4. This evidence suggests that the high frequency extrapolation does not substantially affect the details of the infrared behaviour of the samples under investigation. Nevertheless, it should be understood that extrapolated data can never substitute real data and, therefore, the values of the optical constants at the limits of the experimentally measured region are not expected to be entirely accurate due to the lack of sufficient number of data points necessary for the correct calculation of the KK integrals.
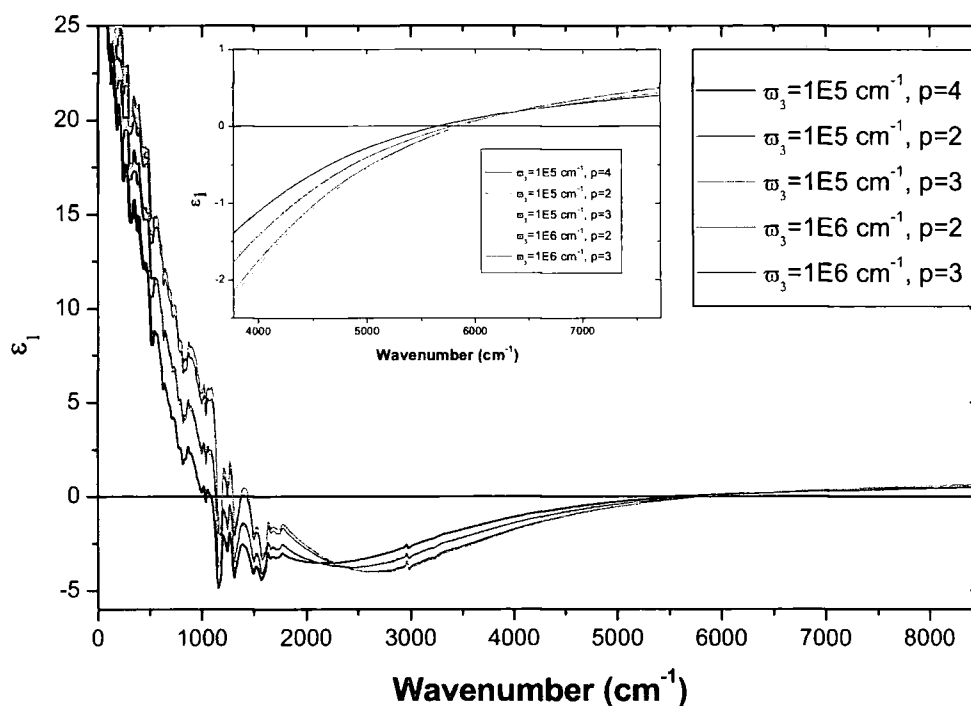
Figure 4-8 The real part ε_1 of the dielectric function as calculated for a polyaniline sample (PANI-AMPSA 30% or sample A1 from Table 4-2) by using the KK transformation of the reflectivity data (Figure 4-7) with different values of the high frequency extrapolation parameters ω_3 and p, as discussed within the text.

4.8.3 Dielectric function $\varepsilon(\omega)$ and energy loss function $Im[-1/\varepsilon(\omega)]$

The real and imaginary parts of the dielectric function $\varepsilon(\omega)$ and the energy loss function $Im[-1/\varepsilon(\omega)]$ for all the samples present in Table 4-2 are shown in Figure 4-9 and in Figure 4-10. In all the samples, the dielectric function shows, after approximately 3500 cm^{-1}, behaviour reminiscent of the free electron response in traditional metals at the plasma frequency region, as discussed in 4.3.3. The plasma frequency Ω_p is principally defined as the frequency where ε_1=0 and ε_2<<1, while the energy loss function, $Im(-1/\varepsilon)$, exhibits a sharp peak [102, 109]. Such a definition clearly distin-

guishes a plasma resonance from an interband transition displayed in Figure 4-4, panel c. All samples satisfy the plasma frequency requirement and their respective values of Ω_p are listed in Table 4-3.

According to the Drude model (Equations (4.49)), the real part of the dielectric function is given by the expression:

$$\varepsilon_1 = \varepsilon_\infty - \frac{\omega_p^2}{\omega^2 + \gamma^2} \tag{4.62}$$

where $\omega_p^2 = \dfrac{4\pi e^2 N}{V m^*}$ is the unscreened plasma frequency mentioned in 4.3.3, which is related to the experimentally determined plasma frequency Ω_p by equation (4.55). Equation (4.62) was fitted to the experimental data curves for frequencies above 3500 cm^{-1}. The fitting procedure generated curves virtually indistinguishable, under the current plot resolution, from the data curves, as the inset of Figure 4-9 testifies. The fitting parameters ω_p, γ and ε_∞ [32] along with the measured values of Ω_p and Im(-1/ε) and the free carrier concentration, N/V^{Drude}, are included in Table 4-3. The values of N/V^{Drude} are extracted from the values of ω_p by taking the effective mass m^* equal to the free electron mass.

Table 4-3 . Experimental values of Ω_p and Im(-1/ε) along with the fitting parameter values ω_p, γ and ε_∞ of the Drude model to the experimental data for frequencies above 3500 cm^{-1} ,and the free carrier concentration N/V^{Drude}. The relative errors for each of the three fitting parameters are approximately 0.5%, 0.75% and 0.3% respectively.

Sample	Ω_p (cm^{-1})	Im(-1/ε)^{peak} (cm^{-1})	ω_p (cm^{-1})	γ (cm^{-1})	ε_∞	N/V^{Drude} (10^{20} cm^{-3})
A1	5662	5943	6603	1671	1.2	4.9
A2	7155	7787	9366	4806	1.2	9.8
A3	7230	8190	9201	4354	1.2	9.4
A4	6344	7372	8862	5050	1.2	8.7
C1	6890	7355	8248	3284	1.2	7.6
C4	6332	7173	8477	4387	1.2	8.0

[32] It has been assumed during the fitting process that ε_∞ does not vary significantly and is in the order of one.

The values of N/V^{Drude} in Table 4-3 are two orders of magnitude smaller than the values of a typical metal referred in Table 4-1. This difference, in conjunction with the larger scattering time by one order of magnitude (10^{-15} sec rather than 10^{-14} sec), can explain, within the framework of the Drude Model, the deviation from the free electron behaviour for frequencies lower than 3500 cm^{-1}. As the inset of Figure 4-9 demonstrates, the Drude model curve for ε_1 deduced from the parameters in Table 4-3 reaches significantly higher values at low frequencies than a curve for a typical metal does (Figure 4-3) and, therefore, the phonon features cannot be eradicated from the dielectric function plots. Hence, the deviation from the free electron behaviour can be primarily attributed to the insufficient screening of the vibrational features by the free charge carriers.
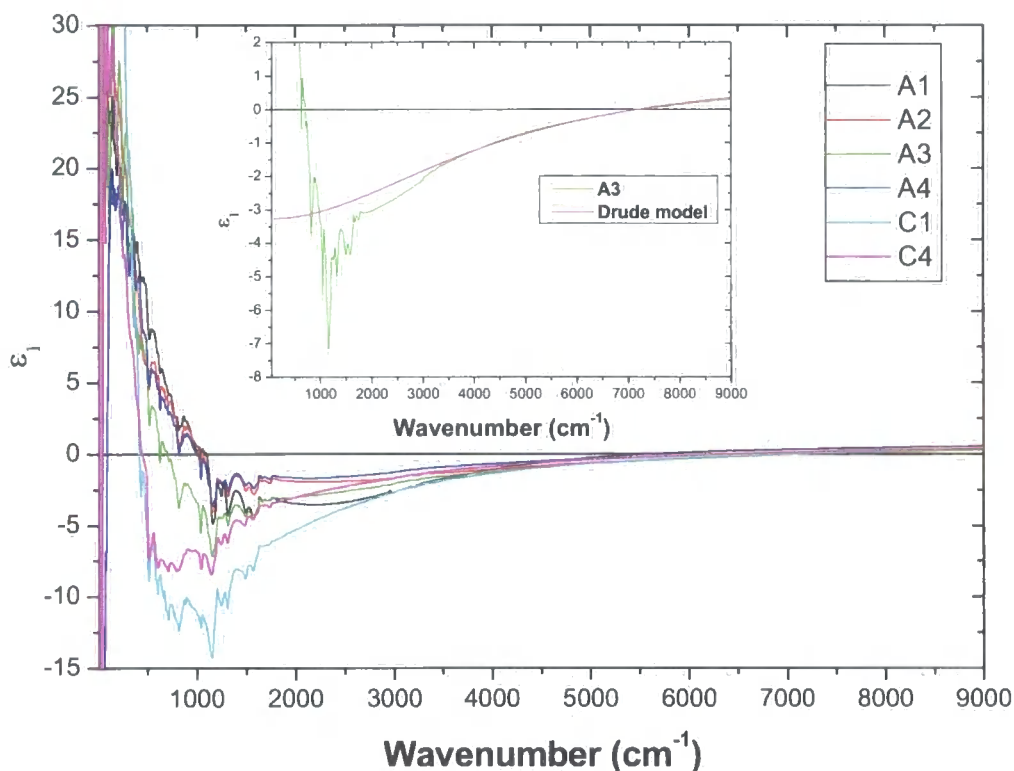
Figure 4-9 The real part ε_1 of the dielectric function as obtained from a KK transformation of the reflectivity data. All samples display Drude-like behaviour after 3500 cm^{-1} with the model curves coinciding with the experimental curves, as the inset for one of the samples studied shows.
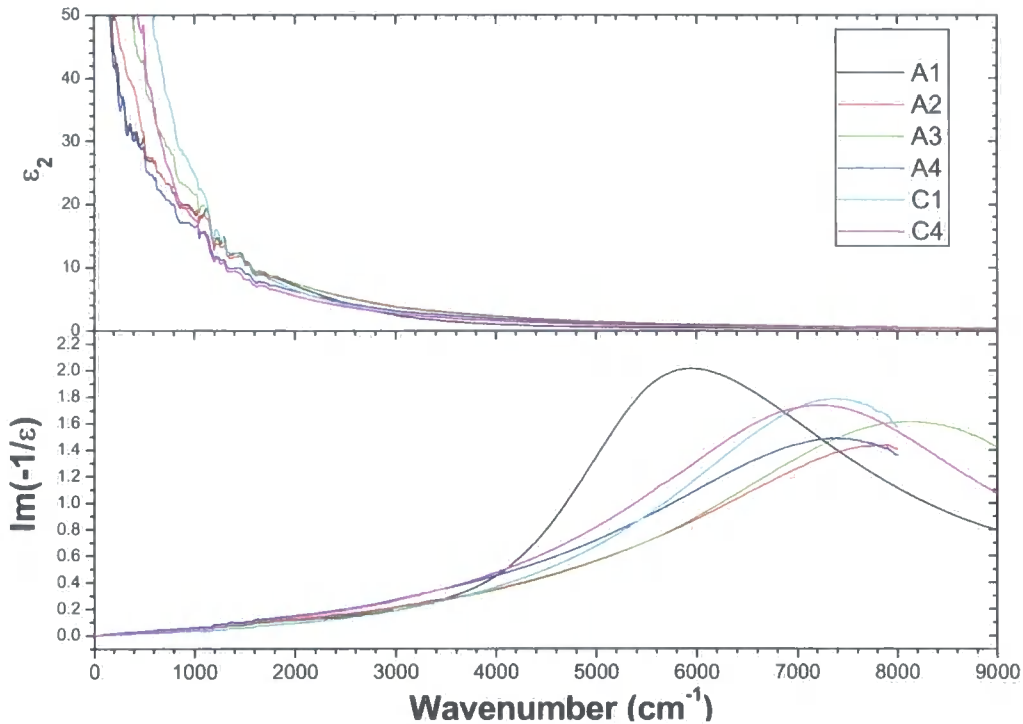
Figure 4-10 The imaginary part ε_2 of the dielectric function along with the energy loss function Im(-1/ε). Note that Im(-1/ε) peaks and $\varepsilon_2 \ll 1$ only at the vicinity of the plasma frequency Ω_p.

4.8.4 The localization modified Drude model as applied to the optical conductivity $\sigma(\omega)$ spectra.

Although the Drude model describes satisfactorily the free-carrier response at high frequencies, the behaviour of the samples below 3000 cm^{-1} does not resemble that of typical metals and therefore cannot be explained by using such a simple model. The localization modified Drude model (LMD)[25, 31, 38] is a more suitable candidate for describing the carrier response in the infrared region since it can account for any disorder present in the sample. According to LMD, the Drude expression (4.51) for the optical conductivity $\sigma(\omega)$ should be modified for disordered materials according to the following expression

$$\sigma_{LMD}(\omega) = \sigma_D(\omega)\left\{1 - \frac{C}{(k_F\lambda)^2}\left[1 - \left(\frac{3\omega}{\gamma}\right)^{1/2}\right]\right\} \tag{4.63}$$

where $\sigma_D(\omega) = \dfrac{\omega_p^2\gamma}{4\pi\left(\omega^2 + \gamma^2\right)}$ is the Drude optical conductivity, C$\approx$1, k_F is the Fermi wavevector, and λ the mean free path. Expression (4.63) was fitted on the experimen-

tal curves plotted in Figure 4-11 with ω_p, γ and $k_F\lambda$ as fitting parameters. The fitting results are listed in Table 4-4. As it can be observed by plotting the Drude and the LMD model curves in Figure 4-12 for the case of sample A3, the optical conductivity is suppressed at low frequencies (long-length scales) in comparison with the Drude formula that could be obtained simply by applying the Boltzmann equation. This effect has been discussed in the context of the weak localization and on the basis of the scaling theory of localization [17, 25, 31, 38, 112] and has been attributed mainly to localization and Coulomb interaction effects. It has been suggested [113] that this conductivity suppression compared to the Drude result at low frequencies necessitates an enhancement at higher frequencies (shorter-length scales). This enhancement occurs at around 18,000 cm^{-1} according to an examination of the two model curves linked to sample A3.

Despite the presence of the vibrational features between 200 and 2000 cm^{-1} that are not accounted for in the model, the fitting is quite successful since it manages to give consistent values with the DC conductivity (Table 4-2) at the zero frequency limit where it takes the form

$$\sigma_{LMD}(0) = \frac{\omega_p^2}{4\pi\gamma}\left\{1 - \frac{1}{(k_F\lambda)^2}\right\} \tag{4.64}$$

This expression cannot be applied for samples with values of $k_F\lambda$ equal or less than 1, i.e. for samples in the limit of the metal-insulator transition. Attempts have been made [25, 38] to provide a correction in (4.64) that accounts for the reduction of energy states due to localization, but not without a considerable ambiguity. However, apart from samples A1 and C1, the values of $\sigma_{LMD}(0)$, as obtained by (4.64), that are listed in Table 4-4 are in a very good agreement with the experimental values in Table 4-2 which were obtained from direct current measurements. Hence the LMD is suitable for estimating the degree of the disorder present on the sample through the parameter $k_F\lambda$, enabling in this way a characterization of its transport regime. Samples with $k_F\lambda>1$ are on the metallic side of the metal-insulator transition that occurs when the disorder becomes sufficiently large such that $k_F\lambda$ crosses unity and decreases until $k_F\lambda<<1$, where all the states are localized and the material becomes a Fermi glass. A typical value of $k_F\lambda$ for a conventional metal like copper is about 500.

From the values of the unscreened plasma frequency ω_p, as obtained from the LMD model, the free carrier concentration, N/V, can be determined. The free carrier

density can then be compared to the effective carrier density, $n_{eff}(\omega_0)$, that contributes to the optical properties up to frequency $\omega_0 = 8000$ cm^{-1} according to the sum rule (4.59) from which the following expression for $n_{eff}(\omega_0)$ is derived

$$n_{eff}(\omega_0) = \frac{2m^*}{\pi e^2} \int_0^{\omega_0} \sigma(\omega)d\omega \qquad (4.65)$$

Predictably enough, $n_{eff}(\omega_0)$ is larger than N/V for all the samples studied, indicating that localized carriers also contribute to optical properties up to 8000 cm^{-1}. Figure 4-13 shows $n_{eff}(\omega_0)$ for ω_0 up to 8000 cm^{-1} for all the samples under study. The carrier density values in Table 4-4 are significantly smaller than in typical metal ($\sim 10^{22}$ cm^{-3}), but also considerably larger than in a typical doped semiconductor ($\sim 10^{15}$ cm^{-3}), denoting the peculiarity of the conjugated polymers in the realm of electrically conducting materials. The values of free carrier concentration, N/V, obtained from the LMD model are noticeably smaller than the Drude values N/V^{Drude} listed in Table 4-3, suggesting, in accordance with the theory [31], that disorder induces the free carrier localization at low frequencies. The mean free path λ for each sample, as obtained by the free carrier density values and the order parameter, are also included in Table 4-4, showing that the most ordered samples have greater values of λ. From the differences in the number of carriers between these two models, the percentage of the localized carriers, L, can be estimated. Since irrespectively of the localization mechanism, there will be a critical energy E_C, the mobility edge, separating localized from extended states [114], L will provide an estimate of the number of carriers close to or below E_C. The results, listed in Table 4-4, show that samples with similar DC conductivities have similar percentages localized carriers, contributing thus to the general consistency of the applied model.

Considering the existence of E_C separating the lower-lying localized states and the higher energy extended states, for a given Fermi-level E_F the free carrier density is given from

$$N/V = \int_{E_c}^{\infty} f_{FD}(E,T)g(E)dE \qquad (4.66)$$

where $f_{FD}(E,T) = \frac{1}{1+e^{(E-E_F)/kT}}$ is the Fermi-Dirac distribution function and $g(E)$ the density of states. If the expression of $g(E)$ is known, by assuming that m^* is independent of T and using the N/V values from Table 4-4, the free carrier parameter $E_F - E_C$ can

be determined. The parameter E_F-E_C is clearly correlated with the Insulator-Metal transition since the metallic and insulating regimes are characterized by E_F-E_C>0 and <0, respectively. It has been contended by Martens et al. [114] that E_F-E_C is a significant physical quantity for the characterisation of the conductive state and they managed to calculate it for PF_6 doped polypyrrole at different temperatures by assuming, however, that $g(E)$ is independent of E. It is well known [115] that such an assumption is valid only for a 2D gas of free electrons and cannot be applied, therefore, without further justification and corroborating evidence in the case of polyaniline. Nevertheless, the importance of E_F-E_C>0 for the understanding of the insulator-metal transition remains undisputed.

Table 4-4 The fitting parameters of the LMD model along with the experimental value of plasma frequency Ω_p and other quantities derived from the model such as, the screened plasma frequency ω_p, the damping constant γ, the order parameter $k_F\lambda$, the mean free path λ, the free charge carrier concentration N/V, the effective number of carriers $n_{eff}(\omega_0)$, the evaluated DC conductivity $\sigma_{LMD}(0)$ and the percentage of the localized carriers L. The relative errors for the fitting parameters ω_p, γ and $k_F\lambda$ are approximately 0.3%, 0.5% and 1% respectively.

Sample	Ω_p (cm^{-1})	ω_p (cm^{-1})	γ (cm^{-1})	$k_F\lambda$	λ (Å)	N/V (10^{20} cm^{-3})	$n_{eff}(\omega_0)$ (10^{20} cm^{-3})	$\sigma_{LMD}(0)$ (S/cm)	L (%)
A1	5662	4774	1324	0.92	4.72	2.5	4.1	-	49
A2	7155	6725	2463	1.16	4.73	5	5.6	79	49
A3	7230	7033	2311	1.36	5.36	5.5	6.0	164	41
A4	6344	6177	2427	1.18	5.06	4.3	4.7	74	50
C1	6890	5228	929	0.99	4.78	3	5.6	-	60
C4	6332	6498	2123	1.82	7.57	4.7	4.8	217	41
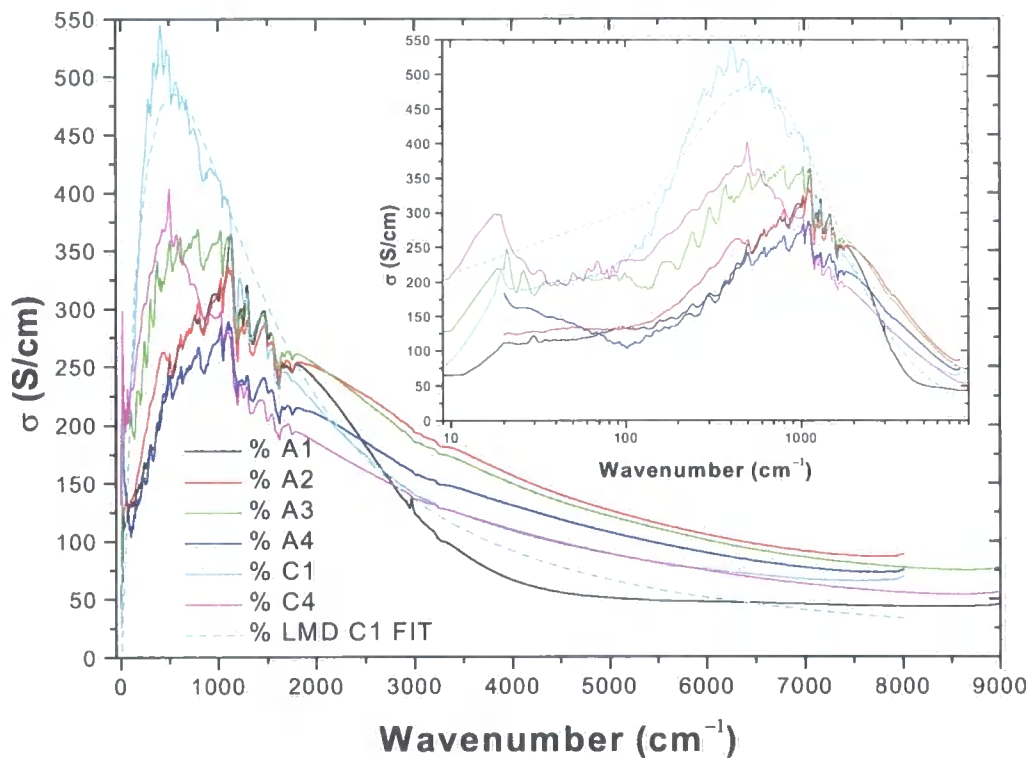
Figure 4-11 The real part $\sigma(\omega)$ of the optical conductivity. For clarity purposes, only one of the LMD model curves is shown along with the experimental curves.
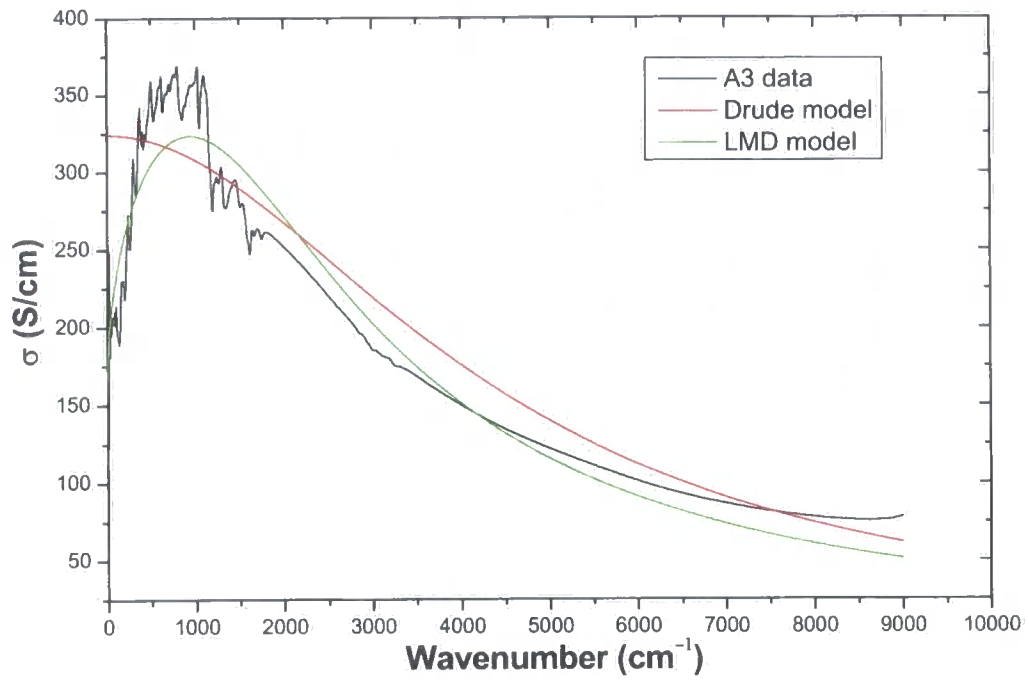
Figure 4-12 The optical conductivity of sample A3 (PANI-AMPSA 50%) along with two model curves: The Drude curve as derived from the fitting data of Table 4-3 and the LMD curve deduced from the values in Table 4-4.
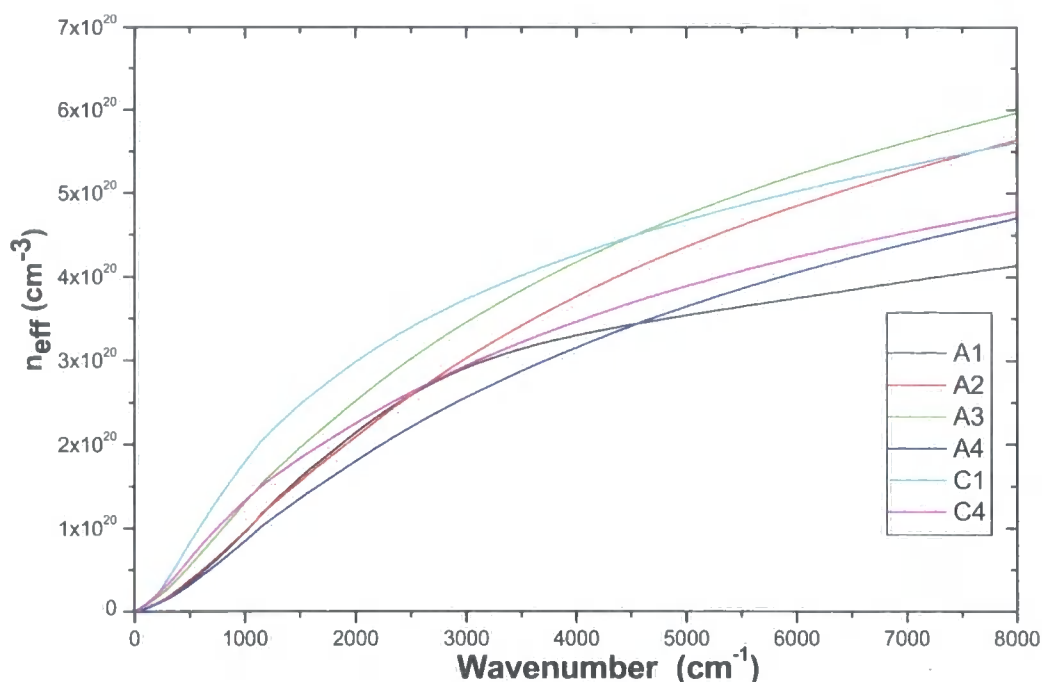
Figure 4-13 The effective carrier density for all the samples studied up until 8000 cm⁻¹. The relative position of the curves is consistent with the conclusions derived from the analysis of the results of Table 4-4.

4.8.5 Homogeneous and inhomogeneous disorder and the nature of the insulator-metal transition in polyaniline.

The above results are consistent with previous studies [108, 116, 117] that examine the transport properties of conjugated polymers within the framework of an Anderson-Mott insulator-metal transition due to weak localization. In this context, disorder is considered homogeneous, which implies a localization length greater than the structural coherence length so that the system sees only an average [10]. Disorder causes localization of the wave functions and while it is below a critical limit, a critical energy E_c (the "mobility edge") separating localized from non-localized states exists. The position of the Fermi level E_F in respect to E_c determines whether the system is either on the insulating ($E_F < E_c$ or $k_F\lambda \ll 1$), metallic ($E_F > E_c$ or $k_F\lambda > 1$) side or at the boundary ($E_F \sim E_c$ or $k_F\lambda \sim 1$) of a disorder driven I-M transition. The recent generation of conducting polymers has given samples with fewer large scale inhomogeneities that dominated the transport properties of previous generations. Hence, the current materials are more highly conducting and homogeneous than before, while the re-

ported localization length (~100-200 Å) [42] is considerably greater than the structural coherence length (~20 Å) [118], justifying partly the application of the homogeneous disorder model for which the Anderson-Mott theory applies.

However, the validity of a model can only be assessed if it can reproduce the experimental data. The above discussion shows a considerable consistency between optical and transport measurements since experimentally measured values of conductivity were reproduced, via equation (4.64), with notable accuracy after the application of the LMD model. The values obtained for the free charge carrier concentration ($\sim 10^{20}$ cm^{-1}) and the relaxation time ($\tau=1/\gamma \sim 10^{-15}$ sec) are characteristic of a dirty metal [27], implying that the mechanism of transport in conducting polymers, despite their structural difference due to the 1D polymer chains, is not fundamentally different from the 3D delocalization that takes place in amorphous metallic bundles. Nevertheless, the subtle details of the transport mechanism such as the relative importance of the interplay between the quasi-1D of the system and the 3D features due to contribution from interchain and counterion interactions are yet to be decided.

The suitability of the conventional homogeneous disorder model for the understanding of the charge transport mechanism in conducting polymers has been contested in some studies [15, 114, 119, 120] and an alternative has been proposed. The inhomogeneous disorder model treats the conducting polymer as a composite system of three dimensional metallic regions with delocalized charge carriers coupled by disordered quasi-1D amorphous regions of polymer chains where one-dimensional disorder induced localization is dominant [4]. The metallic transport occurs when the localization length is larger than the separation between the metallic regions so that charge carriers can percolate through the ordered regions. This model was incited after a zero crossover from positive to negative at the far infrared (~0.01eV or ~80 cm^{-1}) of the real part of the dielectric function of Polypyrrole [121] and PANI [122] was observed. This crossover was attributed to a second plasma frequency due to a small fraction (~10^{16} cm^{-3}) of delocalized carriers with unusually long scattering time $\tau > 10^{-13}$ sec. This crossover was observed only for systems on the metallic side of the I-M transition, while for systems on the insulating side $\varepsilon_1(\omega)$ remains positive for the entire frequency regime. In the case of the samples studied here, a second plasma frequency has not been observed. As Figure 4-10 testifies, the values of ε_2 remain large enough, while the loss function Im(-1/ε) does not show any peaks in the far infrared range, preventing the conditions for the existence of a plasma frequency from being

satisfied. The erratic crossovers of ε_1 that are observed in the case of samples C4 and A3 at the edge of the measurement range (<30 cm^{-1}) can therefore be attributed to errors in the KK transformations because of low data point density at the measurement edge (20 cm^{-1}), which the extrapolation procedure cannot fully compensate for. Therefore, it is conjectured that the inhomogeneous disorder model is not suitable for interpreting the materials under investigation.

The importance of doping for the metallic properties of conductive polymers has been unequivocally acknowledged in the field [50]. The conductivity of the emeraldine base can increase up to 10 orders of magnitude after non-redox doping by a protonic acids, as in the current samples. Although the number of electrons associated with the polymer backbone remains unchanged, the rearrangement of the energy levels after doping affects constructively the charge transport leading to an I-M transition at high doping levels. Due to the lack of a widely accepted microscopic charge transport mechanism in doped polymers that would quantitatively estimate the contributions of various factors (such as the electron-phonon interaction, e-e interaction, interchain interactions and disorder and their extent, quantum lattice fluctuations, extent of intra and interchain delocalization of electronic states etc.) [10], it is very difficult to construct a comprehensive model that solely explains the metallic properties as a function of the doping level. However, individual observations can always be useful for establishing a solid basis from which a new approach may flourish. Hence, from the data on Table 4-2 and Table 4-4, it becomes apparent that the optimum doping level for the PANI-AMPSA samples is 50%, something that is not unexpected regarding the fact that only 2 out of 4 Nitrogen sites in a EB repeat unit can be protonated, whereas for PANI-CSA samples is 60%, possible suggesting that doping with CSA is less straightforward than AMPSA. Samples A1 and C1, i.e. 30% doping level, were found to be at the boundary of the I-M transition, while the rest were found at the metallic side, suggesting that high doping concentrations adversely affect the extent of the disorder present at the samples.

4.9 Summary.

Infrared reflectivity measurements were performed from 20-9000 cm^{-1} on a series of PANI films protonated, at various degrees, with AMPSA and CSA. The experimental setup permitted the absolute determination of the sample reflectivity by accounting for any scattering losses due to surface imperfections. The dielectric function

was obtained from a Kramers-Kronig transformation of the reflectivity data. Subsequently, other optical constants were easily determined. Analysis of the results showed that PANI is a disordered metal close to I-M transition that was more suitably interpreted in the context of an Anderson-Mott localization and strongly affected by the doping level of the sample. The optical results were remarkably consistent with the transport studies, thus, contributing to the suitability of the homogeneous disorder model for the interpretation of the metallic properties of conductive polymers.

5 Concluding Remarks

Throughout a series of conductivity, magnetoconductance and infrared reflectivity measurements, the inherent metallic character of polyaniline has been confirmed. The significant improvement of the sample processing techniques over the past few years has produced samples with notable structural and morphological improvement that enabled a thorough investigation of the metal-insulator transition due to random disorder. The variation of the doping level for both PANI systems studied here (PANI-CSA and PANI-AMPSA), has given samples on either sides of the transition. The most metallic samples, PANI AMPSA 50% and PANI-CSA 60%, have shown typical features of a disordered metal such as

- Considerable dc conductivity values at temperatures as low as 1.5 K and a positive temperature coefficient at higher temperatures. The more metallic the sample, the lower the onset of a positive TCR is.

- A positive slope of the reduced activation energy $W(T)$ at low temperatures.

- Values of the resistivity ratio ρ_r within the limits that characterise the metallic regime.

- Very high (greater than 80%) reflectivity in the far infrared ($\omega < 100$ cm^{-1}) and Drude-like behaviour of the real part of the dielectric function, $\varepsilon = \varepsilon_1 + i\varepsilon_2$ at frequencies over 3500 cm^{-1}.

The application of the localization-interaction model for disordered electronic systems has provided a quantitative method of determining the degree of the disorder present in the sample through the calculation of several order parameters such as $k_F\lambda$, γF_σ, the percentage of localized carriers etc. The results from the optical measurements were consistent with those obtained from the transport measurements, resulting in a similar classification of the studied samples in term of their position in a virtual metal-insulator transition diagram.

The localization-interaction model is an extended version of the Anderson's theory of localization and Mott's theory of the electronic correlations. The success of this model in the case of polyaniline has led to the conclusion that the disorder in polyaniline is homogeneous. This means that the localization length is greater than the struc-

tural coherence length, something which is true for samples of improved quality as the ones studied. An implication of such a conclusion is that the fundamental physical principles for understanding the metal-insulator transition in disordered metals and conjugated polymers remains basically the same.

Despite its noticeable successes, the localization-interaction model has certain shortcomings. It has failed to provide any explanation for the unusual magnetoconductance behaviour of the PANI-AMPSA 50% sample and some of its assumptions regarding the various constants appearing in the magnetic-field corrections to the conductivity remain questionable. Its limits of validity are not rigidly specified, prompting the need for further theoretical development and clarification. Therefore, the theoretical understanding of the magnetic field effects on the charge transport of conjugated polymers is not yet complete.

Another issue that remains unresolved within the context of the localization-interaction model is that of the nature of the charge carriers. Although there have been theoretical models attempting to understand the transport mechanisms in terms of nonlinear excitations present in conjugated systems, rigid experimental confirmation and a common consensus is still lacking, indicating that the investigation of charge transport mechanisms in conjugated polymers remains an open issue.

Publications arising from this work

- G. Tzamalis, N. A. Zaidi, C. C. Homes and A. P. Monkman, *Doping Dependent Optical Properties of Polyaniline Films*, to be published in Synthetic Metals (2002).

- G. Tzamalis, N. A. Zaidi, C. C. Homes and A. P. Monkman, *Doping dependent studies of the Anderson-Mott localization in polyaniline at the metal-insulator boundary.*, Physical Review B, 66 (2002), pp. 085202.

- G. Tzamalis, N. A. Zaidi, C. C. Homes and A. P. Monkman, *Infrared optical properties of polyaniline doped with 2- acrylamido-2-methyl-1-propanesulfonic acid (AMPSA)*, Journal of Physics-Condensed Matter, 13 (2001), pp. 6297-6306.

- J. Zhou, G. Tzamalis, N. A. Zaidi, N. P. Comfort and A. P. Monkman, *Effect of thermal aging on electrical conductivity of the 2- acrylamido-2-methyl-1-propanesulfonic acid-doped polyaniline fiber*, Journal of Applied Polymer Science, 79 (2001), pp. 2503-2508.

- J. Zhou, G. Tzamalis, N. A. Zaidi, N. P. Comfort and A. P. Monkman, *Electrically conductive PANI multifilaments spun by a wet- spinning process*, Journal of Materials Science, 36 (2001), pp. 3089-3095.

List of References

[1]   J. Tsukamoto, *Recent Advances in Highly Conductive Polyacetylene*, Advances in Physics, 41 (1992), pp. 509-546.

[2]   M. Munowitz, *Principles of chemistry*, W.W. Norton, New York, 2000.

[3]   R. Menon, C. O. Yoon, D. Moses and A. J. Heeger, *Metal-Insulator Transition in Doped Conducting Polymers*, in T. A. Skotheim, R. L. Elsenbaumer and J. R. Reynolds, eds., *Handbook of Conducting Polymers*, Marcel Dekker, New York, 1998.

[4]   R. S. Kohlman and A. J. Epstein, *Insulator-Metal Transition and Inhomogeneous Metallic State in Conducting Polymers*, in T. A. Skotheim, R. L. Elsenbaumer and J. R. Reynolds, eds., *Handbook of Conducting Polymers*, Marcel Dekker, New York, 1998.

[5]   R. Kiebooms, R. Menon and K. Lee, *Synthesis, Electrical, And Optical Properties of Conjugated Polymers*, in H. S. Nalwa, ed., *Handbook of advanced electronic and photonic materials and devices*, Academic Press, San Diego, CA, 2001, pp. 10 v.

[6]   E. M. Conwell, *Transport in Conducting Polymers*, in H. S. Nalwa, ed., *Handbook of organic conductive molecules and polymers*, Wiley, New York, 1997.

[7]   A. J. Heeger, S. Kivelson, J. R. Schrieffer and W. P. Su, *Solitons in Conducting Polymers*, Reviews of Modern Physics, 60 (1988), pp. 781-850.

[8]   D. Baeriswyl, D. K. Campbell and S. Mazumdar, *An overview of the Theory of π-Conjugated Polyemrs*, in H. G. Kiess, ed., *Conjugated Conducting Polymers*, Springer, Berlin, 1992.

[9]   E. M. Conwell and H. A. Mizes, *Metallic State of Polymers with Nondegenerate Ground-States*, Physical Review B, 44 (1991), pp. 937-942.

[10]   R. Menon, *Charge Transport in Conducting Polymers*, in H. S. Nalwa, ed., *Handbook of organic conductive molecules and polymers*, Wiley, Chichester ; New York, 1997, pp. 4 v.

[11]   S. Stafstrom, J. L. Bredas, A. J. Epstein, H. S. Woo, D. B. Tanner, W. S. Huang and A. G. Macdiarmid, *Polaron Lattice in Highly Conducting*

Polyaniline - Theoretical and Optical Studies, Physical Review Letters, 59 (1987), pp. 1464-1467.

[12] E. M. Conwell, H. A. Mizes and S. Jeyadev, *Metal-Insulator-Transition in Trans-Polyacetylene*, Physical Review B, 40 (1989), pp. 1630-1641.

[13] E. M. Conwell and S. Jeyadev, *Free Soliton Transport and Photoconductivity in Trans- Polyacetylene*, Synthetic Metals, 28 (1989), pp. D439-D446.

[14] S. Stafstrom and J. L. Bredas, *Evolution of the Electronic-Structure of Polyacetylene and Polythiophene as a Function of Doping Level and Lattice Conformation*, Physical Review B, 38 (1988), pp. 4180-4191.

[15] V. N. Prigodin and A. J. Epstein, *Nature of insulator-metal transition and novel mechanism of charge transport in the metallic state of highly doped electronic polymers*, Synthetic Metals, 125 (2001), pp. 43-53.

[16] R. Zallen, *The physics of amorphous solids*, Wiley, New York, 1983.

[17] P. A. Lee and T. V. Ramakrishnan, *Disordered Electronic Systems*, Reviews of Modern Physics, 57 (1985), pp. 287-337.

[18] D. Belitz and T. R. Kirkpatrick, *The Anderson-Mott Transition*, Reviews of Modern Physics, 66 (1994), pp. 261-390.

[19] D. Cottevieille, A. Le Mehaute, C. Challioui, P. Mirebeau and J. N. Demay, *Industrial applications of polyaniline*, Synthetic Metals, 101 (1999), pp. 703-704.

[20] R. H. Bube, *Electronic properties of crystalline solids; an introduction to fundamentals*, Academic Press, New York,, 1974.

[21] F. Blatt, J., *Physics of electronic conduction in solids*, McGraw-Hill 1968, New York, 1968.

[22] O. Madelung, *Introduction to solid-state theory*, Springer, Berlin ; New York, 1996.

[23] H. P. Myers, *Introductory solid state physics*, Taylor & Francis, London ; New York, 1990.

[24] C. C. Tsuei, *Anderson localization : proceedings of the international symposium, Tokyo, Japan, August 16-18, 1987*, in T. Ando and H. Fukuyama, eds., *Springer proceedings in physics ; v. 28*, Springer-Verlag, Berlin ; New York, 1988, pp. xi, 376.

[25] N. F. Mott and M. Kaveh, *Metal-Insulator Transitions in Non-Crystalline Systems*, Advances in Physics, 34 (1985), pp. 329-401.

[26] A. F. Ioffe and A. R. Regel, *Non-Crystalline, Amorphous, and Liquid Electronic Semiconductors*, Progress in Semiconductors, 4 (1960), pp. 237-291.

[27] N. F. Mott and E. A. Davis, *Electronic processes in non-crystalline materials*, Clarendon Press, Oxford, 1979.

[28] N. F. Mott, *Conduction in non-crystalline materials*, Oxford University Press, Oxford, 1987.

[29] K. Morigaki, *Physics of Amorphous Semiconductors*, World Scientific, London, 1999.

[30] O. Madelung, *Introduction to solid-state theory*, Springer-Verlag, Berlin ; New York, 1978.

[31] N. F. Mott, *Metal-Insulator Transitions in Doped Semiconductors; A Survey*, in D. M. Finlayson, ed., *Proceedings of the Thirty First Scottish Universities Summer School in Physics*, Scottish Universities Summer School in Physics, St. Andrews, 1986.

[32] A. Kawabata, *A Self-Consistent Treatment of Anderson Localization*, Solid State Communications, 38 (1981), pp. 823-825.

[33] N. F. Mott, *Metal-Insulator Transitions*, Philosophical Magazine B-Physics of Condensed Matter Statistical Mechanics Electronic Optical and Magnetic Properties, 50 (1984), pp. 161-167.

[34] N. F. Mott, *The Conductivity Near a Mobility Edge*, Philosophical Magazine B-Physics of Condensed Matter Statistical Mechanics Electronic Optical and Magnetic Properties, 49 (1984), pp. L75-L82.

[35] G. Bergmann, *Physical Interpretation of Weak Localization - a Time-of-Flight Experiment with Conduction Electrons*, Physical Review B, 28 (1983), pp. 2914-2920.

[36] G. Bergmann, *Consistent Temperature and Field-Dependence in Weak Localization*, Physical Review B, 28 (1983), pp. 515-522.

[37] N. F. Mott and M. Kaveh, *Conductivity Near a Mobility Edge .2*, Philosophical Magazine B-Physics of Condensed Matter Statistical Mechanics Electronic Optical and Magnetic Properties, 52 (1985), pp. 177-183.

[38] N. F. Mott, *Metal-Insulator Transitions*, Taylor & Francis, London, 1990.

[39]   E. Abrahams, P. W. Anderson, D. C. Licciardello and T. V. Ramakrishnan, *Scaling Theory of Localization: Absence of Quantum Diffusion in Two Dimensions*, Physical Review Letters, 42 (1979), pp. 673-676.

[40]   A. Mobius, C. Frenzel, R. Thielsch, R. Rosenbaum, C. J. Adkins, M. Schreiber, H. D. Bauer, R. Grotzschel, V. Hoffmann, T. Krieg, N. Matz, H. Vinzelberg and M. Witcomb, *Metal-insulator transition in amorphous Si1-xNix: Evidence for Mott's minimum metallic conductivity*, Physical Review B, 60 (1999), pp. 14209-14223.

[41]   B. I. Shklovskii and A. L. Efros, *Electronic properties of doped semiconductors*, Springer-Verlag, Berlin ; New York, 1984.

[42]   M. Reghu, Y. Cao, D. Moses and A. J. Heeger, *Counterion-Induced Processibility of Polyaniline - Transport At the Metal-Insulator Boundary*, Physical Review B-Condensed Matter, 47 (1993), pp. 1758-1764.

[43]   A. I. Larkin and D. E. Khmelnitsky, *Activation Conductivity in Disordered-Systems With Large Localization Lengths*, Zhurnal Eksperimentalnoi I Teoreticheskoi Fiziki, 83 (1982), pp. 1140-1149.

[44]   A. Mobius and C. J. Adkins, *Metal-insulator transition in amorphous alloys*, Current Opinion in Solid State & Materials Science, 4 (1999), pp. 303-314.

[45]   A. G. Zabrodskii and K. N. Zinoveva, *Conductivity in the Metal-Dielectric Transition Range and Its Application in Wide-Range Low-Temperature Converters*, Fizika Nizkikh Temperatur, 10 (1984), pp. 1151-1159.

[46]   A. Mobius, *Critical-Behavior of the Zero-Temperature Conductivity in Compensated Silicon, Si-(P,B) - Comment*, Physical Review B, 40 (1989), pp. 4194-4195.

[47]   R. V. Gregory, *Solution Processing of Conductive Polymers: Fibers and Gels from Emeraldine Base Polyaniline*, in T. A. Skotheim, R. L. Elsenbaumer and J. R. Reynolds, eds., *Handbook of Conducting Polymers*, Marcel Dekker, New York, 1998.

[48]   A. G. Macdiarmid and A. J. Epstein, *Polyanilines - a Novel Class of Conducting Polymers*, Faraday Discussions (1989), pp. 317-&.

[49]   A. G. Macdiarmid, J. C. Chiang, A. F. Richter and A. J. Epstein, *Polyaniline - a New Concept in Conducting Polymers*, Synthetic Metals, 18 (1987), pp. 285-290.

[50]   A. G. MacDiarmid, *Synthetic metals: a novel role for organic polymers*, Synthetic Metals, 125 (2001), pp. 11-22.

[51]   A. P. Monkman, *Physics of Conductive Polymers*, in M. C. Petty, M. R. Bryce and D. Bloor, eds., *An introduction to molecular electronics*, Oxford University Press, New York, 1995, pp. xiv, 387.

[52]   P. Rannou, B. Dufour, J. P. Travers and A. Pron, *New PANI/dopant/solvent associations for processing of metallic PANI*, Synthetic Metals, 119 (2001), pp. 441-442.

[53]   P. N. Adams, P. J. Laughlin, A. P. Monkman and A. M. Kenwright, *Low temperature synthesis of high molecular weight polyaniline*, Polymer, 37 (1996), pp. 3411-3417.

[54]   P. N. Adams, P. J. Laughlin and A. P. Monkman, *Synthesis of high molecular weight polyaniline at low temperatures*, Synthetic Metals, 76 (1996), pp. 157-160.

[55]   M. Trznadel and P. Rannou, *Effect of solvent-dopant competition on the conductivity of polyaniline films*, Synthetic Metals, 101 (1999), pp. 842-842.

[56]   R. Menon, C. O. Yoon, D. Moses, A. J. Heeger and Y. Cao, *Transport in Polyaniline Near the Critical Regime of the Metal- Insulator-Transition*, Physical Review B-Condensed Matter, 48 (1993), pp. 17685-17694.

[57]   J. Zhou, G. Tzamalis, N. A. Zaidi, N. P. Comfort and A. P. Monkman, *Electrically conductive PANi multifilaments spun by a wet- spinning process*, Journal of Materials Science, 36 (2001), pp. 3089-3095.

[58]   J. Zhou, G. Tzamalis, N. A. Zaidi, N. P. Comfort and A. P. Monkman, *Effect of thermal aging on electrical conductivity of the 2- acrylamido-2-methyl-1-propanesulfonic acid-doped polyaniline fiber*, Journal of Applied Polymer Science, 79 (2001), pp. 2503-2508.

[59]   P. Rannou, M. Nechtschein, J. P. Travers, D. Berner, A. Wolter and D. Djurado, *Ageing of PANI: chemical, structural and transport consequences*, Synthetic Metals, 101 (1999), pp. 734-737.

[60]   P. Rannou, A. Wolter, J. P. Travers, B. Gilles and D. Djurado, *A model for PANI-HCl ageing*, Journal De Chimie Physique Et De Physico-Chimie Biologique, 95 (1998), pp. 1396-1399.

[61] C. O. Yoon, M. Reghu, D. Moses and A. J. Heeger, *Transport Near the Metal-Insulator-Transition - Polypyrrole Doped With Pf(6)*, Physical Review B-Condensed Matter, 49 (1994), pp. 10851-10863.

[62] M. Ahlskog, R. Menon, A. J. Heeger, T. Noguchi and T. Ohnishi, *Metal-insulator transition in oriented poly(p- phenylenevinylene)*, Physical Review B-Condensed Matter, 55 (1997), pp. 6777-6787.

[63] M. Ahlskog, M. Reghu and A. J. Heeger, *The temperature dependence of the conductivity in the critical regime of the metal-insulator transition in conducting polymers*, Journal of Physics-Condensed Matter, 9 (1997), pp. 4145-4156.

[64] E. R. Holland, S. J. Pomfret, P. N. Adams and A. P. Monkman, *Conductivity studies of polyaniline doped with CSA*, Journal of Physics-Condensed Matter, 8 (1996), pp. 2991-3002.

[65] P. N. Adams, P. Devasagayam, S. J. Pomfret, L. Abell and A. P. Monkman, *A new acid-processing route to polyaniline films which exhibit metallic conductivity and electrical transport strongly dependent upon intrachain molecular dynamics*, Journal of Physics-Condensed Matter, 10 (1998), pp. 8293-8303.

[66] A. N. Aleshin, N. B. Mironkov, A. V. Suvorov, J. A. Conklin, T. M. Su and R. B. Kaner, *Transport properties of ion-implanted and chemically doped polyaniline films*, Physical Review B-Condensed Matter, 54 (1996), pp. 11638-11643.

[67] N. W. Ashcroft and N. D. Mermin, *Solid state physics*, Saunders College, Philadelphia, 1976.

[68] R. K. Wangsness, *Electromagnetic fields*, Wiley, New York, 1986.

[69] J. D. Jackson, *Classical electrodynamics*, John Wiley & Sons, New York ; Chichester, 1999.

[70] S. Blundell, *Magnetism in condensed matter*, Oxford University Press 2001, Oxford, 2001.

[71] J. M. Ziman, *Electrons and phonons : the theory of transport phenomena in solids*, Oxford University Press, Oxford, 2001.

[72] G. Bergmann, *Influence of Spin-Orbit Coupling on Weak Localization*, Physical Review Letters, 48 (1982), pp. 1046-1049.

[73] A. C. Smith, J. F. Janak and R. B. Adler, *Electronic conduction in solids*, McGraw-Hill, New York,, 1967.

[74] A. Kawabata, *Theory of Negative Magnetoresistance in Three-Dimensional Systems*, Solid State Communications, 34 (1980), pp. 431-432.

[75] A. Kawabata, *Positive Magnetoresistance Induced by Zeeman Splitting in Two- Dimensional Systems*, Journal of the Physical Society of Japan, 50 (1981), pp. 2461-2462.

[76] B. L. Altshuler and A. G. Aronov, *Fermi-Liquid Theory of the Electron-Electron Interaction Effects in Disordered Metals*, Solid State Communications, 46 (1983), pp. 429-435.

[77] B. L. Altshuler, A. G. Aronov and D. E. Khmelnitskii, *Negative Magnetoresistance in Semiconductors in the Hopping Conduction Region*, Jetp Letters, 36 (1982), pp. 195-198.

[78] B. L. Altshuler and A. G. Aronov, *Magnetoresistance of Thin-Films and of Wires in a Longitudinal Magnetic-Field*, Jetp Letters, 33 (1981), pp. 499-501.

[79] B. L. Altshuler, A. G. Aronov and A. Y. Zuzin, *Spin Relaxation and Interaction Effects in the Disordered Conductors*, Solid State Communications, 44 (1982), pp. 137-139.

[80] A. L. Efros and M. Pollak, *Electron-electron interactions in disordered systems*, North-Holland ; New York N.Y. U.S.A. : Sole distributors for the U.S.A. and Canada Elsevier Science Pub. Co. 1985, Amsterdam ; New York, 1985.

[81] A. Aleshin, R. Kiebooms, R. Menon, F. Wudl and A. J. Heeger, *Metallic conductivity at low temperatures in poly(3,4- ethylenedioxythiophene) doped with PF6*, Physical Review B-Condensed Matter, 56 (1997), pp. 3659-3663.

[82] A. N. Aleshin, N. B. Mironkov, A. V. Suvorov, I. O. Usov, J. A. Conklin, T. M. Su and R. B. Kaner, *Conductivity and magnetoconductivity of polyaniline films implanted with Ar+ and Ga+ ions near the critical regime of the metal-insulator transition*, Journal of Physics-Condensed Matter, 10 (1998), pp. 4867-4875.

[83] M. Reghu, K. Vakiparta, Y. Cao and D. Moses, *Pressure-Dependence of the Conductivity and Magnetoconductance in Oriented Iodine-Doped Polyacetylene*, Physical Review B, 49 (1994), pp. 16162-16170.

[84]   P. Dai, Y. Z. Zhang and M. P. Sarachik, *Magnetoconductance of Metallic Si-B Near the Metal-Insulator- Transition*, Physical Review B-Condensed Matter, 46 (1992), pp. 6724-6731.

[85]   P. H. Dai, Y. Z. Zhang and M. P. Sarachik, *Electrical-Conductivity of Metallic Si-B Near the Metal- Insulator-Transition*, Physical Review B-Condensed Matter, 45 (1992), pp. 3984-3994.

[86]   S. Bogdanovich, P. H. Dai, M. P. Sarachik and V. Dobrosavljevic, *Universal Scaling of the Magnetoconductance of Metallic Si-B*, Physical Review Letters, 74 (1995), pp. 2543-2546.

[87]   M. Ahlskog and R. Menon, *The localization-interaction model applied to the direct- current conductivity of metallic conducting polymers*, Journal of Physics-Condensed Matter, 10 (1998), pp. 7171-7181.

[88]   D. Belitz and K. I. Wysokinski, *Electronic Inelastic Lifetime Near a Mobility Edge*, Physical Review B-Condensed Matter, 36 (1987), pp. 9333-9336.

[89]   G. Bergmann, *Quantitative-Analysis of Weak Localization in Thin Mg Films by Magnetoresistance Measurements*, Physical Review B, 25 (1982), pp. 2937-2939.

[90]   M. Ahlskog, M. Reghu, A. J. Heeger, T. Noguchi and T. Ohnishi, *Electronic transport in the metallic state of oriented poly(p- phenylenevinylene)*, Physical Review B-Condensed Matter, 53 (1996), pp. 15529-15537.

[91]   M. Ahlskog and M. Reghu, *Magnetoconductivity in doped poly(p-phenylenevinylene)*, Journal of Physics-Condensed Matter, 10 (1998), pp. 833-845.

[92]   Y. Nogami, H. Kaneko, H. Ito, T. Ishiguro, T. Sasaki, N. Toyota, A. Takahashi and J. Tsukamoto, *Low-Temperature Electrical-Conductivity of Highly Conducting Polyacetylene in a Magnetic-Field*, Physical Review B, 43 (1991), pp. 11829-11839.

[93]   A. Aleshin, R. Kiebooms, R. Menon and A. J. Heeger, *Electronic transport in doped poly(3,4-ethylenedioxythiophene) near the metal-insulator transition*, Synthetic Metals, 90 (1997), pp. 61-68.

[94]   F. Wooten, *Optical properties of solids*, Academic Press, 1972.

[95]   J. S. Toll, *Causality and the Dispersion Relation: Logical Foundations*, Physical Review, 104 (1956), pp. 1760-1770.

[96]   E. Kreyszig, *Advanced engineering mathematics*, Wiley, New York, 1993.

[97]   F. Stern, *Elementary Theory of the Optical Properties of Solids*, in F. Seitz and D. Turnbull, eds., *Solid State Physics*, Academic Press, New York, 1963.

[98]   E. N. Economou, *Solid State Physics (in Greek)*, University of Crete Press, 1997.

[99]   G. Burns, *Solid state physics*, Academic Press, Boston, 1990.

[100] C. Kittel, *Introduction to solid state physics*, Wiley, New York, 1996.

[101] P. Y. Yu and M. Cardona, *Fundamentals of semiconductors : physics and materials properties*, Springer, Berlin ; New York, 2001.

[102] H. Ehrenreich, *Electromagnetic Transport in Solids: Optical Properties and Plasma Effects*, in J. Tauc, ed., *Proceedings of the International School of Physics "Enrico Fermi", Course XXXIV*, Academic Press, Varenna on Lake Como, 1966.

[103] D. Y. Smith, *Dispersion Theory, Sum Rules, and their application to the Analysis of Optical Data*, in E. D. Palik, ed., *Handbook of Optical Constants of Solids*, Academic Press, New York, 1998.

[104] M. Altarelli, D. L. Dexter, M. Nussenzveig and D. Y. Smith, *Superconvergence and Sum Rules for the Optical Constants*, Physical Review B-Condensed Matter, 6 (1972), pp. 4502-4509.

[105] D. Y. Smith and E. Shiles, *Finite-energy f-sum rules for valence electrons*, Physical Review B-Condensed Matter, 17 (1978), pp. 4689-4694.

[106] D. E. Aspnes, *The Accurate Determination of Optical Properties by Ellipsometry*, in E. D. Palik, ed., *Handbook of Optical Constants of Solids*, Academic Press, New York, 1998.

[107] G. Tzamalis, N. A. Zaidi, C. C. Homes and A. P. Monkman, *Infrared optical properties of polyaniline doped with 2- acrylamido-2-methyl-1-propanesulfonic acid (AMPSA)*, Journal of Physics-Condensed Matter, 13 (2001), pp. 6297-6306.

[108] K. H. Lee, A. J. Heeger and Y. Cao, *Reflectance of Polyaniline Protonated With Camphor Sulfonic- Acid - Disordered Metal On the Metal-Insulator Boundary*, Physical Review B-Condensed Matter, 48 (1993), pp. 14884-14891.

[109] H. Ehrenreich and H. R. Philipp, *Optical Properties of Ag and Cu*, Physical Review, 128 (1962), pp. 1622-1629.

[110] R. S. Kohlman, J. Joo, Y. Z. Wang, J. P. Pouget, H. Kaneko, T. Ishiguro and A. J. Epstein, *Drude Metallic Response of Polypyrrole*, Physical Review Letters, 74 (1995), pp. 773-776.

[111] K. Lee, M. Reghu, E. L. Yuh, N. S. Sariciftci and A. J. Heeger, *Infrared Reflectance of Polypyrrole - Metal With a Gap in the Spectrum of Charged Excitations*, Synthetic Metals, 68 (1995), pp. 287-291.

[112] T. Ando and H. Fukuyama, *Anderson localization : proceedings of the international symposium, Tokyo, Japan, August 16-18, 1987*, Springer-Verlag, Berlin ; New York, 1988.

[113] H. K. Ng, M. Capizzi, G. A. Thomas, R. N. Bhatt and A. C. Gossard, *Short-Length-Scale Conductivity Enhancement in a Superlattice*, Physical Review B-Condensed Matter, 33 (1986), pp. 7329-7331.

[114] H. C. F. Martens, H. B. Brom and R. Menon, *Metal-insulator transition in PF6 doped polypyrrole: Failure of disorder-only models - art. no. 201102*, Physical Review B, 64 (2001), pp. 201102-+.

[115] F. Reif, *Fundamentals of statistical and thermal physics*, McGraw Hill, New York,, 1965.

[116] K. Lee and A. J. Heeger, *Optical reflectance studies of conducting polymers on the metal-insulator boundary*, Synthetic Metals, 84 (1997), pp. 715-718.

[117] A. J. Heeger, *Disorder-induced metal-insulator transition in conducting polymers*, Journal of Superconductivity, 14 (2001), pp. 261-268.

[118] J. P. Pouget, Z. Oblakowski, Y. Nogami, P. A. Albouy, M. Laridjani, E. J. Oh, Y. Min, A. G. Macdiarmid, J. Tsukamoto, T. Ishiguro and A. J. Epstein, *Recent Structural Investigations of Metallic Polymers*, Synthetic Metals, 65 (1994), pp. 131-140.

[119] H. C. F. Martens, J. A. Reedijk, H. B. Brom, D. M. de Leeuw and R. Menon, *Metallic state in disordered quasi-one-dimensional conductors - art. no. 073203*, Physical Review B, 63 (2001), pp. 073203-+.

[120] J. Joo, S. M. Long, J. P. Pouget, E. J. Oh, A. G. MacDiarmid and A. J. Epstein, *Charge transport of the mesoscopic metallic state in partially crystalline polyanilines*, Physical Review B-Condensed Matter, 57 (1998), pp. 9567-9580.

[121] R. S. Kohlman, Y. Min, A. G. Macdiarmid and A. J. Epstein, *Optical Conductivity of Doped Polyaniline - Effects of Disorder*, Synthetic Metals, 69 (1995), pp. 211-212.

[122] R. S. Kohlman, J. Joo, Y. G. Min, A. G. MacDiarmid and A. J. Epstein, *Crossover in electrical frequency response through an insulator-metal transition*, Physical Review Letters, 77 (1996), pp. 2766-2769.